EFFECTS OF ELECTRICAL DYNAMIC RESPONSE OF DOUBLY FED INDUCTION GENERATOR TYPE WIND TURBINES ON THEIR MECHANICAL SYSTEMS DURING SINGLE AND MULTIPLE FAULTS

A Thesis Submitted to
the Graduate School of Engineering and Sciences of
İzmir Institute of Technology
in Partial Fulfillment of the Requirements for the Degree of

MASTER OF SCIENCE

in Energy Engineering

by
Mert COŞGUN

December 2023
İZMİR

We approve the thesis of **Mert COŞGUN**

Examining Committee Members:

Prof. Dr. Engin KARATEPE
Institute of Solar Energy, Ege University

Prof. Dr. Levent ÇETİN
Mechatronic Engineering Department, İzmir Katip Çelebi University

---

Assoc Prof. Dr. Z. Haktan KARADENİZ
Energy System Engineering, İzmir Institute of Technology

11 December 2023

Assoc Prof. Dr. Z. Haktan KARADENİZ
Supervisor, Energy System Engineering
İzmir Institute of Technology

Dr. Müfit ALTIN
Co-Supervisor, Siemens Gamesa
Renewables Energy

Prof. Dr. Gülden GÖKÇEN AKKURT
Head of Energy System Engineering

Prof. Dr. Mehtap EANES
Dean of the Graduate School of
Engineering and Sciences

ACKNOWLEDGEMENT

Words cannot express my gratitude to my Energy System Engineering department professors and head of ESE, Prof Dr. Gülden GÖKÇEN AKKURT for their valuable support. I would like to express my deepest appreciation to my supervisors who generously provided knowledge and expertise, Assoc. Prof. Dr. Z. Haktan KARADENİZ and Dr. Müfit ALTIN for their invaluable patience and feedback during this long journey. I also could not have undertaken this journey without my defense committee with their valuable feedback.

I am also grateful to my company, FEV Türkiye and especially my colleagues and managers for their support. This endeavor would not have been possible without their generous understanding of them.

Lastly, I would be remiss in not mentioning my family, especially my parents, parents-in-law, sister, and brother-in-law. Their belief in me has kept my spirits and motivation high during this process. And, I am deeply indebted to my dear wife, Melike TURGUT COŞGUN, and my beloved son, Bulut COŞGUN, without them and their love, patience, support, I could not have undertaken this thesis study. I achieved everything with all this big family's endless support.

ABSTRACT

EFFECTS OF ELECTRICAL DYNAMIC RESPONSE OF DOUBLY FED INDUCTION GENERATOR TYPE WIND TURBINES ON THEIR MECHANICAL SYSTEMS DURING SINGLE AND MULTIPLE FAULTS

In the early stages of wind turbine technology, the focus was on the separate development of mechanical and electrical systems and research was carried out only in these areas. Today's modern wind turbine designs, which have reached megawatt sizes, continue to be more cost-effective and dependable for countries to achieve their renewable energy targets. In this direction, wind turbine research and development processes have now started to focus on both mechanical and electrical systems and their subsystem interactions. In this thesis study, it is aimed to investigate the effects of the response of electrical control systems on towers components during grid faults. A doubly fed induction generator is used for power generation and power systems including converters and control systems are modelled in MATLAB/Simulink. Simulations were designed in Simulink to test the grid-connected wind turbine model and the Fault Ride Through condition that causes voltage drops in the grid connection lines; the response of the control system and electromagnetic torque output in the relevant case were sent to the mechanical system analysis tool Horizonal Axis Wind Turbine Simulation Code 2 to observe the effects on the mechanical system. In Horizonal Axis Wind Turbine Simulation Code 2, the interaction of the main bodies against forces and limits is analyzed and the results are reported graphically. The state of the system without fault and data with the faults are analyzed comparatively. It has been observed that the reactions of the electrical power systems during grid failure influence the mechanical systems.

ÖZET

ÇİFT BESLEMELİ İNDÜKSİYON JENERATÖR TİPİ RÜZGAR TÜRBİNLERİNİN TEK VE ÇOKLU ARIZA DURUMUNDA ELEKTRİKSEL DİNAMİK TEPKİLERİNİN MEKANİK SİSTEMLER ÜZERİNDEKİ ETKİLERİ

Rüzgâr türbini teknolojisinin ilk dönemlerinde, mekanik ve elektrik sistemlerin ayrı ayrı geliştirilme süreçlerine odaklanılmış ve sadece bu alanlarda araştırmalar yapılmıştır. Günümüzdeki megavat boyutlarına ulaşan modern rüzgâr türbin tasarımlarının ülkelerin yenilenebilir enerji hedeflerine ulaşması için daha uygun maliyetli ve güvenilir olması için çalışmaları sürmektedir. Bu doğrultuda, rüzgâr türbini araştırma ve geliştirme süreçleri artık hem mekanik hem de elektrik sistemlere ve bunların alt sistem etkileşimlerine de odaklanmaya başlamıştır. Şebeke bağlantılarının gereksinimleri, şebeke kodları, sadece güç sistemleri ve bileşenleri için değil, mekanik sistem ve bileşenleri için de sorumluluklar getirmektedir. Bu çalışmada, şebeke de meydana gelen arızalar sırasında, elektrik kontrol sistemlerinin tepkisinin, kule ve kanatlardaki etkilerinin incelenmesi amaçlanmıştır. Güç üretimi için Çift Beslemeli Endüksiyon Jeneratörü kullanılmış; AC/DC, DC/DC çevirici ve kontrol sistemlerini içeren güç sistemleri MATLAB/Simulink'te modellenmiştir. Şebekeye bağlı rüzgâr türbini modeli ile şebeke bağlantı hatlarında meydana gelen voltaj düşümüne neden olan hatalarının üstesinden gelebilme durumunu test etmek için Simulink'te simülasyonlar tasarlanmış; ilgili durumda kontrol sisteminin tepkisi ve elektromanyetik tork çıkışı, mekanik sistem üzerindeki etkileri gözlemlemek için mekanik sistemi analiz aracı Horizontal Axis Wind Turbine Simulation Code 2 (HAWC2) programına gönderilmiştir. HAWC2'de ana gövdelerin kuvvetlere ve limitlere karşı etkileşimi analiz edilerek; sonuçlar grafiksel olarak raporlanmıştır. Hata olmayan sistemin durumu ile hata geldiği anda elde edilen veriler karşılaştırılmalı olarak incelenmiştir. Hata anında elektrik güç sistemlerinin şebekeye bağlı kalmak için verdiği tepkilerin mekanik sistemler üzerinde etkisi olduğu gözlenmiştir.

TABLE OF CONTENTS

LIST OF FIGURES

Figure **Page**

LIST OF TABLES

Table **Page**

CHAPTER 1
INTRODUCTION

Today's wind turbines, which are larger in size and have more power capacity, are designed to function in challenging environmental circumstances and meet the growing demands of power systems. Creating an affordable and dependable wind turbine design requires expertise in multiple fields. Wind turbine design and research focus on specific areas such as aeroelastic and mechanical systems, electrical and control systems, and grid integration problems, which are crucial for the development of new technologies. Field observations of wind turbines indicate a requirement to integrate expertise from several design domains in order to accomplish this objective (Barahona et al. 2013).

The objective of modern wind turbine design has shifted from medium-sized turbines linked to distribution grids to big offshore wind power facilities connected to the transmission level of power networks (Barahona et al. 2013). Contemporary engineering design heavily depends on computational codes for dynamic analysis during the design process. However, in the field of wind turbine design, these codes are tailored to specific areas of expertise (Barahona et al. 2013). Fields such as aero-elasticity, power systems, power electronics, control systems, etc. all contribute to the design process with the use of specialized software (Hansen and Michalke 2007).

The growing interest in wind energy in recent years resulted in power system regulators revising the grid connection requirements and adding new ones. Essentially, the grid regulations for wind energy necessitate an operating behavior that mirrors that of traditional power plants. The primary problem in wind turbine design is ensuring that they maintain grid connectivity both during and after a voltage decrease. These new grid rules have prompted extensive research efforts to develop sophisticated control systems for wind turbines that meet the needs of the electrical grid. These systems are also known to impact the structural loads on the wind turbines (Barahona et al. 2013).

The main trend of modern wind turbines and wind farms is to be able to operate at variable-speed and to be connected to a grid through a power converter interface. The variable speed wind turbine concept has a significant dominance in the market today. One of the well-known variable-speed wind turbine concepts with partial-scale power converter is doubly fed induction generator (DFIG) wind turbines (Hansen and Michalke 2007). These generators, however, during their operation can be affected by different

types of faults such as current sensor faults, voltage drops, frequency variation and line break, grounding. These electrical faults remain a serious concern. Voltage sags are severe faults that can damage electrical systems of wind turbine by causing an increase in the stator current which subsequently increases the voltage at the DC busbar. Such electrical faults propagate rapidly and affect other system components such as the wind turbine, converters, and the generator, degrading the quality of electrical energy generation (Abdelmalek et al. 2019).

Power systems have a significant impact on the structural loads of wind turbines and the performance and reliability of wind turbine components. In their study, Barahona et al. is investigating the impact of balanced voltage faults on wind turbine loads. In their study outlines a two-step simulation process for analyzing the dynamic behavior of a wind turbine during a grid fault (Barahona et al. 2013). The technique involves the use of two complementary simulation tools, specifically DigSILENT and HAWC2. This approach allows for the evaluation of both the electrical and structural design components of the wind turbine in the event of grid faults. HAWC2 is used as aeroelastic modeling code that incorporates a comprehensive model for the flexible structure of wind turbines. It is aim as accurately considering the flexibility of the tower, blades, and other components of the turbines. The wind turbine loads are simulated and analyzed in HAWC2, while the wind turbine's electrical interaction with the grid during grid faults is evaluated in DigSILENT. However, in this study variable speed turbine design is not considered.

In their study, Tarnowski and Claudio 2012 proposed to examine the incorporation of extensive wind power generation into power systems and its active power control (Tarnowski and Claudio 2012). In this study focuses on innovative approaches and resolutions that explicitly address the stability of electric frequency and the successful integration of high levels of wind power, particularly in isolated islanding scenarios. An analysis is conducted on the ability of variable speed wind turbines to provide Inertial Response. In order to conduct this evaluation, a control algorithm is formulated to regulate the inertial response of a wind turbine. The effectiveness of this algorithm is then simulated for a single wind turbine. Evidence demonstrates that wind power can offer significant inertial response by integrating a substantial quantity of wind turbines within a wind plant. The study focuses on examining the synchronization between the advanced control systems and the typical reactions of conventional plants. This paper presents a methodology for calculating the required wind power reserve and control parameters, including the frequency response characteristic and dead band. The computer simulations

demonstrated the performance and capabilities of supporting the grid both in regular operation and during large load events.

The objective of the study (Barahona et al. 2013) is to create a comprehensive design methodology for analyzing the dynamic behavior of wind turbines in relation to certain power system conditions. The objective is to examine the effects of power system circumstances on wind turbine loads and derive conclusions regarding their influence on wind turbine design. To achieve this primary objective, it is important to incorporate dynamic models of electrical components, controllers, and power systems into the dynamic analysis codes used for wind turbines. The incorporation of these models results in a comprehensive framework or setting for conducting integrated analysis and design of wind turbines. The purpose of this study is to outline a comprehensive dynamic analytic environment integrating HAWC2-Matlab/Simulink, which is the central component of this project. Due to its multibody dynamic formulation, HAWC2 is appropriate for integration with other simulators. The shared libraries, also known as dynamic-link libraries (DLLs), encompass external forces, soil dynamics, hydrodynamics, and control. The inclusion of the MATLAB/Simulink interface is an integral component of this work.

In their study, Slootweg, Polinder, and Kling 2003 observed that the integration of electrical systems with mechanical systems in wind turbines has significant implications for their performance and the overall power system dynamics. The interaction between the electrical and mechanical components of wind turbines affects their behavior and the power system as a whole (Slootweg, Polinder, and Kling 2003).

In the study, Hansen and Michalke suggest using a computer-based method to accurately measure the structural loads on wind turbines resulting from the grid requirements for fault ride-through (Hansen and Michalke 2007). This methodology, demonstrated using a 2MW active stall wind turbine as an example, depends on integrating information from various modeling tools that possess expertise in distinct aspects of wind turbine design. The dynamic reaction of wind turbines to grid disturbances is assessed using two complementary modeling tools: Power Factory from DigSILENT, which is a thorough power system simulation tool, and HAWC2, an advanced aeroelastic computer code. These two tools are connected in a sequential manner in an offline approach to gain a comprehensive understanding of both the structural and electrical reaction of wind turbines during grid failures. The influence of grid requirements on the structural loads of wind turbines is measured by doing a rain flow study for fatigue loads and a statistical analysis for ultimate structural loads. Two

scenarios are being compared: one in which the turbine is promptly disconnected from the grid when a grid fault occurs, and another in which the turbine is fitted with a fault ride-through controller, allowing it to stay connected to the grid even during a grid fault.

In this thesis study, a wind turbine model with a double-fed induction generator is used to monitor the effects of the electrical system response on the mechanical system during a single one phase to short or successive one-phase and three-phase short circuit faults. Unlike the two dynamically coupled simulation in other studies, electromagnetic torque data was first obtained in MATLAB/Simulink and tried to be input to HAWC2 with dll executable file. In similar studies, Power Factory or DigSilent tools as advanced power systems analysis are used for electrical system design for grid connected wind turbines as well as FAST for aeroelastic analysis. In this thesis study, MATLAB/Simulink is used to design wind turbine and power system. Moreover, voltage drop faults are considered as faults and uniquely successive faults are implemented for effect analysis. It is aimed to observe the effects on the turbine tower top deflections during faults. In addition to this, it is objected to see different effects of wind speed for mechanical system during fault by comparing the worst case in HAWC2. In the end, eventually, the correlation between electrical system and mechanical systems are presented by showing engineering methods for future researches.

In Chapter 1, Introduction for background and motivation behind that thesis can be found. In Chapter 2, Design environments and materials are introduced. The contribution of this chapter is to develop software interfaces of simulation tools. In Chapter 3, wind turbine design models and power systems are presented. In Chapter 4, MATLAB/Simulink power system model and HAWC2 DTU 10MW wind turbine model's simulations and their verifications by simulations are presented. In Chapter 5, discussion of results can be found. Chapter 6 is final consideration and outlook for future researched on that topic.

CHAPTER 2
DESIGN ENVIRONMENTS AND MATERIALS

Simulation stands as a crucial method in assessing engineering solutions currently. There is a variety of simulation software available for various applications such as power converters, generators, power systems, mechanical components, and the aeroelastic characteristics of wind turbines. However, it is not feasible for a single tool to address every detail simultaneously. Thus, when enhancing electrical models, it is vital to ensure their compatibility with chosen tools and to have a clear understanding of the model's components. These tools ought to be utilized in alignment with the specific area of interest of the designer (Florin Iov, Frede Blaabjerg, and Anca Daniela Hansen 2002), (Hansen, Soerensen and Blaabjerg 2004).

The primary concept behind this innovative simulation platform is to enhance the capabilities of current wind turbine design software. This enhancement focuses on simulating both the dynamic responses of wind turbines and their interactions with the electrical grid. To facilitate this, the model database should be equipped to analyze how the wind turbine's mechanical structure interacts with the electrical grid under various operational conditions (Florin Iov, Frede Blaabjerg, and Anca Daniela Hansen 2002), (Hansen, Soerensen and Blaabjerg 2004).

2.1. MATLAB/Simulink

MATLAB stands out as a dynamic language tailored for technical computing. It combines calculation, visual representation, and programming in a user-friendly setting, using familiar mathematical expressions to define problems and solutions. Common applications of MATLAB include mathematical computations, algorithm creation, data gathering, modeling, simulation, prototyping, data analysis and exploration, visualization, scientific and engineering graphics, and creating applications with graphical user interfaces (Pratap 2009).

The MATLAB system is composed of five primary components:

1. Development Environment: This comprises tools and features aiding in utilizing MATLAB functions and files, many of which are graphical interfaces. It encompasses the MATLAB desktop, Command Window, a command history log, an editor, and

debugger, as well as browsers for accessing help, workspace, files, and the search path.

2. MATLAB Mathematical Function Library: A comprehensive repository of computational algorithms, ranging from basic functions like addition, trigonometric functions, and complex arithmetic to more advanced ones such as matrix inversion, eigenvalues, Bessel functions, and fast Fourier transforms.
3. MATLAB Language: This high-level language focuses on matrix/array handling with control flow statements, functions, data structures, input/output, and object-oriented programming capabilities. It is designed for both small-scale, quick programming tasks and large-scale, complex applications.
4. Graphics: MATLAB offers extensive tools for graphically representing vectors and matrices, along with annotating and printing these graphs. It provides high-level functions for 2D and 3D visualization, image processing, animation, and presentation graphics, along with low-level functions for detailed customization of graphics and development of graphical user interfaces in MATLAB applications.
5. MATLAB Application Program Interface (API): This library allows for writing C and Fortran programs that interface with MATLAB. It includes features for calling functions from MATLAB, using MATLAB as a computational engine, and for reading and writing MAT-files.

Simulink, a graphical software package, is utilized for the purpose of modeling, simulating, and evaluating dynamic systems. This software is built upon the foundation of MATLAB. The software provides support for both linear and nonlinear systems, which can be modeled using continuous time, sampled time, or a combination of both. Simulink offers a graphical user interface (GUI) that facilitates the construction of models through the utilization of click-and-drag mouse actions, specifically in the form of block diagrams. This interface facilitates the construction of required dynamic systems with ease. Simulink encompasses an extensive assortment of blocks inside its library, encompassing sinks, sources, linear and nonlinear components, as well as connectors.

S-Functions can be utilized to customize and generate user-defined blocks as well. Hierarchical models can be constructed using either top-down or bottom-up methodologies. The system can be observed from a macro perspective, and users can navigate to lower levels of model information by double-clicking on individual blocks. This methodology offers a comprehensive understanding of the structural organization and interplay of components inside a model. Once a model has been defined, it is possible

to simulate it by employing various integration methods. This can be done either through the Simulink menus or by inputting commands in the MATLAB Command Window.

The utilization of menus is notably advantageous for facilitating interactive tasks, however the command-line methodology becomes highly beneficial for executing a series of simulations, such as Monte Carlo simulations or parameter sweeping across a certain range. By utilizing scopes and other display blocks, it is possible to analyze the simulation results in real-time throughout the execution of the simulation. Furthermore, the parameters have the capability to be modified throughout the simulation to facilitate "what if" analysis. The obtained simulation results can be stored in the MATLAB workspace for subsequent postprocessing and display purposes. The available model analysis tools encompass linearization and trimming tools, which can be accessible using the MATLAB command line, in addition to the diverse array of tools provided by MATLAB and its associated application toolboxes. The integration of MATLAB and Simulink allows for the seamless simulation, analysis, and revisitation of models within any environment, offering flexibility and convenience to users (Pratap 2009), (Ali 2018).

MATLAB/Simulink Toolbox can be designed specifically for the purpose of wind turbine applications in the context of wind energy projects. To examine the dynamic and steady state characteristics of a wind turbine, a comprehensive model can be developed. These models encompass the fundamental elements of a wind turbine, which have been organized into seven distinct libraries: Mechanical Components, Electrical Machinery, Power Converters, Common Models, Transformations, Measurements, and Control (Florin Iov, Frede Blaabjerg, and Anca Daniela Hansen 2002).

2.2. Horizontal Axis Wind Turbine Simulation Code 2nd Generation (HAWC2)

2.2.1. HAWC2 General Information

The HAWC2, also known as Horizontal Axis Wind turbine simulation Code 2nd generation, is a computational tool designed to analyze the aeroelastic behavior of wind turbines by simulating their reaction in the time domain.

The primary development of the code took place predominantly between the years 2003 and 2007, under the supervision of the Aeroelastic Design Research Program at

DTU Wind, located at DTU Risø Campus in Denmark. HAWC2, a software program, has been developed and supplied by DTU Wind Energy. It has been extensively utilized in various research projects and industrial applications related to wind turbine performance, wake modeling, aeroelasticity, and structural responses, making it a crucial tool for research and analysis in the field of wind energy.

The HAWC2 software is a widely used aeroelastic code for wind turbine simulations, particularly in the context of offshore wind power. It has been employed in various studies to analyze turbine wakes, aeroelastic behavior, and structural responses. For instance, Gaertner et al. utilized HAWC2 for load and performance analysis of offshore wind turbines, while Lio, Larsen, and Thorsen, Asmuth et al are both incorporated the Dynamic Wake Meandering (DWM) module within HAWC2 to generate turbine wakes and model wind turbine responses in waked inflow, respectively (Gaertner et al. 2020), (Lio, Larsen, and Thorsen 2021), (Asmuth et al. 2022). Additionally, Tuhfe Göçmen et al, Tang and Cao compared experimental findings with simulation results from HAWC2 models, demonstrating their significance in validating wind turbine performance (Tuhfe Göçmen et al. 2022), (Tang and Cao 2023). Moreover, HAWC2 is used to study fatigue sensitivity, reliability, and wave kinematics associated with wind turbines, further highlighting its relevance in assessing turbine behavior under various conditions (Chen et al. 2021), (Wang and Larsen 2019).

Furthermore, HAWC2 has been used in structural reliability analysis (Jiang et al. 2017), wake characteristics of floating offshore wind turbines (Tang and Cao 2023), and ice-induced load analysis for offshore wind turbines (Shi et al. 2016). The software has also been utilized in aeroelastic simulations for wind turbine design optimization (Barlas et al. 2021), investigating fault ride-through capability (You et al. 2013), and studying the influence of inflow angles on wind turbine blade vibrations (Horcas et al. 2022). Additionally, it has been integrated with hydraulic transmission systems in Jiang et al study and used in the development of control-oriented models for floating wind turbines (Betti et al. 2014), (Jiang et al. 2017).

In Appendix A, license information and starting and running HAWC2 process can be found in detail.

2.3. MATLAB/Simulink and HAWC2 Integration

The integration of HAWC2 with MATLAB/Simulink has been extensively studied for various purposes. In their study, Ren et al. discussed the interface between HAWC2 and MATLAB/Simulink, emphasizing the drawbacks of using TCP/IP or DLLs for control implementation (Ren et al. 2018). You et al. utilized an integrated simulation environment, based on HAWC2 and MATLAB/Simulink to investigate the fault ride-through capability of a novel wind turbine concept, demonstrating the practical application of this integration in studying structural loads during grid faults (You et al. 2013). For their study, Gallego-Calderon, Natarajan, and Cutululis employed an online co-simulation approach with HAWC2 and MATLAB/Simulink to analyze the ultimate design load of planetary gearbox bearings, highlighting the use of detailed generator models for realistic torque response (Gallego-Calderon, Natarajan, and Cutululis 2016). In their study, Barahona et al. also emphasized the significance of an integrated simulation environment based on HAWC2 and MATLAB/Simulink for dynamic analysis considering aeroelastic, electrical, and control dynamics (Barahona et al. 2013).

These references collectively underscore the utilization of HAWC2 in conjunction with MATLAB/Simulink for various purposes, including control system implementation, fault ride-through capability studies, realistic torque response analysis, and dynamic analysis encompassing aeroelastic, electrical, and control dynamics. The integration of these tools offers a comprehensive approach to wind turbine research and development, enabling in-depth investigations into structural loads, control strategies, and overall turbine performance.

In this study, HAWC2 and MATLAB developments are based on keeping both as a stand-alone application while letting MATLAB manage Electrical Systems responses as input to HAWC2. This solution can only be achieved by using DLL files. The primary purpose of DLLs is to manage the speed and pitch of turbines. However, due to the flexible nature of the DLL format, it can also be employed for other purposes such as external loading of the turbine. There exist two distinct dynamic-link library (DLL) techniques, namely hawc_dll and type2_dll. Both interfaces display distinct characteristics, with one notable distinction: the hawc_dll undergoes updates during each aero-structure iteration, frequently occurring many times during a time step, but the type2_dll is updated just once each time step. The durability of the new type2_dll interface in relation to the solver is slightly higher compared to that of the hawc_dll interface (Larsen, Hansen, and Melchior 2007).

2.3.1. Hawc.dll Format

The hawc_dll format allows the creation of a subroutine within an externally written DLL. This subroutine involves the transfer of two one-dimensional arrays between the HAWC2 core and the DLL function. One data stream transfers information from the HAWC2 core to the DLL, while the second data stream transfers information from the DLL to the core. It is crucial to acknowledge that the transfer of data occurs between HAWC2 and the DLL throughout each time step and iteration. The responsibility of managing the iteration within the Dynamic Link Library (DLL) lies with the user (Larsen, Hansen, and Melchior 2007).

If the dll file contains further subroutines, two more subroutines will be invoked. The first step involves making an initialization call, which includes a text string specified in the init_string parameter throughout the subsequent calls. That phrase represents the potential designation of a file that contains localized input parameters for the data transfer function. The execution of this function occurs only once. The subroutine in question shares its name with the data transfer subroutine defined with the command dll_subroutine, with the additional suffix "_init". Consequently, if the data transfer subroutine is named "test", the initialization subroutine will be named "test_init" (Larsen, Hansen, and Melchior 2007).

The second function pertains to a message exchange mechanism, enabling the transmission of messages authored within the Dynamic Link Library (DLL) to the HAWC2 core for the purpose of writing to the logfile. The subroutine in question shares the identical name as the data transfer subroutine, which is defined using the command dll_subroutine. However, it includes an additional suffix '_message' (Larsen, Hansen, and Melchior 2007).

2.3.2 Type2.dll Format

This version of the DLL interface is a revised and somewhat altered iteration of the hawc_dll interface. The type2_dll format involves the establishment of a function within a DLL that has been built externally. This subroutine involves the transfer of two one-dimensional arrays between the HAWC2 core and the DLL function (Larsen, Hansen, and Melchior 2007).

The first dataset comprises information transmitted from the HAWC2 core to the DLL, whereas the secondary dataset covers data transmitted from the DLL to the core. It

is crucial to acknowledge that the transfer of data between HAWC2 and the DLL occurs during the initial call of each time step, in which the outgoing variables rely on the most recently iterated values from the preceding time step. The output and actions of the sub command are similar between the hawc_dll and type2_dll interfaces. The type2_dll interface should include two subroutines. There are two key routines in the simulation process: an initialization procedure, which is executed just once before the beginning of the time simulation, and an update routine, which is executed at each time step. The calling format of these two subroutines is similar, involving the exchange of two arrays of double precision (Larsen, Hansen, and Melchior 2007).

2.3.3. External Force and Moment

These command blocks can be used to specify a user-defined constant external force and/or moment on a node on the structure. DLL file should be prepared to include external forces or moments for HAWC2 simulation. The DLL command block is utilized in cases where an externally defined force or moment is exerted against the structure. One famous distinction between the DLL format under consideration and the conventional DLL control interface employed with external controllers is in the first calculation of increased stiffness, which contributes to a more resilient and expedient resolution of the interconnected system. The utilization of this force module has demonstrated favorable outcomes when employed to account for external soil-springs or hydrodynamic forces in the context of floating constructions or mooring lines (Larsen, Hansen, and Melchior 2007).

DLL interface can be written with fortran90; subroutines can be defined inside that fortran90 code piece. Strings and values are passed into variables in those routines. Related main body and its node information as well as actions shall be defined with that value passing. DLL creation can be possible with Lazarus and Pascal builder. An example of dll subroutine can be seen in APPENDIX B.

DLL files would be passed into HAWC2 simulation file, namely “HTC” file. HTC file can be updated using “Notepad++” tool before running with simulation. While calling DLL files with “type2.dll” format. Comments can be used. DLL commands for external force or moment can be seen from table in APPENDIX C. An example of type2.dll code

portion of HTC file can be seen in APPENDIX D. Output variables and actions detailly examined in these code section.

2.4. Grid Codes

Wind turbines must adhere to grid codes, which are particular technical standards that ensure their seamless integration into the electrical grid. The codes provide the criteria and benchmarks that wind turbines must satisfy in order to guarantee the stability and dependability of the grid. The introduction and enforcement of grid rules have had a substantial influence on wind turbine technology and operation, compelling manufacturers to modify their systems to comply with these requirements (Altın et al. 2010). Grid codes cover multiple factors, including fault ride-through capabilities, low voltage ride-through (LVRT) requirements, reactive power supply, and power quality considerations. For example, contemporary grid standards require wind turbine generators (WTGs) to be connected to electrical networks even when there are voltage disruptions that are significantly lower than the normal values (Mullane, Lightbody, and Yacamini 2005). Furthermore, LVRT regulations dictate that WTGs must maintain their connection to the grid within specific voltage thresholds and time intervals during failures (Chandrasekaran et al. 2013). In addition, grid regulations require wind turbines to supply reactive currents in order to assist in the restoration of voltage after the clearance of grid faults (Thapa, Kim, and Yong Cheol Kang 2016).

The development of grid codes has also impacted the design and control techniques of wind turbines. Recent grid code requirements have prompted the advancement of wind turbine active power control (APC) systems. These systems allow wind turbines to contribute to grid frequency management and offer stabilizing responses to abrupt fluctuations in grid frequency (Sim et al 2012). Moreover, the growing enthusiasm for linking wind farms to electrical grids has resulted in the adaptation or expansion of grid codes to suit the distinct capabilities and needs of wind turbine generators (WTGs) (Florin Iov et al. 2006). Furthermore, according to the grid code, wind turbines must stay linked even under grid fault conditions. This requires the development of enhanced control techniques and technologies to assure compliance (Pao 2021).

The influence of grid codes extends beyond the technical features of wind turbines to embrace the wider wind power sector. Grid codes serve as essential directives for wind

turbine manufacturers and wind farm planners, exerting influence over the market adoption of various wind turbine models and technologies (Gashi et al. 2012). Moreover, the progress of wind turbine technology is unavoidably influenced by the updated grid codes, which require wind power plants to assist the system and offer supplementary services comparable to traditional power plants (Siavash Beheshtaein 2014).

The consolidation of the above sources emphasizes the substantial impact of grid codes on wind turbine technology, functioning, and the wind power sector as a whole. The rigorous technical specifications specified in grid regulations have stimulated the invention of sophisticated control systems, technologies, and market penetration tactics to guarantee adherence and improve the incorporation of wind power into electrical grids.

2.4.1. Wind Turbine Fault Ride Through Requirements

The increase and growth of wind power has introduced new challenges to the electrical system. The integration of a large-scale wind power system would give rise to challenges not only during normal operation but also during emergency situations. Fault Ride Throughs (FRTs) must ensure that wind turbines remain connected to the power grid during disturbances in order to enhance the stability of the power transmission system. Researchers have conducted numerous studies on the behaviors of WTs. The given references clearly indicate that fault ride-through capability is a crucial factor in the functioning of wind turbines, especially when it comes to integrating with the power grid. Grid codes require wind turbines to maintain their connection to the grid and sustain operation even in the event of grid faults, thereby guaranteeing the stability and dependability of the grid. Multiple studies have concentrated on improving the ability of wind turbines to withstand faults by implementing diverse control systems and technology.

The fault ride-through capability of wind turbines is a crucial feature of their performance, particularly when encountering grid faults. Multiple research investigations have been carried out to improve the ability of wind turbines, namely those equipped with doubly-fed induction generators (DFIG) to withstand faults during operation, known as fault ride-through (FRT) capabilities. These studies have suggested multiple control systems and technologies to allow wind turbines to stay linked during grid disturbances and endure faults. Furthermore, there have been suggestions to utilize adaptive control

algorithms that rely on stator current transient components in order to improve the reactive power support and fault ride-through capability of wind turbines based on Doubly Fed Induction Generators (DFIG) (Wang, Fu, and Zhang 2023).

In addition, researchers have investigated the application of superconducting fault current limiters and energy storage systems to improve the ability of wind turbines, especially those with doubly-fed induction generators (DFIGs), to withstand faults (Sitharthan and Geethanjali 2015). Additionally, researchers have suggested the use of electronic power transformer control techniques and better crowbar protection to boost the ability of wind turbines with permanent magnet synchronous generators and doubly-fed induction generators (DFIGs) to withstand low voltage conditions. These proposals were made by Huang et al. and Kalyani et al. (Huang et al. 2014), (Kalyani et al). In addition, research has specifically examined the adherence of wind turbines to low-voltage ride-through capability regulations and the influence of fault ride-through requirements on the structural stresses of fixed-speed wind turbines (Hansen et al. 2011), (Jerin, Palanisamy Kaliannan, and Subramaniam 2017).

Wind turbines, particularly those equipped with Doubly Fed Induction Generators (DFIGs), have been thoroughly investigated for their ability to withstand faults. This has resulted in the development of many control systems, technologies, and compliance measures to assure the uninterrupted operation of wind turbines when grid faults occur.

In addition, Thapa, Kim, and Kang highlight the importance of the low voltage ride-through (LVRT) requirement outlined in grid standards (Thapa, Kim, and Kang 2016). This requirement dictates that wind turbine generators (WTGs) must remain connected to the grid within a specific voltage range and for a designated duration in the event of a fault. This emphasizes the complete technical prerequisites associated with fault ride-through in grid codes.

2.5. Method

This Thesis study method is established by following Figure 2.1.

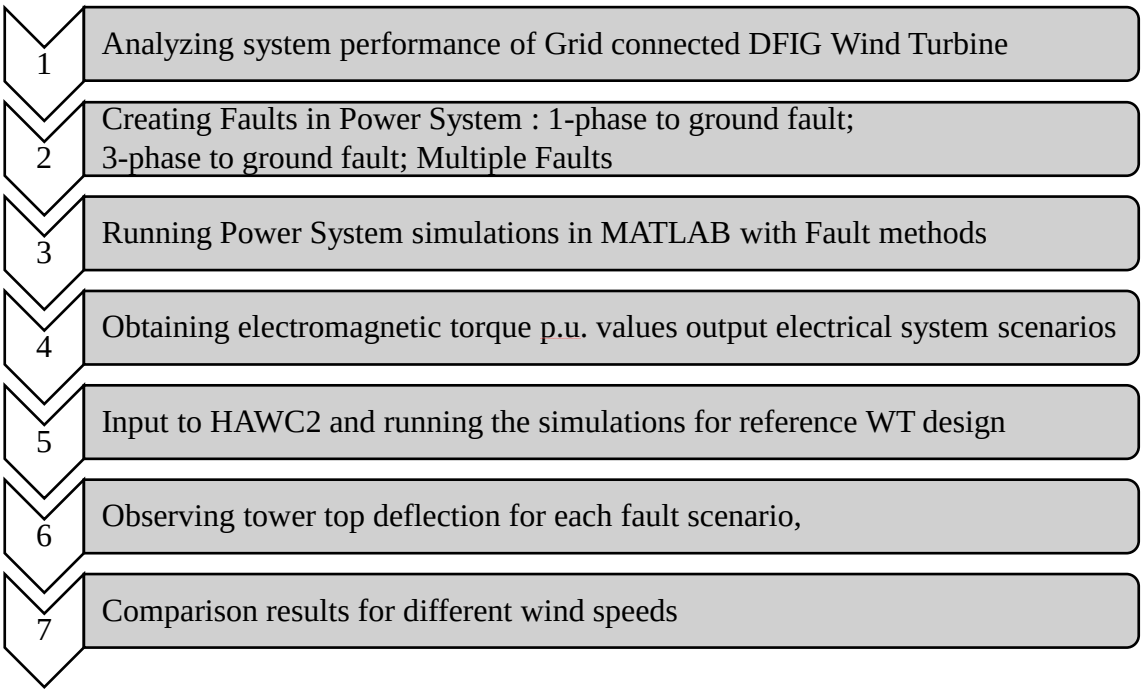

Figure 2.1. Thesis study method

First step is starting with designing Power System for Double Fed Induction Generator Type Wind Turbine that is connected to a Grid. Analyzing performance of power system and verifying is the first simulation of the study. Grid faults, namely one-phase to ground and three-phase to ground, would be introduced to system as next step. For all scenarios, by changing grid voltage, are simulated to observe effects of grid faults on to electrical system of DFIG Wind Turbine. Electromagnetic Torque values per unit are recorded to see the changes.

In following step, HAWC2 simulations are prepared. Firstly, base model for HAWC2 model is run for reference wind turbine and then electromagnetic torque changes are introduced into HAWC2 model to show the effects of faults on mechanical system. It can be achieved by introducing tower and shaft deflections in axial and transversal ways. Comparing results against different fault situations and wind speeds to obtain the results.

CHAPTER 3
SYSTEM DESCRIPTIONS

3.1. Double Fed Induction Generator Wind Turbine

DFIG, Doubly Fed Induction Generator, is a type of generator commonly used in wind turbines. DFIG is characterized by its ability to control both rotor and stator currents, which makes it suitable for variable speed operation (Abad et al. 2011). Some of the main features of DFIG wind turbines are as follows:

1. Variable speed operation: DFIG wind turbines are designed to operate at variable speeds, allowing them to capture more energy from the wind compared to fixed speed turbines. The rotor speed is controlled independently of the grid frequency, ensuring optimum power generation at different wind speeds.

2. Power converter system: The DFIG system includes a power converter located in the rotor circuit. This converter, known as rotor-side converter (RSC), allows bidirectional power flow between the rotor and the grid. By controlling the rotor currents, it enables the turbine to run at different speeds and adjusts the reactive power output of the generator.

3. Slip rings and brushes: The DFIG rotor is equipped with slip rings and brushes that facilitate the transfer of electrical power and control signals between the rotor and the stator. These components enable the RSC to be connected to the rotor windings.

4. Mains connection: The DFIG stator is directly connected to the grid, allowing the generator to supply power to the electrical grid. The stator operates at a constant frequency and voltage, typically synchronized with the grid.

5. Control system: DFIG wind turbines require sophisticated control systems to regulate rotor and stator currents. The control system adjusts the operation of the power converter to optimize the performance of the generator and ensure grid compatibility.

6. Capacity to remain connected to the grid during failure: DFIG wind turbines are designed with the capability to remain grid-connected during fault (FRT), which allows them to remain grid-connected during grid failures or outages. The control system detects and responds to grid faults by adjusting rotor currents to maintain stability and support grid voltage.

DFIG wind turbines offer several advantages, including enhanced energy capture, improved grid compatibility and the ability to provide reactive power support. However, they are more complex and costly than fixed speed turbines. However, DFIG technology has been widely adopted in the wind energy industry due to its ability to achieve high energy conversion efficiency in varying wind conditions. Figure 3.1 shows a schematic representation of a DFIG wind turbine.

Rotor and stator connections, inverter connections and grid connection example are given (Abad et al. 2011).

Doubly Fed Induction Generator (DFIG) wind turbines have gained recognition in the wind energy industry due to their variable speed operation and improved energy capture performance (Ekanayake et al. 2003). However, a major drawback of variable-speed wind turbines, especially those with DFIGs, is their operation during grid faults, which can affect their performance and stability (Morren and deHaan 2005). To address this, research has focused on developing control strategies for DFIG wind turbines to regulate active and reactive power, enhance fault ride-through capability, and improve low voltage ride through (LVRT) capability (Hu et al. 2010), (Wu, Zhu, and Hu 2013), (Kumar, Sushil, and Shilpa 2013). These control strategies are crucial for ensuring the reliable and stable operation of DFIG wind turbines under varying grid conditions.

Furthermore, studies have shown that DFIG wind turbines can contribute to primary frequency control and provide advanced grid support, making them an efficient and cost-effective solution for wind power integration (Engineering 2019), (Hansen et al. 2006). The integration of DFIGs with variable-speed wind turbines has been found to increase the transient stability margin of electrical grids compared to fixed-speed wind systems with cage generators (Nunes et al. 2004). Additionally, DFIG technology allows for the extraction of maximum energy from the wind at low wind speeds while minimizing mechanical stresses on the turbine during gusts of wind Kumar, 2015).

It is important to note that the control and protection of the power converter during and after grid faults are critical for the controllability of DFIG variable speed wind turbines (Kumar, Sushil, and Shilpa 2013). Research has also focused on improving the fault ride-through capability of DFIG wind turbines to mitigate the impact of extreme voltage sags on the rotor circuit, which can lead to damage and undue fatigue on the turbine components (Yan et al. 2011).

3.2. DFIG Design

The DFIG consists of two sets of three-phase windings: one in the stator and one in the rotor. These two three-phase windings need to be fed independently and can also be bidirectionally energized. The rotor three-phase windings can be connected in star or delta configuration and are fed by means of brushes and slip ring assembly.

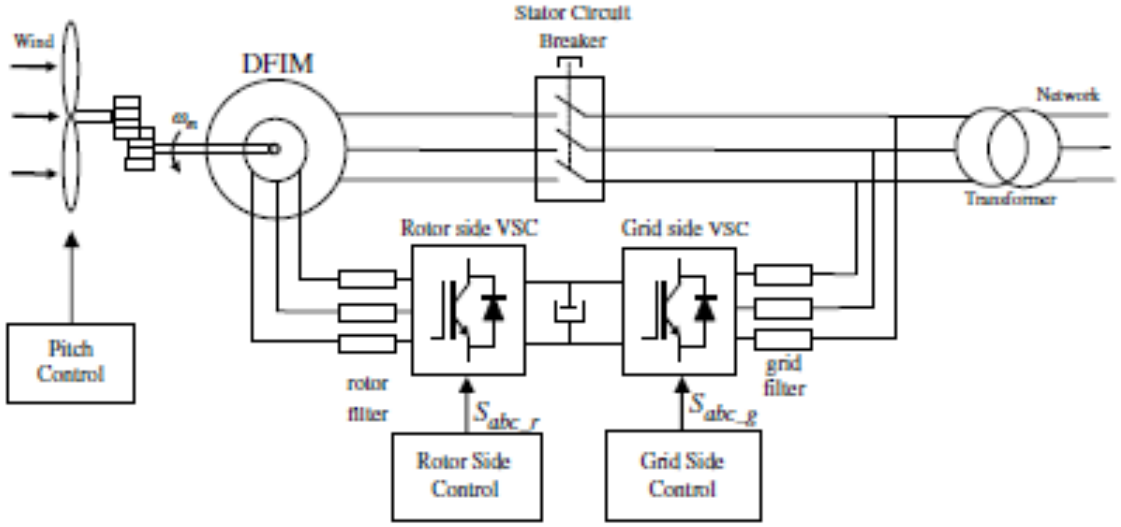

Figure 3.1. Double fed induction generator wind turbine rotor and stator overview

The stator therefore consists of three windings spatially offset by 120° and p number of double poles. When these three stator windings are supplied with a balanced three-phase voltage of frequency fs, the stator flux is induced. This stator flux rotates at constant speed. That is, the synchronous speed (ns) is given by the following expression:

$$n_s = \frac{60 f_s}{p} \tag{1}$$

In principle, this rotational stator flux induces an electromotive force in the rotor windings according to Faraday's law. Due to this voltage induced in the rotor windings and the voltage that can be injected externally via the brushes, a current is induced in the rotor windings. This current generates an induced force in the rotor of the machine according to Laplace's law. The angular frequency of the induced rotor voltages and currents is in a relationship expressed as follows:

$$\omega_r = \omega_s - \omega_m \tag{2}$$

$$\omega_m = p\Omega_m \tag{3}$$

ω_r : Rotor windings voltage and current angular frequency (rad/s)

ω_s : Stator windings voltage and current angular frequency (rad/s)

ω_m: Rotor electrical speed (rad/s)

Ω_m : Mechanical rotational speed at the rotor (rad/s)

The term commonly used to describe the relationship between the stator speed and the rotor angular frequency is slip, (s) is given by:

$$s = \frac{\omega_s - \omega_m}{\omega_s} \tag{4}$$

When we combine both equations (2) and (3), the relationship between slip, ω_r and ω_s is obtained as follows:

$$\omega_r = s\omega_s \tag{5}$$

The slip concept plays an important role in solving the equations for the rotor or stator side to calculate the basic DFIG parameters.

The steady state equations can be simply written with respect to one-phase equivalent electric circuit of DFIG where rotor side is referred to stator. It is assumed that both rotor and stator side have the same frequency. Therefore, DFIG electric equations for voltages and fluxes can be expressed as follows:

$$\overrightarrow{V_s} = R_s\overrightarrow{I_s} + j\omega_s L_{\sigma s}\overrightarrow{I_s} + j\omega_s L_m(\overrightarrow{I_s} + \overrightarrow{I_r}) \tag{6}$$

$$\frac{\overrightarrow{V_r}}{s} = \frac{R_r}{s}\overrightarrow{I_r} + j\omega_s L_{\sigma r}\overrightarrow{I_r} + j\omega_s L_m(\overrightarrow{I_s} + \overrightarrow{I_r}) \tag{7}$$

$$\overrightarrow{\varphi_s} = L_m\overrightarrow{I_r} + L_s\overrightarrow{I_s} \tag{8}$$

$$\overrightarrow{\varphi_r} = L_m\overrightarrow{I_s} + L_r\overrightarrow{I_r} \tag{9}$$

where $L_s = L_m + L_{\sigma s}$; $L_r = L_m + L_{\sigma s}$

$\overrightarrow{V_s}$: Supplied stator voltage phasor; $\overrightarrow{V_r}$: Supplied rotor voltage phasor. $\overrightarrow{I_s}$: Stator current phasor; $\overrightarrow{I_r}$: Rotor current phasor.

R_s : Stator resistance, R_r : Rotor resistance, L_m: Mutual inductance, $L_{\sigma s}$: Stator leakage inductance, L_m: Mutual inductance, $L_{\sigma r}$: Rotor leakage inductance

Equivalent torque T_{em} $(electromagnetic\ torque)$ expressions can be derived using voltage and flux expressions as follow:

$$T_{em} = 3\frac{L_m}{\sigma L_r L_s} p\ Im\{\overrightarrow{\varphi_s} * \overrightarrow{\varphi_s}\} \quad (10)$$

where $\sigma = \frac{1-L_m^2}{L_r L_s}$

For developing dynamic model of DFIG, *αβ* model can be applied to the steady state equations when the machine can be thought of as ideal and linear. Typical rotating reference frame for equations can be transferred to stationary stator reference frame. Therefore, the three windings of stator and rotor separately, by using space vector theory can be represented by two stationary *αβ* coils for stator and *DQ* rotating coils for rotor. If it will be rewritten both side equations with respect stationary from then *αβ* model transformation can be successfully obtained. After transformation following equations can be obtained:

$$v_{\alpha s} = R_s i_{\alpha s} + \frac{d\varphi_{\alpha s}}{dt} \quad (11)$$

$$v_{\beta s} = R_s i_{\beta s} + \frac{d\varphi_{\beta s}}{dt} \quad (12)$$

$$v_{\alpha r} = R_r i_{\alpha r} + \frac{d\varphi_{\alpha r}}{dt} + \omega_m \varphi_{\beta r} \quad (13)$$

$$v_{\beta r} = R_r i_{\beta r} + \frac{d\varphi_{\beta r}}{dt} - \omega_m \varphi_{\alpha r} \quad (14)$$

In similar way fluxes can be derived in space vector form with stationary frame:

$$\varphi_{\alpha s} = L_s i_{\alpha s} + L_m i_{\alpha r} \quad (15)$$

$$\varphi_{\beta s} = L_s i_{\beta s} + L_m i_{\beta r} \quad (16)$$

$$\varphi_{\alpha r} = L_r i_{\alpha r} + L_m i_{\alpha s} \quad (17)$$

$$\varphi_{\beta r} = L_r i_{\beta r} + L_m i_{\beta s} \quad (18)$$

$$T_{em} = \frac{3}{2} p(\varphi_{\beta r} i_{\alpha r} - \varphi_{\alpha r} i_{\beta r}) \quad (19)$$

The parameters used in this study are shown in Table 3.2 with reference to a 2MW DFIG wind turbine (Abad et al. 2011).

Table 3.1. Reference parameters for 2MW DFIG wind turbine

Basic Parameters	**Value**	**Description**
Synchronism	1500 rev/min	Synchronous speed at 50 Hz
Rated Power	2MW	Nominal stator three-phase active power
Rated Stator Voltage	690 V_{rms}	Line-to-line nominal stator voltage in rms
Rated Stator Current	1760 A_{rms}	Each phase nominal stator current in rms
Rated Torque	12.7 kNm	Nominal torque at generator or motor modes
Stator Connection	Star	
p	2	Pair of poles
Rated Rotor Voltage	2070 V_{rms}	Line-to-line nominal rotor voltage in rms
Rotor Connection	Star	
u	0.34	Coefficient at the stator and rotor turns per phase
Rs	2.6 mOhm	Stator resistance
Lss	87 uH	Stator leakage inductance
Lm	2.5 mH	Magnetizing inductance
R0r’	26.1 mOhm	Rotor resistance
L0sr’	783 uH	Rotor leakage inductance
Rr	2.9 mOhm	Rotor resistance referred to the stator
Lsr	87 uH	Rotor leakage inductance referred to the stator
Ls	2.587 mH	Stator Inductance
Lr	2.587 mH	Rotor Inductance

3.3. DFIG Wind Turbine Power System Design on MATLAB/Simulink

3.3.1. Aerodynamic Model in Simulink

The aerodynamic model is utilized to quantify the power extraction of the rotor by determining the mechanical torque based on the airflow acting upon the blades. Wind speed can be defined as averaging the incident wind speed across the swept area by the blades, with the purpose of assessing the average torque in the low-speed axle.

The torque generated by the rotor has been defined by the following expression:

$$T_t = \frac{1}{2}\rho\pi R^3 V_v^2 C_t \tag{20}$$

One of the most direct methods for expressing the torque and power coefficient C_p is using analytical equations that are dependent on the tip step ratio (λ) and the pitch angle (β).

$$C_p = k1\left(\frac{k_2}{\lambda_i} - k_3\beta - k_4\beta^{k_5} - k_6\right)\left(e^{k_7/\lambda_i}\right) \tag{21}$$

$$\lambda_i = \frac{1}{\lambda + k_8} \tag{22}$$

where the tip step ratio;

$$\lambda = \frac{R\Omega_t}{V_v} \tag{23}$$

MATLAB m-file script is written to initialize aerodynamic and mechanical model parameters. Running initialization file before Simulink model; C_t and λ curves can be obtained as in Figure 3.2. C_t is calculated by C_p divided by λ. Power curve against wind speed is also defined as parameter.

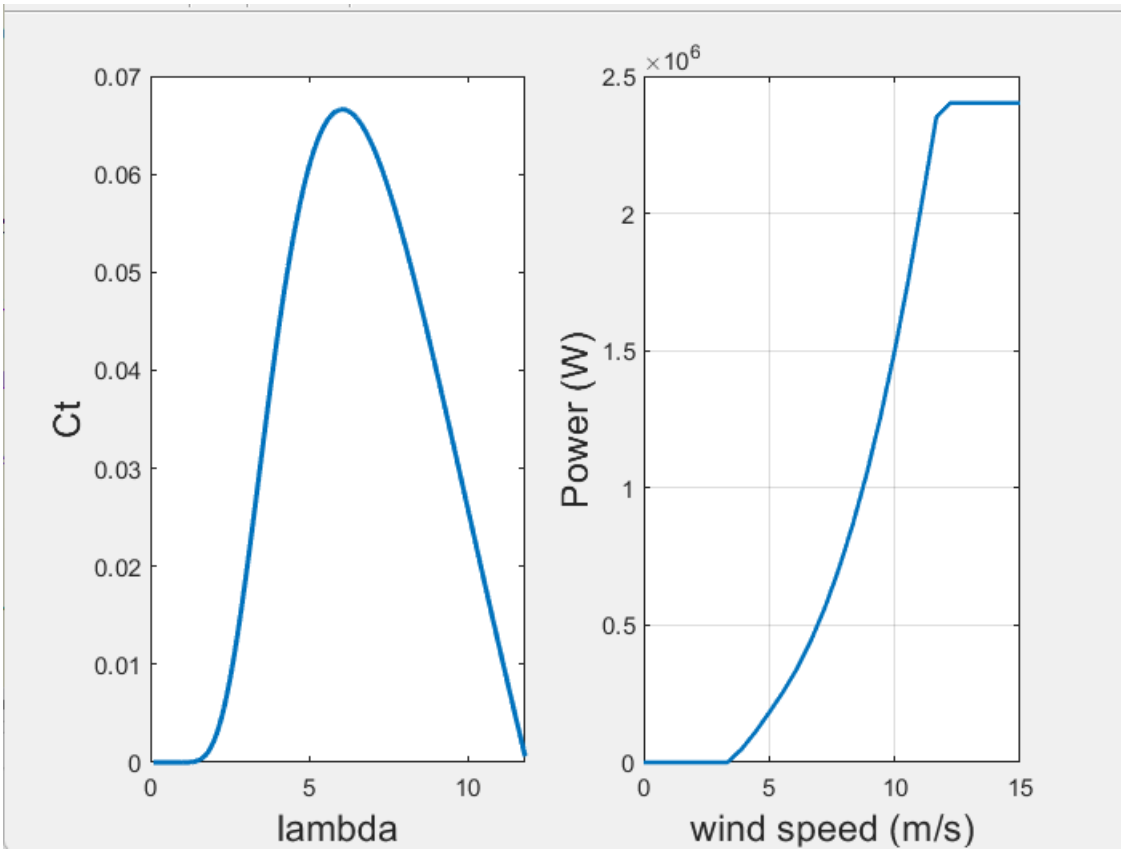

Figure 3.2. MATLAB initialization m-file Ct and λ curves

In Simulink model, these parameters are represented by block shown in Figure 3.3. Wind speed is input for this block as constant parameter. The output of this block is mechanical torque which is calculated and inserted into generator block. Inside calculations can be seen from Figure 3.4.

Figure 3.3. Wind turbine aerodynamic model block in Simulink

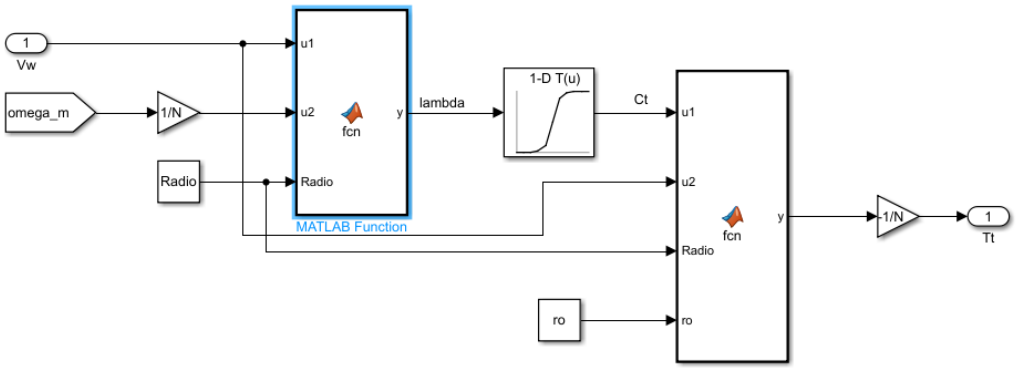

Figure 3.4. Wind turbine aerodynamic model inside in Simulink

3.3.2. DFIG Model in Simulink

DFIG can be modeled as using an electrical machine block by passing parameters in Table 3.1. DFIG block can be seen from Figure 3.5. DFIG needs a calculated mechanical torque against wind speed as input. The left side of generator is connected to rotor side while right and side is connected to grid side. Electromagnetic torque, rotor speed and rotor angle values are collected as output of DIFG. In Figure 3.6, Simulink block configuration would be seen as well as in Figure 3.7 DFIG parameters in which Table 3.2.

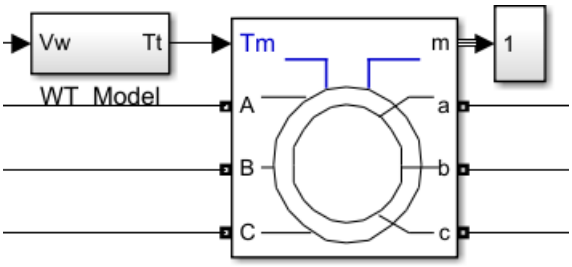

Figure 3.5. DFIG Simulink block

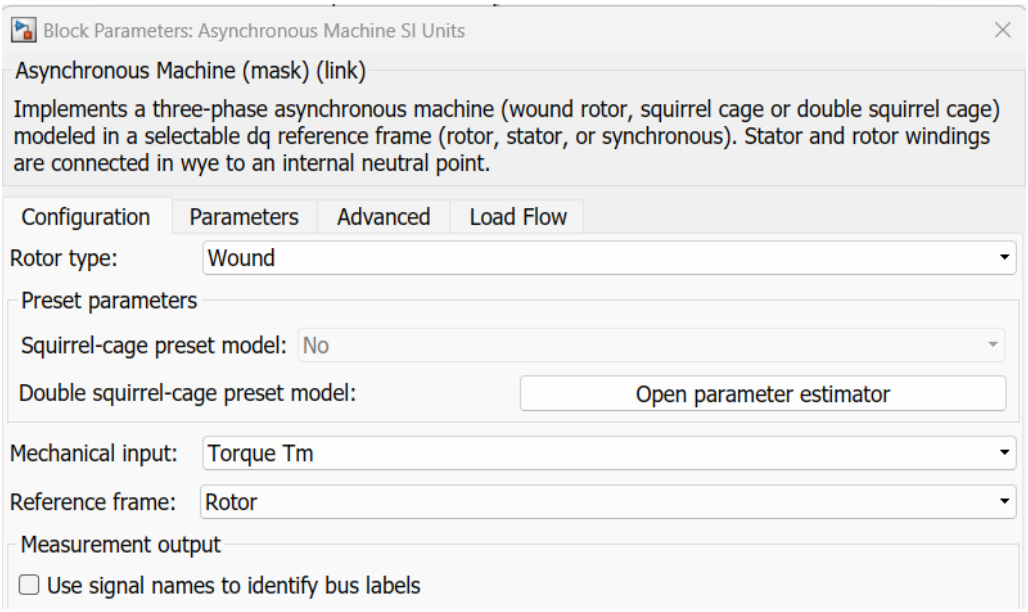

Figure 3.6. DFIG block configurations Simulink block

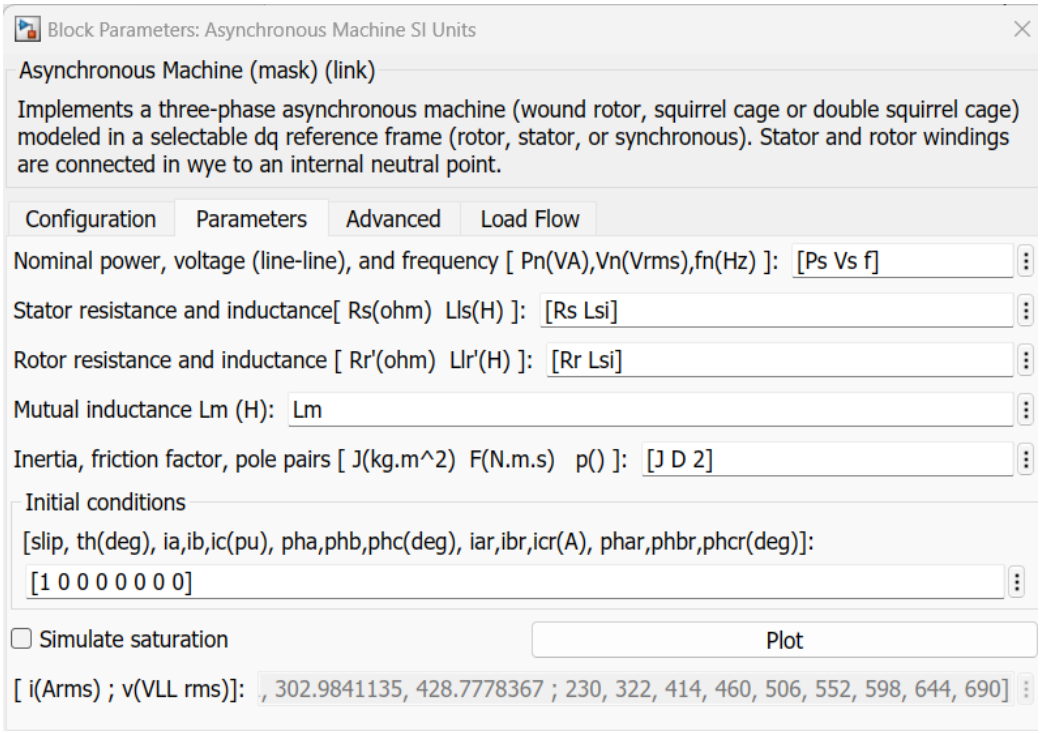

Figure 3.7. DFIG block parameters Simulink block

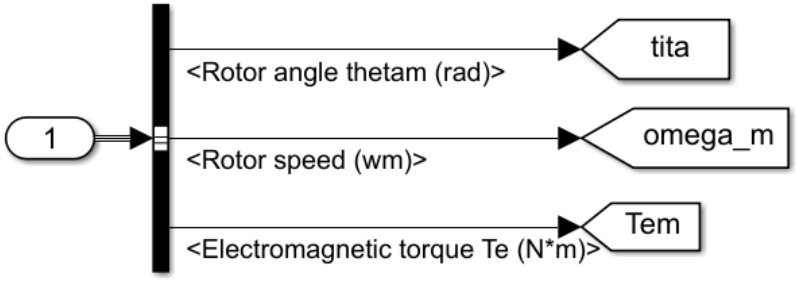

Figure 3.8. DFIG block measured variables

DFIG output variables can be seen in Figure 3.8. These variables particularly rotor angle and rotor speed would be input rotor controller. Electromagnetic torque value is crucial for this study to collect changes for effects on other systems.

3.3.3. DFIG Rotor and Grid Side Control Model in Simulink

The primary aim of the control mechanism is to effectively track and adhere to the trajectory that allows for the optimal extraction of power. Various approaches have been suggested in the literature to control wind turbines during partial load conditions in order to track the trajectory of maximum power extraction.

Two distinct types of controllers have been examined. The first type involves utilizing the electromagnetic torque reference derived from the maximum power curve for each value of turbine rotational speed. This approach capitalizes on the variable speed wind turbine inherent dynamic stability in the vicinity of this curve. The device in question is commonly referred to as the indirect speed controller.

The second controller determines the turbine's optimal rotational speed, which is directly related to the ideal tip speed ratio, for every wind speed value. This optimal rotational speed is then employed as the reference for the turbine's rotational speed. Subsequently, the turbine rotational speed is regulated by the utilization of a control mechanism. The device is commonly referred to as the direct speed controller.

In the MATLAB/Simulink model of the study, indirect speed controller method is chosen for extraction maximum power from system. The dynamic stability of the wind turbine can be demonstrated when considering any position along the maximum power curve depicted in Figure 3.2. This implies that when there is a deviation in rotational speed around a specific point within the maximum power curve, the wind turbine inherently returns to its designated operating position.

In Figure 3.9, DFIG connections with Rotor side and Grid side control blocks can be seen. At the rotor side, DFIG rotor windings are connected to a converter, and measurement block. Rotor controller block output is connected to rotor converter. Rotor controller block expect speed reference, rotor current and reference, stator voltage, rotor speed and angle as input for calculations. Output variable is passed a block to creation pulse signal for which the converter expects, “g” input pin.

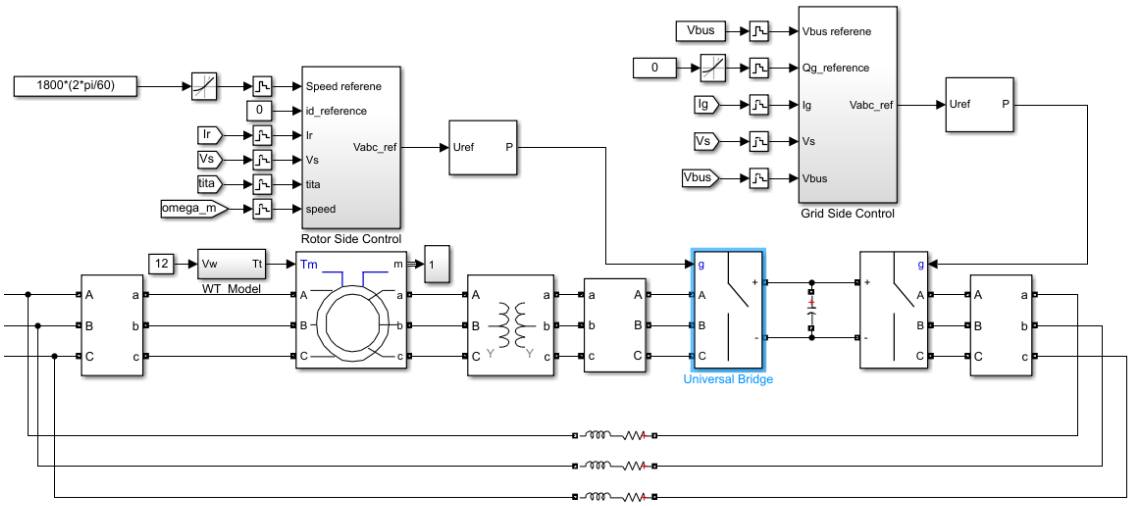

Figure 3.9. Rotor and grid side controller blocks connections

3.3.3.1. Rotor Side Converter Control Design

Rotor Side Converter Control is designed to optimize and maximize power while eliminating errors.

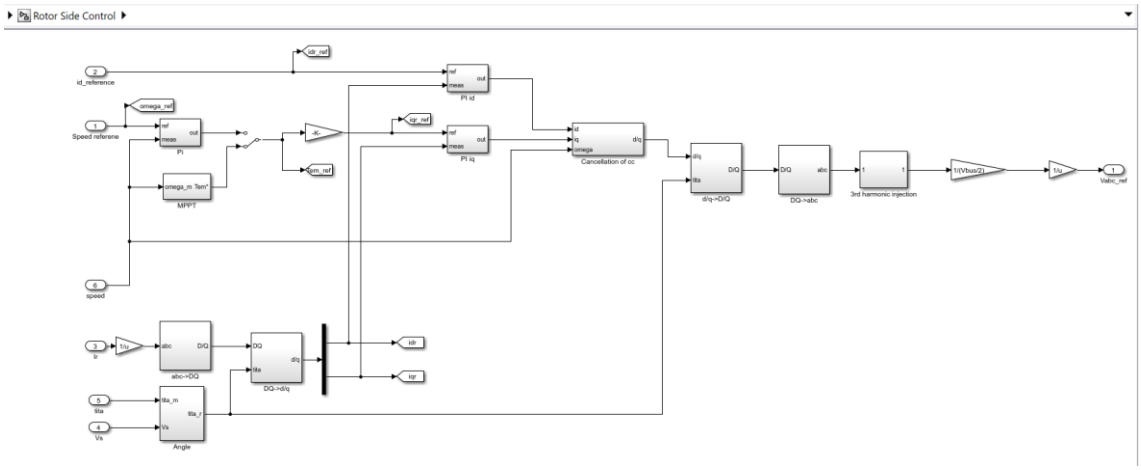

Figure 3.10. Rotor side controller blocks inside

In Figure 3.10, inside of rotor controller block can be seen. In the rotor controller, 3-phase inputs are transformed to 2-phase rotating frame DQ which or rotor side transformer. PI control blocks are established to improve the performance of rotor side converter controllers.

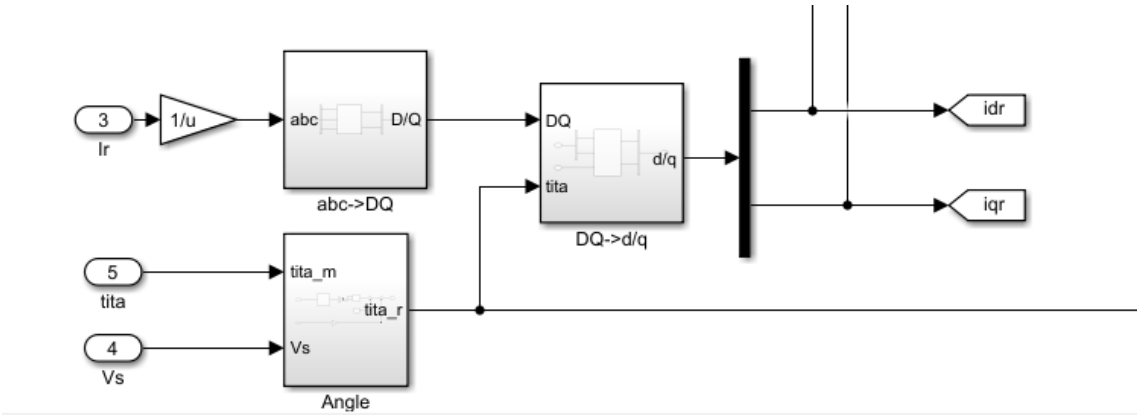

Figure 3.11. Rotor current DQ transformation blocks representing

Rotor current I_r which is input to controller; is 3-phase variable to be transferred to 2-phase reference frame. For that ABC->DQ block in Figure 3.11 is used to obtain i_{Dr} and i_{Qr}. From rotor angle "tita" input and stator voltage (3-phase) rotating frame angle can be obtained with "angle" conversation block in Figure 3.12, whose inside would be seen from Figure 3.13.

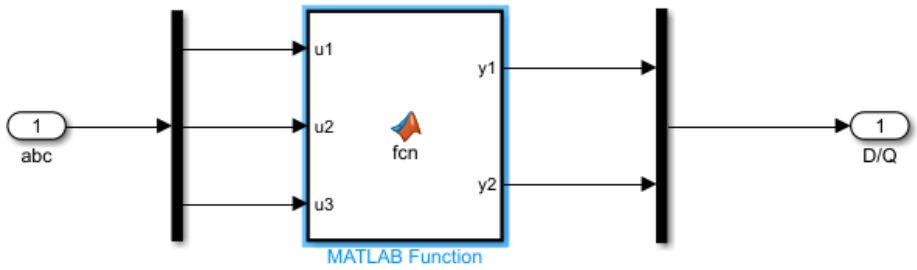

Figure 3.12. Angel conversation block inside representation

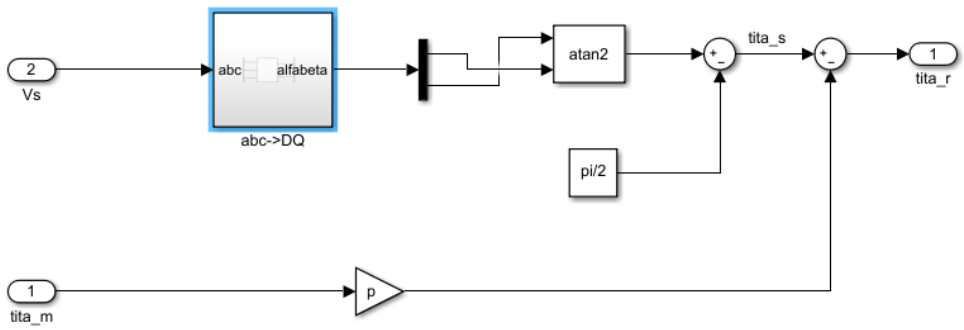

Figure 3.13. Angel conversation block inside representation

In order to obtain reference values of rotor current DQ parts, block definition can be seen from Figure 3.14. "i_{dr} reference "current value directly passed into controller as input; however, "i_{qr} refence" current value should be obtained by using electromagnetic torque which multiplied by a gain which expressing can be seen in Figure 3.15.

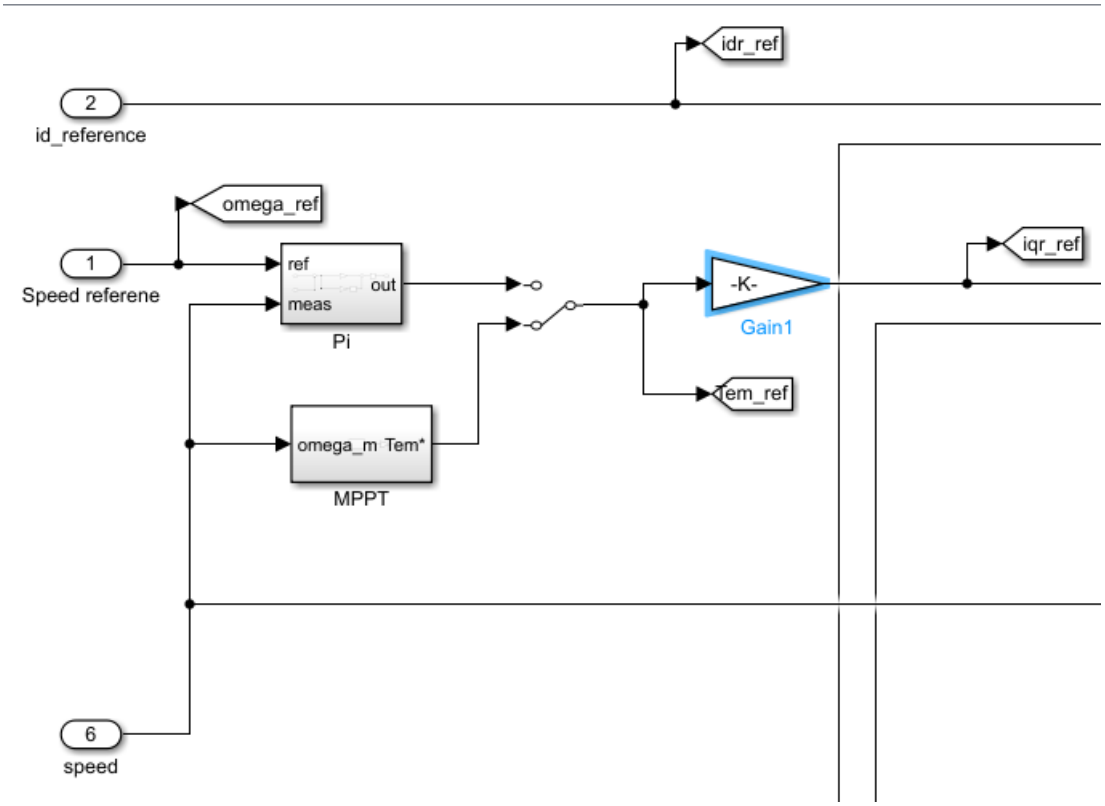

Figure 3.14. Reference rotor current DQ components derivation blocks

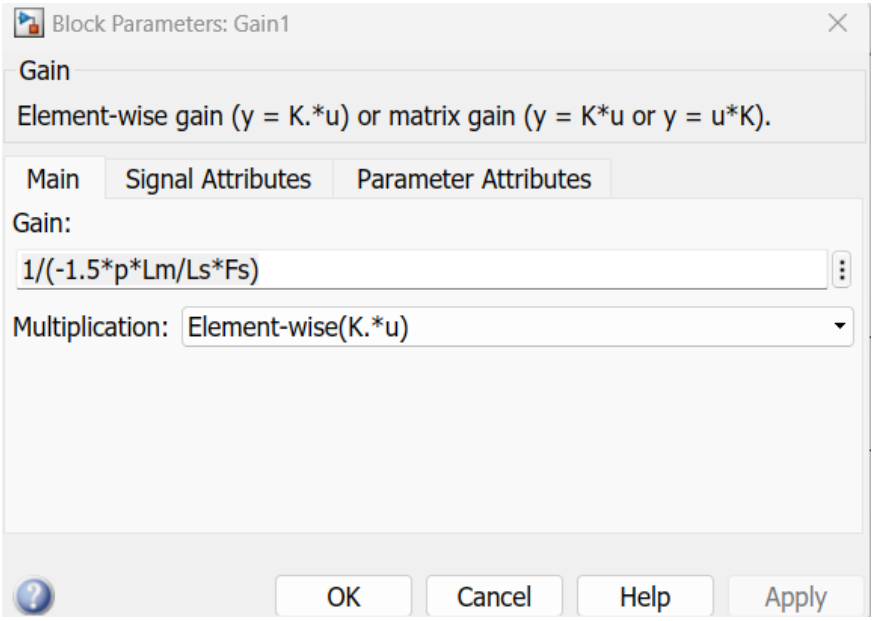

Figure 3.15. "K" gain block expression

Rotor side reference current's DQ components are important values for PI blocks in order to compare with actual rotor current DQ components. Hence, those all signals are passed into PI blocks separately to eliminate errors by applying PI control strategy, which is figured out with Figure 3.16.

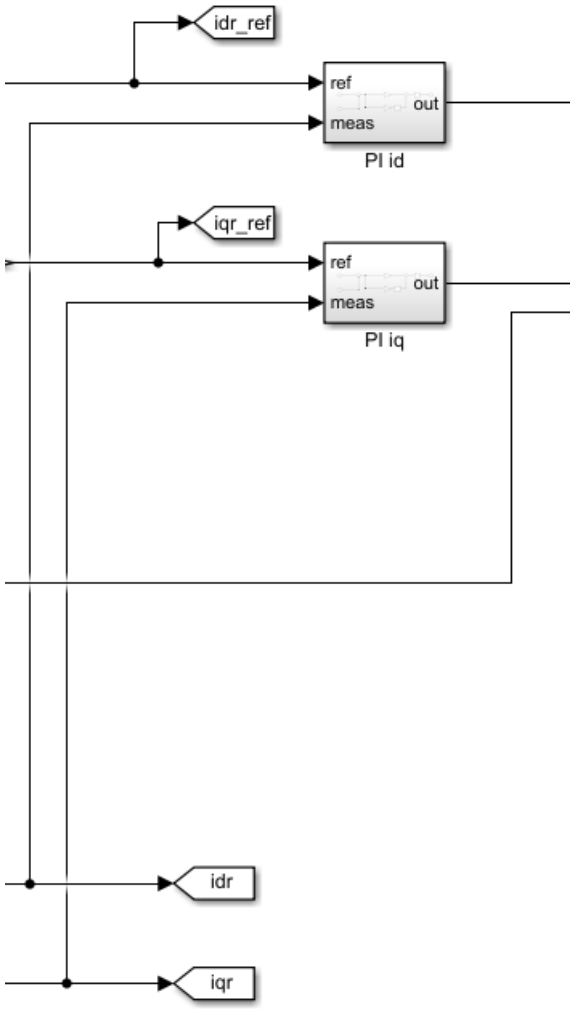

Figure 3.16. Input to PI blocks

The Proportional-Integral (PI) controller is a feedback controller that is extensively employed in industrial control systems. The system integrates both Proportional and Integral control modes in order to deliver control action that is tailored to meet the specific requirements of the process.

The Proportional control mode produces a control response that is directly proportionate to the present error value. The error can be defined as the inconsistency between a predetermined setpoint and the present value of the process variable. The

utilization of proportional control in isolation does not consistently result in the complete elimination of error, as it frequently leads to the presence of a steady-state error.

The Integral control mode is characterized by the accumulation of errors over a period of time, resulting in the generation of a control action that is determined by the summation of these accumulated errors. The purpose of its design is to mitigate the occurrence of steady-state error, which may arise when employing proportional control. The utilization of integral control in a system may result in the occurrence of overshoot and extended settling times if it is not adequately tuned.

The PI controller is a control mechanism that integrates the immediate reaction of proportional control with the error-correcting capability of integral control. In general, the process entails adjusting two variables, namely the proportional gain (Kp) and the integral gain (Ki). The parameters mentioned earlier are modified in order to attain the intended control response. In Figures 3.17, the parameters inside each PI block are presented individually. Both PI blocks have the same representation for each DQ component.

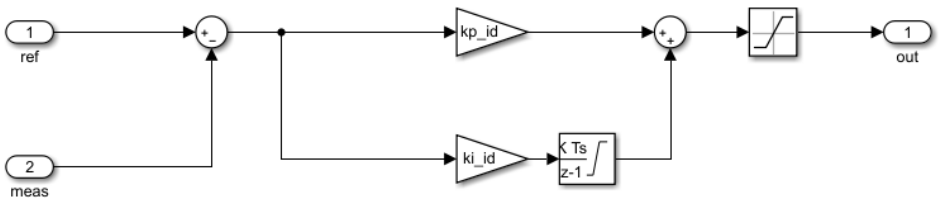

Figure 3.17. Rotor current “D” component and “Q” component PI block inside

Kp and Ki gain expressions can be obtained for both rotor current components as follows. Those expressions are written into initialization m-file and these values are passed to Kp and Ki gain blocks in Simulink:

```
kp_id=(2*wni*sigma*Lr)-Rr;
kp_iq=kp_id;
ki_id=(wni^2)*Lr*sigma;
ki_iq=ki_id;
kp_n=(2*wnn*J)/p;
ki_n=((wnn^2)*J)/p;
```

Therefore, in this study, Kp and Ki calculated by MATLAB as:

kp_id = 0.5771,

kp_iq = 0.5771,

ki_id = 491.5995,

ki_iq = 491.5995.

After regulation of current values with PI control blocks, there should be cancellation of terms which can be established with “Cancelation cc” blocks with expression can be seen from Figure 3.18. The output of this block would be alpha-beta voltage representation of rotor side.

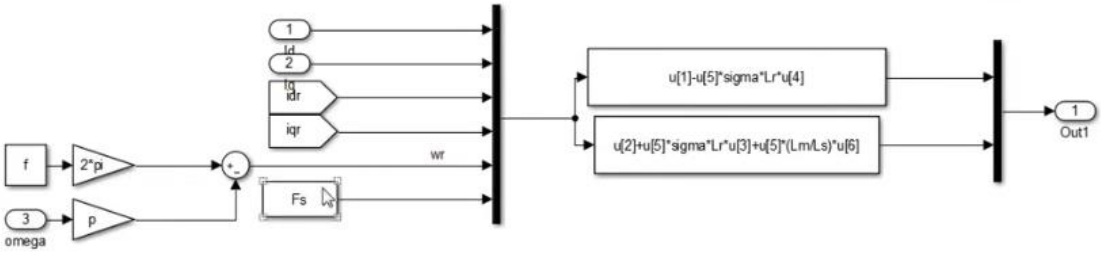

Figure 3.18. “Cancellation cc” block inside

When voltage components in dq frame are obtained there is need to inject rotor angle to obtain DQ representation of rotor voltage in 2-phase reference frame. For this alpha-beta->DQ conversation block can be used as shown in Figure 3.19. Finally, from 2-phase DQ frame, it would be beneficial to transfer 3-phase reference frame for outputs of rotor side converter control. This can be achieved by adding another block which models the transformation from DQ frame to 3-phase reference frame. In Figure 3.20, this block can be seen with its 3rd harmonics injection block representation. As a result, output of rotor side voltage in 3-phase can be obtained with whole models in Figure 3.10.

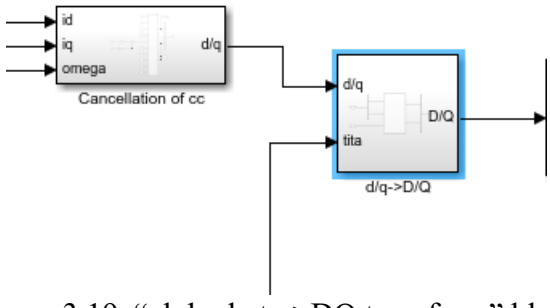

Figure 3.19. “alpha-beta->DQ transform” block

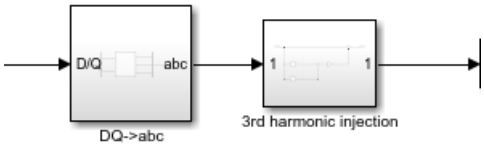

Figure 3.20. “DQ->3-phase frame transform block with 3rd harmonic injection block

3.3.3.2. Grid Side Converter Control Design

Grid Side Converter Control is designed to optimize and maximize power while eliminating failures effects on grid side. In Figure 3.21, connections of Grid Side Controller block can be seen. Inputs are bus voltage and its reference, reactance power refence, grid current in 3-phase and stator voltage in 3-phase. After control block, voltage of stator side in 3-phase again obtains to be passed into grid side converter with pulse signal.

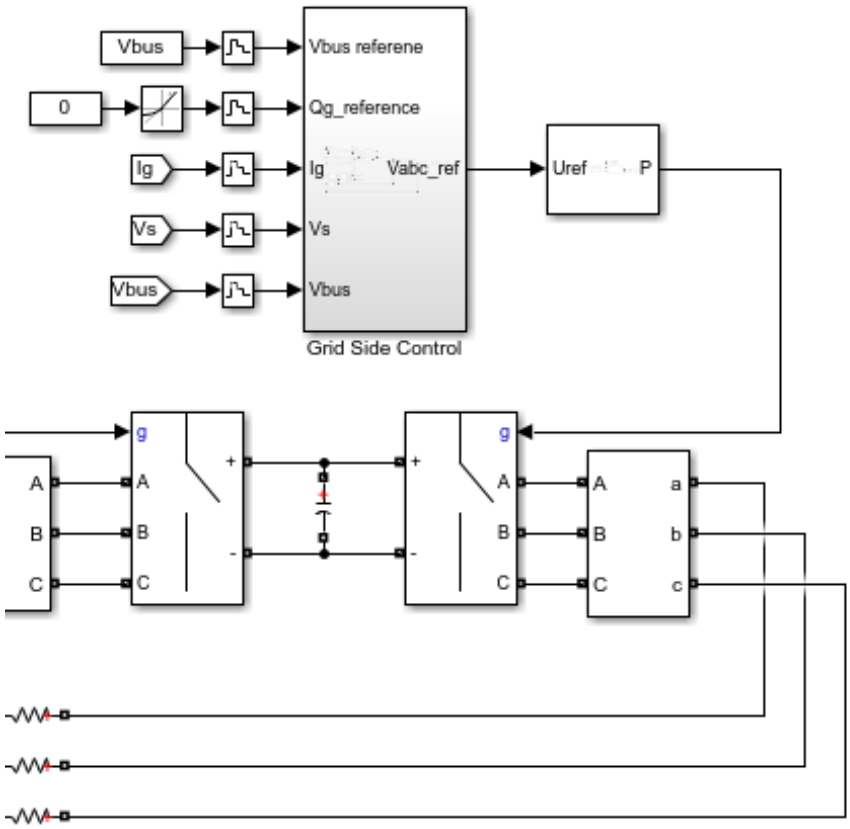

.

Figure 3.21. Grid side converter control block connections

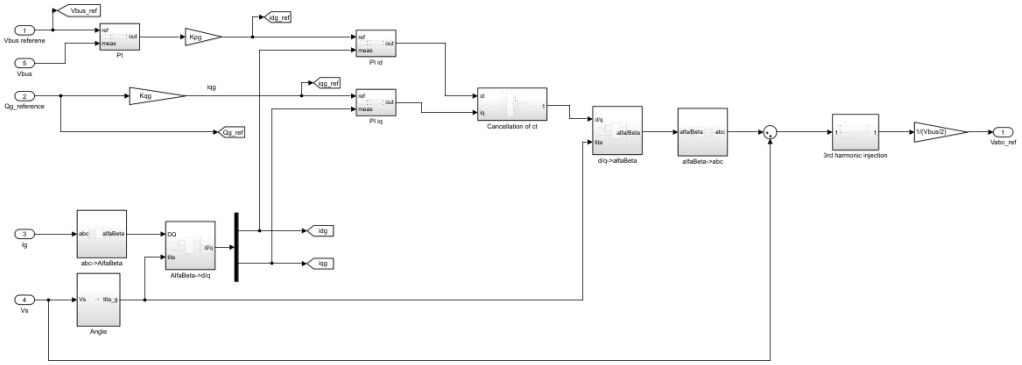

Figure 3.22. Grid side converter control block inside

In Figure 3.22, grid side converter control system can be seen. It is similar to Rotor side converter control system as comparing actual current values and references to obtain stator voltage 3-phase signals as pulse to input into grid side converter.

3.3.4. DFIG Wind Turbine Power System Model in Simulink

In previous sections, it is mentioned to established DFIG machine and control mechanism for convert of both rotor and stator side. In this part, wind turbine connection to grid with modeling transformers, cables, loads etc. Complete modeling of DFIG wind turbine in Simulink can be seen in Figure 3.23.

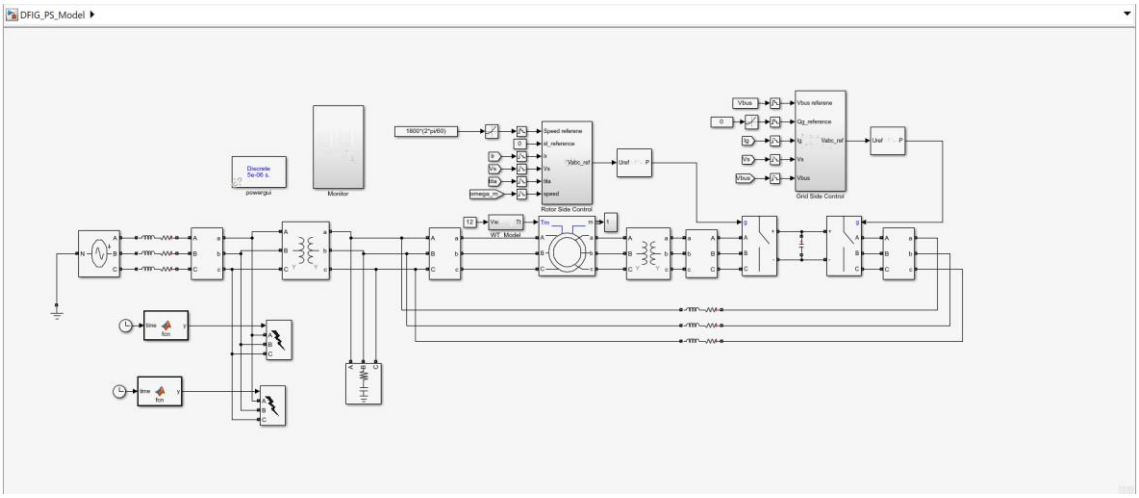

Figure 3.23. Complete modeling of DFIG wind turbine

DFIG stator side connected to a measurement block to get Vs and Is, where stator 3-phase voltage and current values are measured from directly output of DFIG block.

A transformer block is connected to stator side of DFIG machine for set-up process. This transformers configuration can be seen in Figure 3.24 and parameters can be seen in Figure 3.25. Both side of transformer connected as star connection to obtain in the left and side 25kV while right hand side is 690V. Between transformer and DFIG, an RLC load is defined. It is assigned as constant Z load with resistive 1kW load. This block is presented in Figure 3.26.

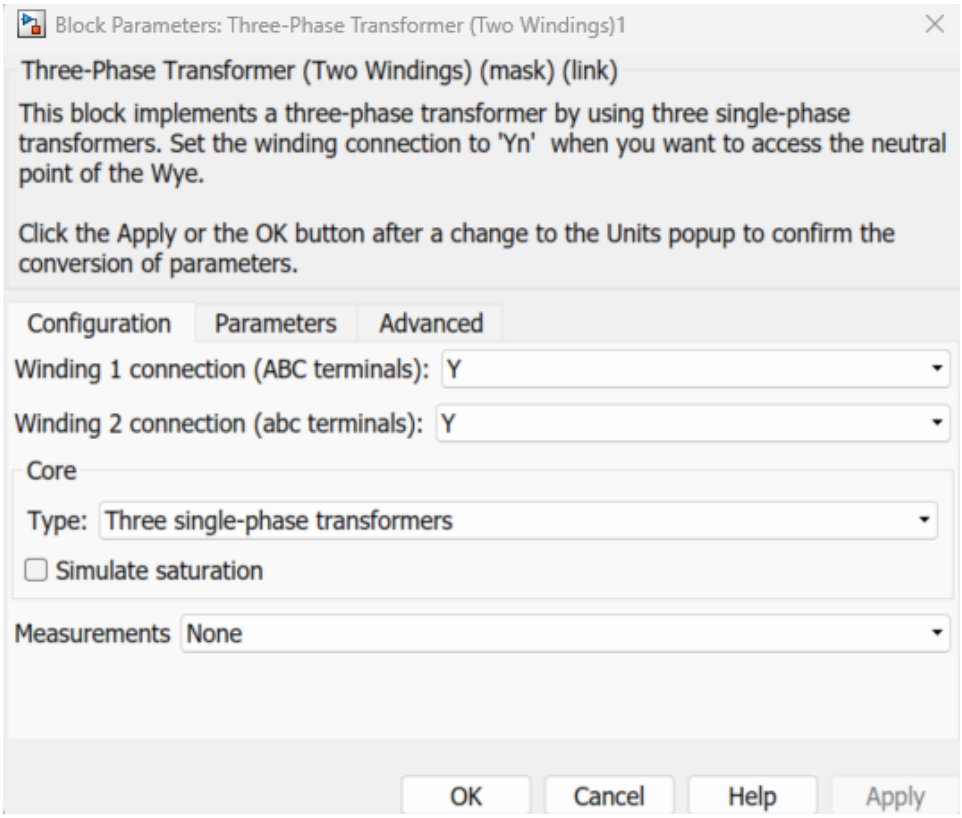

Figure 3.24. Step-up transformer configuration

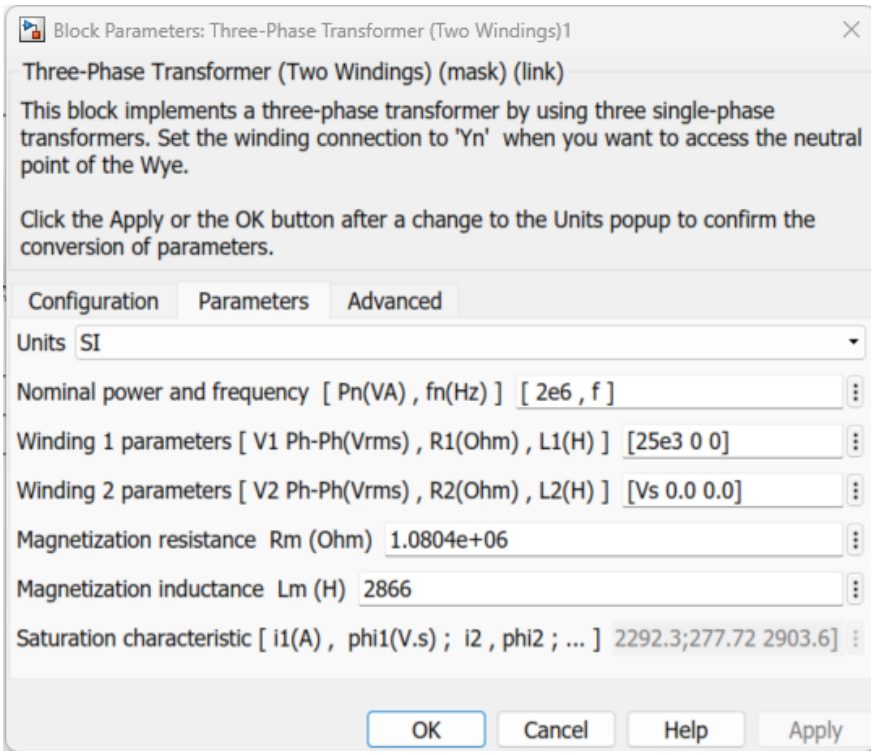

Figure 3.25. Step-up transformer defined parameters

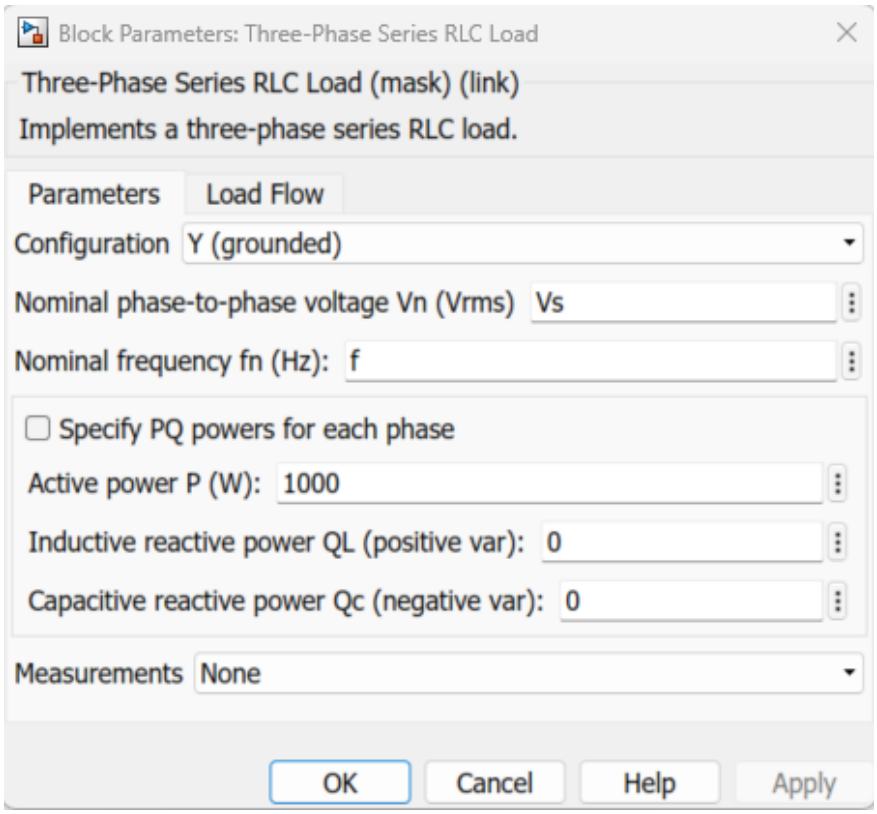

Figure 3.26. RLC load defined parameters

In order to represent grid, a three-phase programmable voltage source is connected to high side of transformer with R and L connections to represent transmit cables. Configuration of this block can be seen from Figure 3.27.

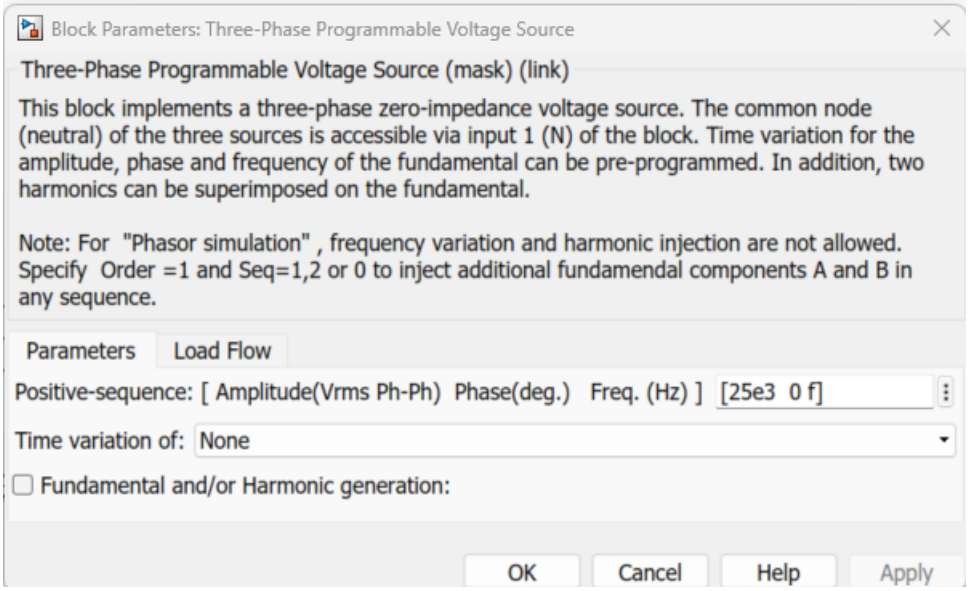

Figure 3.27. Three-phase voltage source as grid configuration

In the model, in order to represent failures in the transmission line there are three-phase fault blocks. This blocks are controlled via timer to represent the fault at a certain time and duration. These blocks configuration can be changed according to fault level on Vs.

3.4. DTU 10MW Wind Turbine HAWC2 Model

The model is derived from the virtual DTU 10-MW reference wind turbine, which was developed as a component of the Light Rotor project. This project is a joint effort between the Wind Energy Department at the Technical University of Denmark and Vestas. DTU 10MW HAWC2 model visualization can be seen in Figure 3.28.

The DTU 10MW wind turbine aims to develop a comprehensive design process that incorporates advanced airfoil design, considering both aerodynamic and structural goals and limitations. It also includes optimizing the blade through aero-servo-elastic techniques, utilizing high-precision 3D simulation tools like CFD and FEM, and employing structural topology optimization. Model's technical details can be seen from Table 3.2.

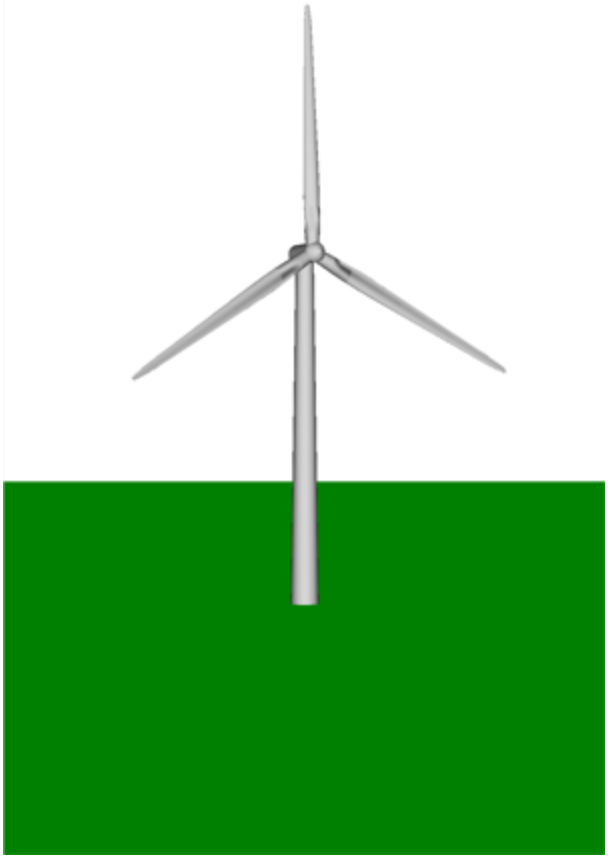

Figure 3.28. HAWC2 DTU 10MW visualization

Table 3.2. DTU 10MW wind turbine model technical details

Description	**Value**
Rating	10MW
Rotor orientation, configuration	Upwind, 3 blades
Control	Variable speed, collective pitch
Drivetrain	Medium speed, Multiple stage gearbox
Rotor, Hub diameter	178.3m, 5.6m
Hub height	119m
Cut-in, Rated, Cut-out wind speed	4m/s, 11.4m/s, 25m/s
Cut-in, Rated rotor speed	6RPM, 9.6RPM
Rated tip speed	90m/s
Overhang, Shaft tilt, Pre-cone	7.07m, 5°, 2.5°
Pre-bend	3m
Rotor mass	229tons (each blade ~41tons)
Nacelle mass	446tons
Tower mass	605tons

In the field of wind energy, the DTU 10MW wind turbine model is widely used for many purposes. For example, it is utilized together with the DTU Wind Energy controller in the HAWC2 aeroelastic program (Dimitrov et al. 2018). Furthermore, wake-flow response and behavior of the DTU 10MW wind turbine model have been investigated in wind tunnel experiments (Fontanella, Zasso, and Belloli 2022).

Additionally, it has been used in machine learning and load estimation research; for the DTU 10MW wind turbine, an artificial neural network (ANN) load model was created (Xu, Yu, and Kim 2022). Additionally, for aeroelastic load simulations and analysis, the DTU 10MW wind turbine model has been incorporated into aero-servo-elastic algorithms like HAWC2 (Papi et al. 2022).

The primary purpose of the DTU Wind Energy controller is to operate pitch-regulated, variable speed wind turbines. The controller possesses the ability to operate at both partial and full load and is equipped with switching mechanisms that provide seamless transition between these two modes of operation.

The partial and full load controllers utilize classical proportional-integral control theory. They also incorporate additional features, including a drivetrain and tower damper, a rotor speed exclusion zone, and a notch filter that reduces the impact of rotor speed-dependent variations in the feedback. The controller depends on the speed of the generator as its main source of feedback. Furthermore, the reference generator power serves as a feedback parameter to facilitate the transition between partial and full load operation. A wind speed measurement that has been filtered to remove high-frequency components can be optionally utilized to determine the minimum blade pitch required for partial load operation. The controller utilizes the combined blade pitch angle and electromagnetic generator torque to regulate the wind turbine. During full load operation, the proportional-integral controller adjusts its gains based on the feedback term from the collective blade pitch angle. This is done to compensate for the varying dynamics of the wind turbine at different wind speeds.

The DTU 10MW wind turbine model is widely recognized as a crucial point of reference in various research domains, encompassing aerodynamics, aeroelasticity, structural engineering, control systems, and design optimization, specifically within the wind energy sector. The extensive acceptance and application of this technology in diverse research industries highlights its importance as a standard for evaluating and progressing wind turbine technology.

3.4.1 HAWC2 Model Output

Pdap, short for Python Data Analysis Program, is software designed for the purpose of processing, analyzing, visualizing, and presenting data, such as simulation

results and measurements. Its scope encompasses wind turbines; however, it is not exclusively confined to them. The software integrates a user-friendly graphical interface with python scripting, enabling the automation and execution of personalized functions.

For this study, tower, generator, and shafts graphics are examined among many graphical output. According to coordinate system shown in APPENDIX E, tower top moments which are the moments on tower yaw bearing are in y-axis; shaft moment which are the main shaft bearing moments are in z-axis. Moreover, tower axial and transversal deflection plots are crucial to examine mechanical system response.

CHAPTER 4
SIMULATION RESULTS

4.1. Simulink Model Run

Simulation Model run plan can be found in the following table. In Table 4.1, each simulation session the output of the simulations is defined.

Table 4.1. Simulation Plan

	Low Voltage Fault 1 Phase to Ground	**Low Voltage Fault 3 Phase to Ground**	**Simulink Plots for Voltage, Current, Power and Electromagnetic Torque**	**Description**
Scenario 1	No	No	Yes	MATLAB/Simulink Model Verification
Scenario 2	Yes	No	Yes	1-phase to ground fault at Vgrid*1.0
Scenario 3	Yes	No	Yes	1-phase to ground fault at Vgrid*0.5
Scenario 4	Yes	No	Yes	1-phase to ground fault at Vgrid*0.1
Scenario 5	No	Yes	Yes	3-phase to ground fault at Vgrid*1.0
Scenario 6	No	Yes	Yes	3-phase to ground fault at Vgrid*0.5
Scenario 7	No	Yes	Yes	3-phase to ground fault at Vgrid*0.1
Scenario 8	Yes	Yes	Yes	1-phase to ground and 3-phase to ground fault at Vgrid*1.0

4.1.1. Running Simulations of Power System Model:

Simulink model is run without any fault generation on the steady state form to verify DFIG, rotor and stator controls and power system designs. In Simulink simulation environment, discrete simulation time with 5e-06 s is selected and simulations are run for 10 secs.

4.1.1.1. Scenario 1 – Simulink Model Verification

From Table 4.1, Scenario 1 is run in Simulink. Grid side converter control parameters, rotor side converter control parameters, power analysis and grid side medium voltage analysis report are presented.

In Figure 4.1, active power values are graphically presented. According to model, active power values are expected to be 2MW, and in Figure 4.1, model without any fault introduction is reaching rated value. After 4.5 secs, active power value is reaching to rated value. In Figure 4.2, electromagnetic torque measurement is presented.

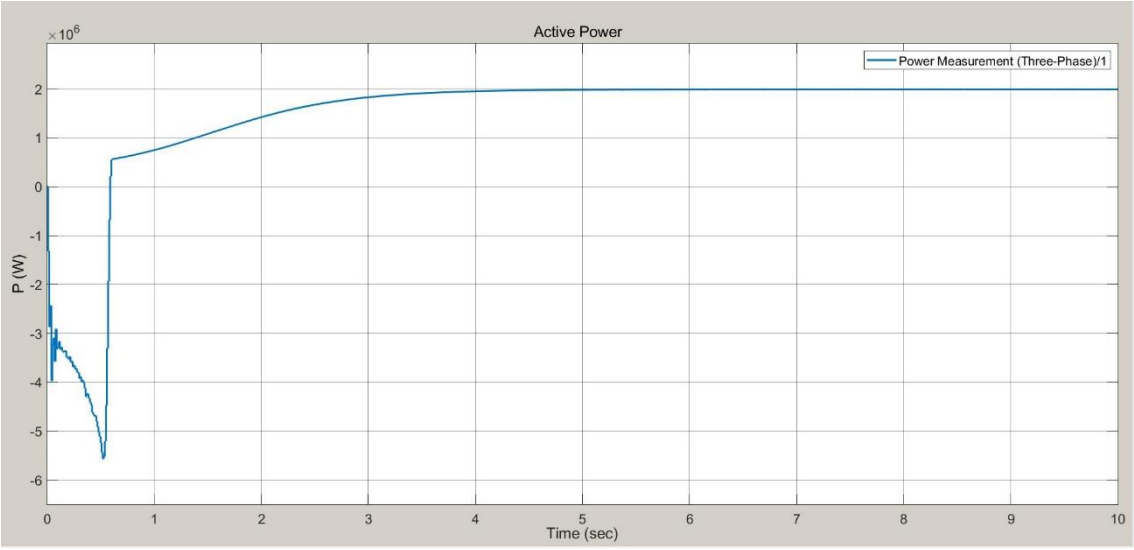

Figure 4.1. Active power measurement in graphical form during scenario 1

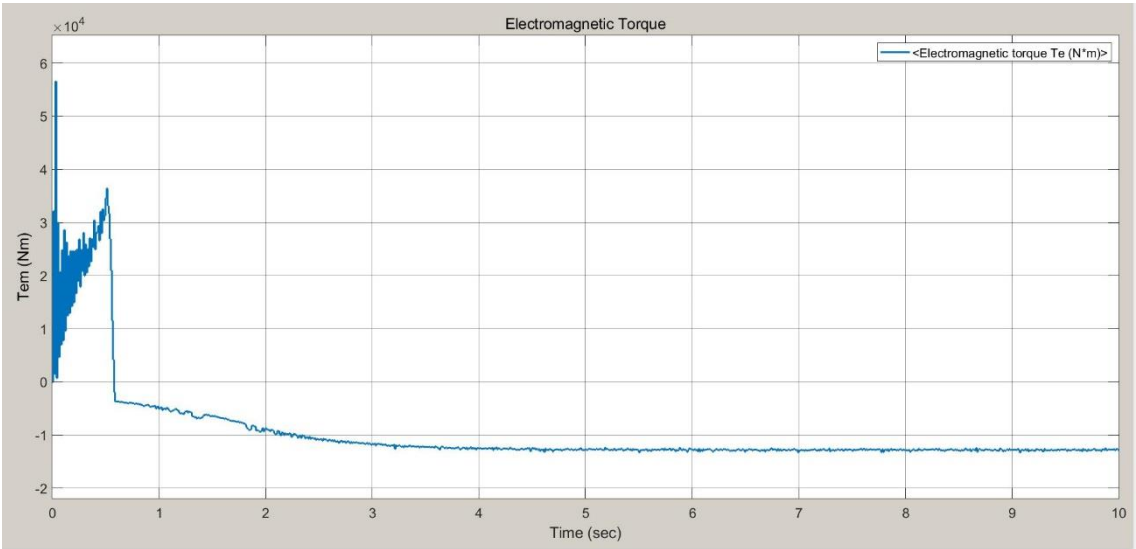

Figure 4.2. Electromagnetic torque measurement in graphical form during scenario 1

In Figure 4.3, rotor side converter measured values are graphically presented for rotor speed, around 200 rad/s is measured at steady state during the simulation.

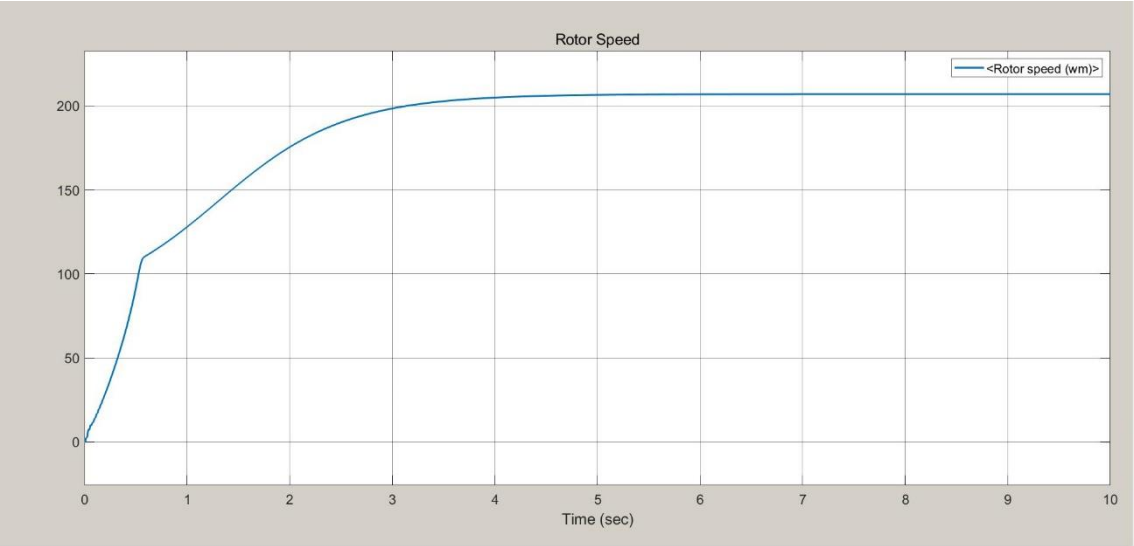

Figure 4.3. Rotor side measurements in graphical form during scenario 1

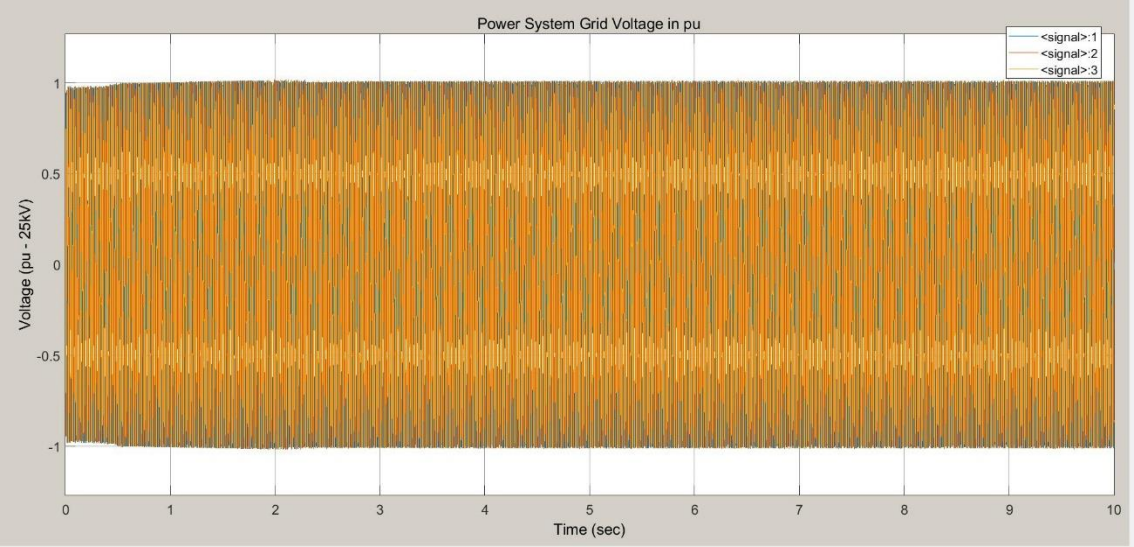

Figure 4.4. Grid voltage measurement in graphical form during scenario 1 – (p.u.)

Figure 4.4 shows medium voltage (25kV) side voltage three-phase measurements. Voltage measurement in per unit (p.u.) form.

According to result obtained in Scenario 1, it was used to verify DFIG design by comparing it with (Abad et al. 2011). Rotor side converter and grid side converter control outputs namely, rotor current, voltage values in d and q forms, rotor speed form, stator voltage, active power values are compared with graphics shown in the 2MW DFIG Wind Turbine design part. APPENDIX F shows whole graphics used for verification.

4.1.1.2. Scenario 2

One-Phase to ground fault would be represented. At t=6 sec, for 400ms, one-phase to ground fault is applied.

Power and Electromagnetic Torque measurements would be examined. In Figure 4.5, Scenario 2 measured values can be seen, P for Active power, and Tem, electromagnetic torque.

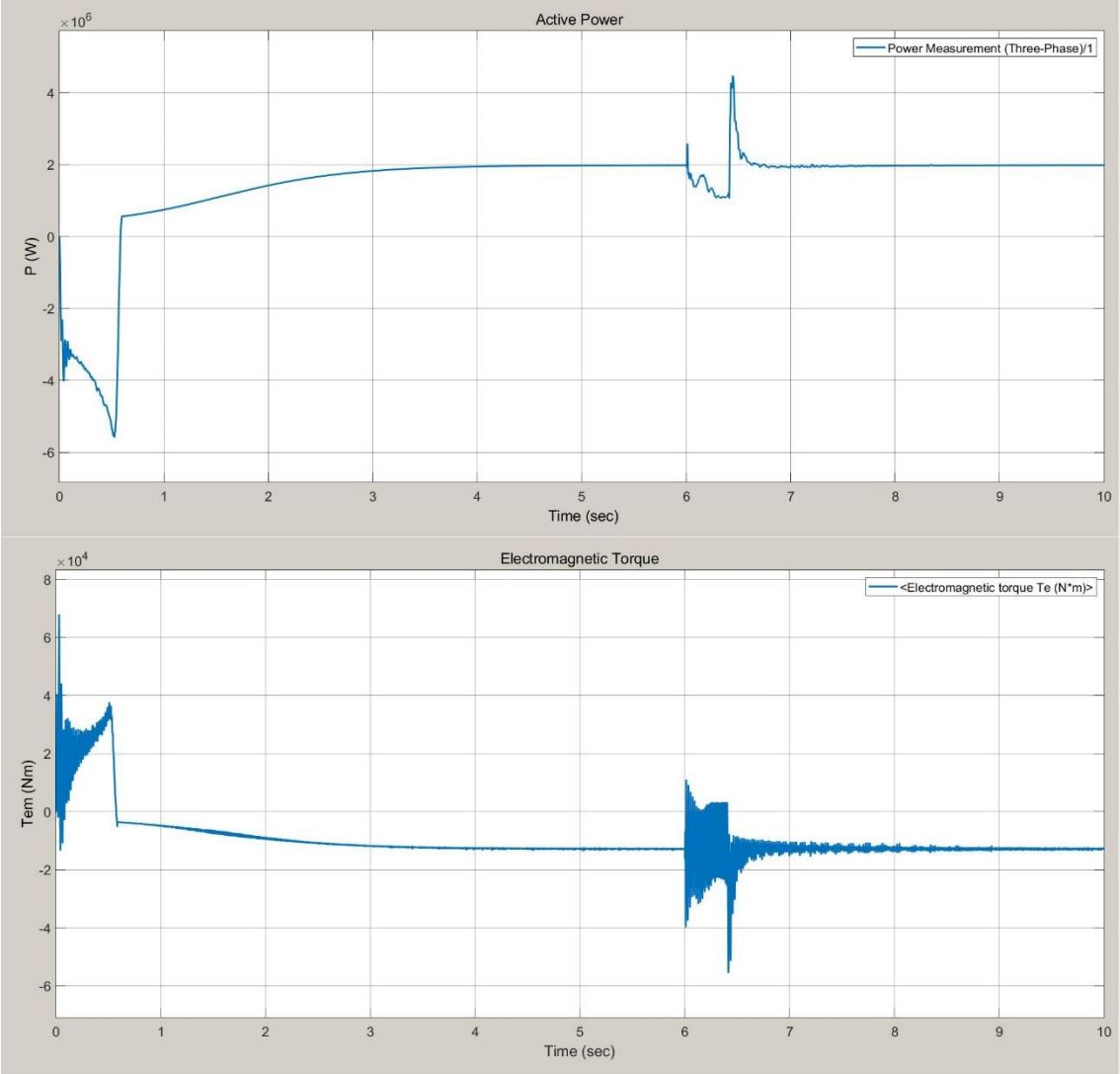

Figure 4.5. Scenario 2 active power and electromagnetic torque analysis

In Figure 4.6, Vgrid plot shows the grid voltage in three phase and one phase to ground fault clearly seen at T=6sec. Furthermore, in the P plot, active power is dropped around its 50% of peak value. Electromagnetic torque values fluctuate during one-phase to ground fault.

After fault is clear from system, Active power is going higher values than nominal power rates for a while and couple of seconds takes to settle down again 2MW level.

Grounded phase is connected again, however for a while signals of that phase have disturbance. It takes long time for T_{em} to be settle down, fluctuation is continued until end of simulation.

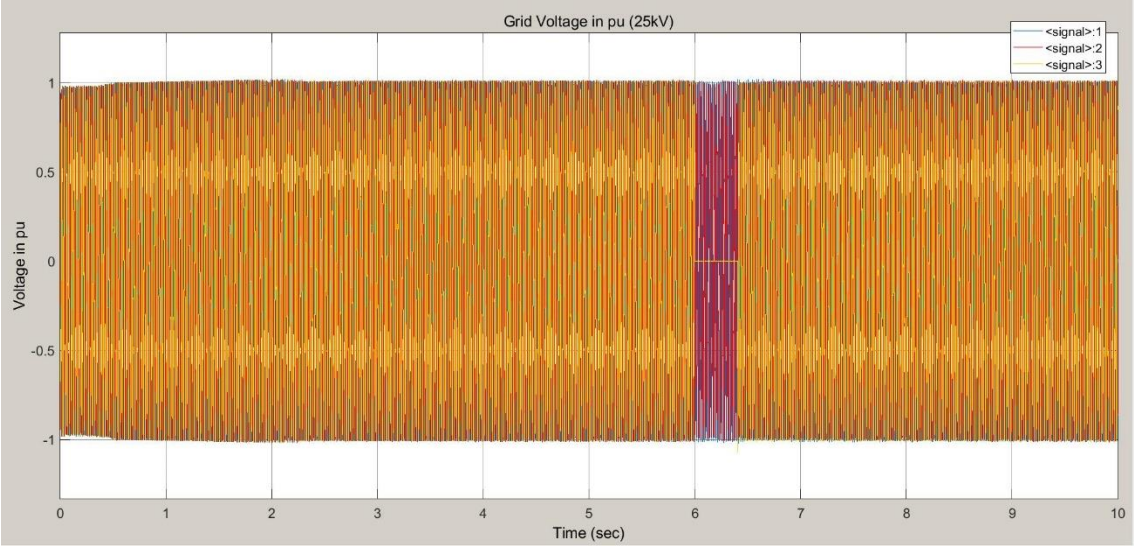

Figure 4.6. Grid voltage in three-phase

4.1.1.3. Scenario 3

One-Phase to ground fault would be represented while V_{grid}*0.5. At t=6 sec, for 400ms, one-phase to ground fault is applied.

Power and Electromagnetic Torque measurements would be examined. In Figure 4.7, Scenario 3 measured values can be seen, P for Active power and Tem, electromagnetic torque.

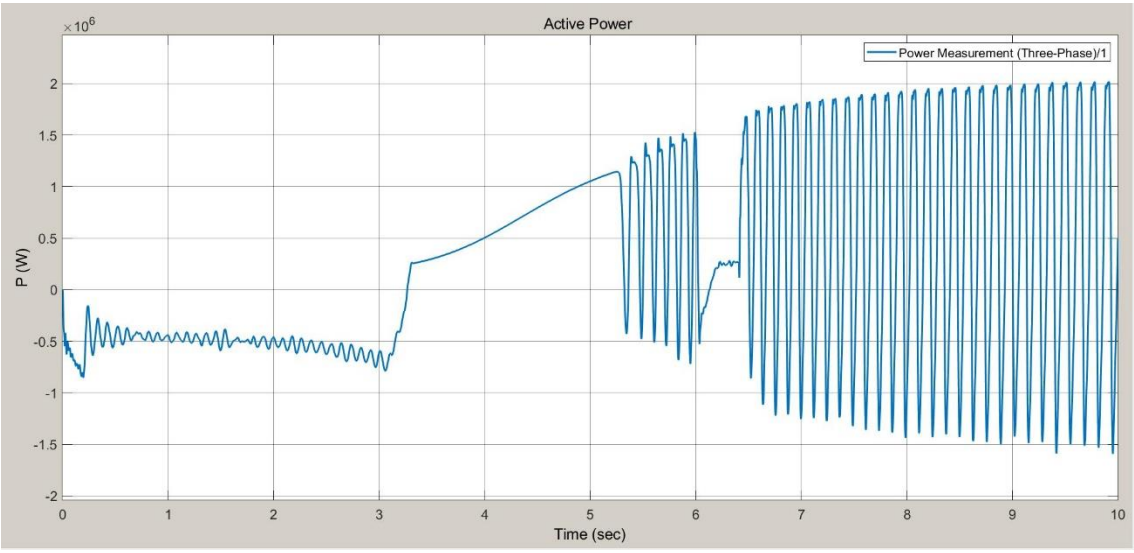

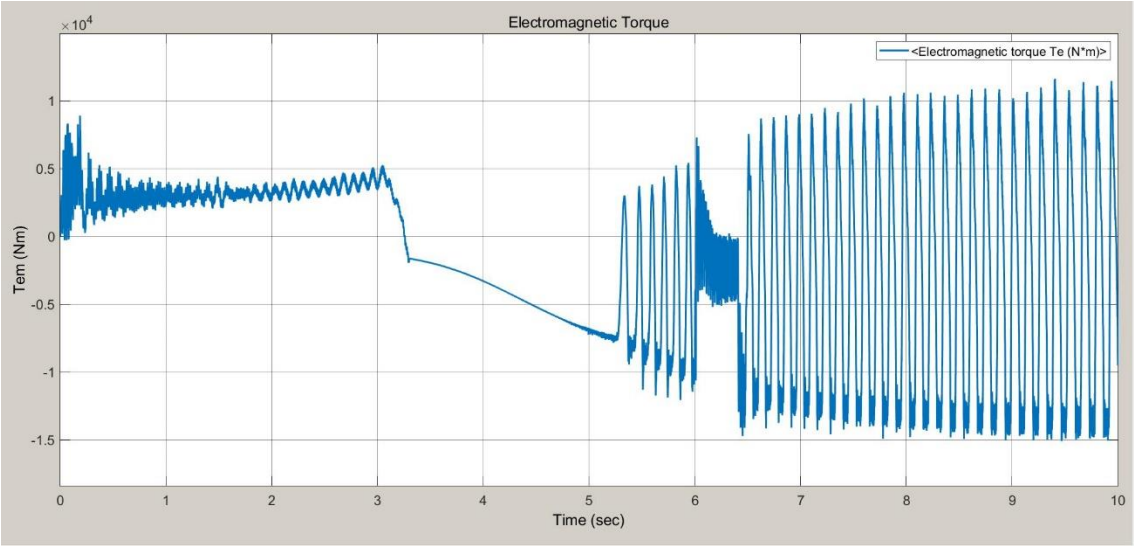

Figure 4.7. Scenario 3 power, electromagnetic torque analysis

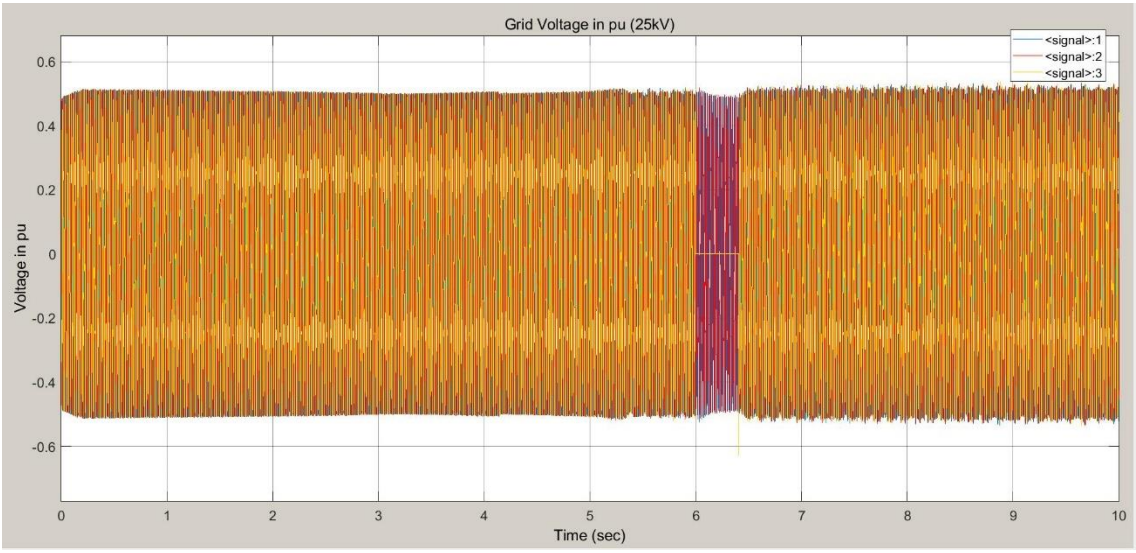

Figure 4.8. Grid voltage in three-phase for scenario 3

In Figure 4.8, since grid voltage is at its 50% value nominal power generation could not be achieved until fault, Furthermore, in the P plot, active power is dropped dramatically during fault. At V_{grid} plot, one phase to ground can be seen. Electromagnetic torque values fluctuate during one-phase to ground fault.

After fault is clear from system, Active power is going higher towards to nominal values but there is fluctuation at its. Grounded phase is connected again, however for a while signals of that phase have disturbance. T_{em} is not to be settled down; fluctuation is continued until end of simulation.

4.1.1.4. Scenario 4

One-Phase to ground fault would be represented while V_{grid}*0.1. At t=6 sec, for 400ms, one-phase to ground fault is applied.

Power and Grid Voltage would be examined. In Figure 4.9, Scenario 4 measured values can be seen, P for Active power, and T_{em}, electromagnetic torque.

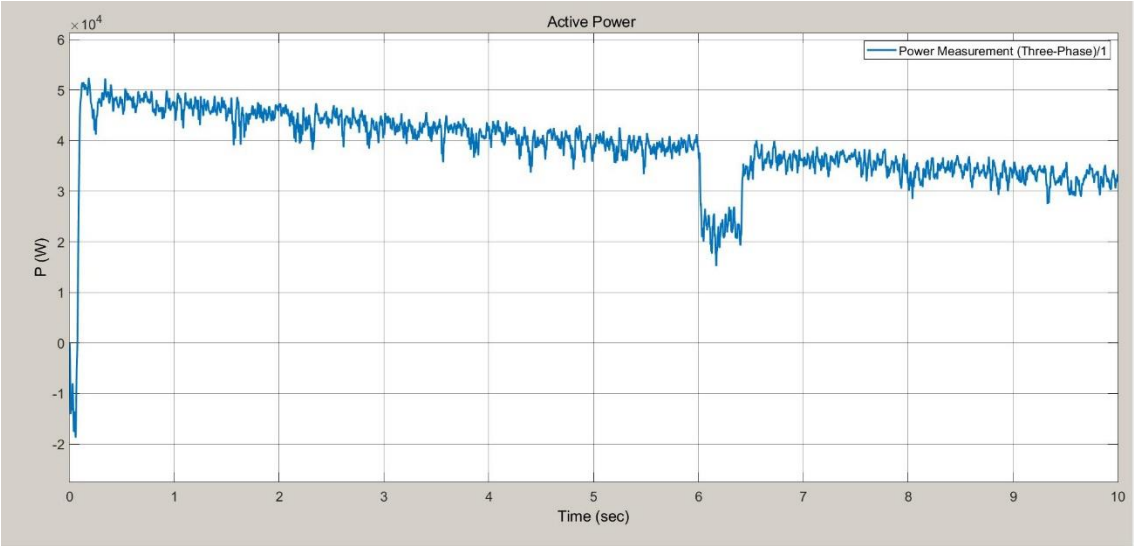

cont. on next page

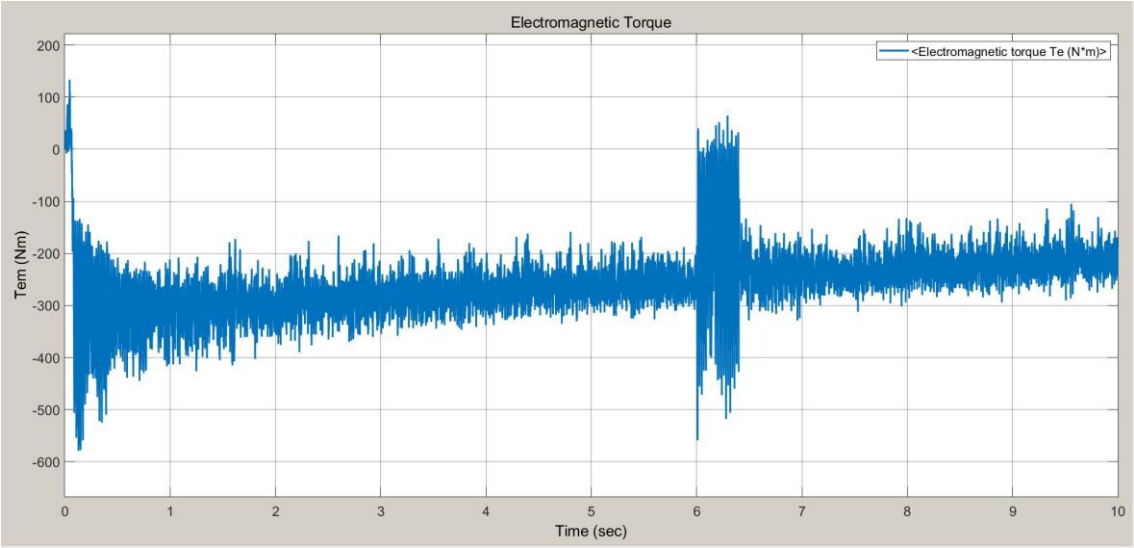

Figure 4.9. Scenario 4 power and electromagnetic torque

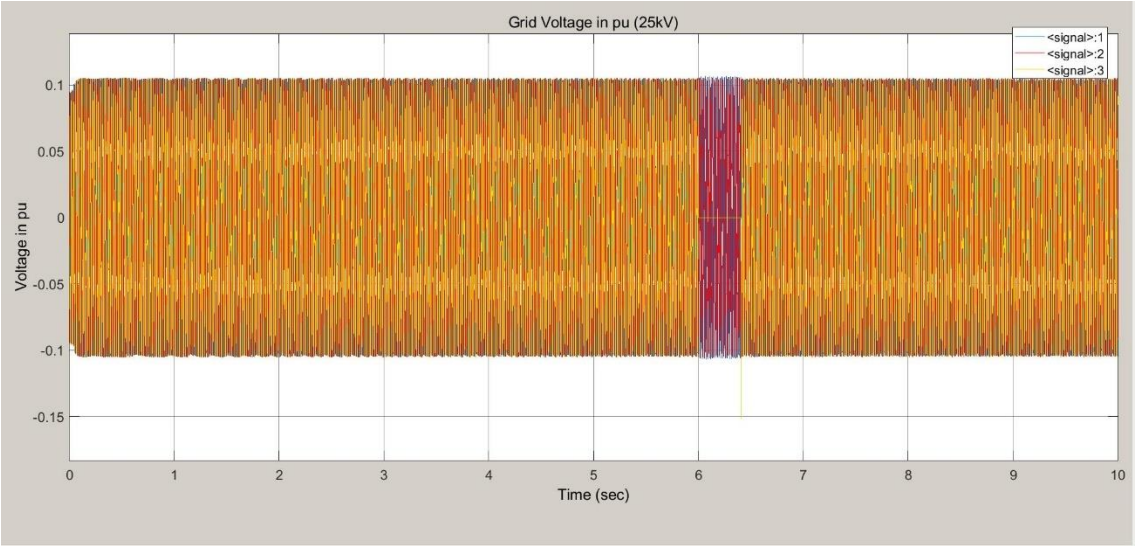

Figure 4.10. Scenario 4 grid voltage analysis during fault

In Figure 4.10, since grid voltage is at its 10% value nominal power generation could not be achieved until fault, Furthermore, in the P plot, active power is dropped dramatically during fault. At V_{grid} plot, one phase to ground can be seen. Electromagnetic torque values fluctuate during one-phase to ground fault.

After fault is clear from system, Active power is going higher towards to nominal values but there is fluctuation at its. Grounded phase is connected again, however for a while signals of that phase have disturbance. T_{em} is not to be settled down; fluctuation is continued until end of simulation.

4.1.1.5. Scenario 5

Three-Phase to ground fault would be represented while Vgrid at 1p.u. At t=6 sec, for 400ms, three-phase to ground fault is applied.

Power and Grid Voltage would be examined. In Figure 4.11, Scenario 5 measured values can be seen, P for Active power, and T_{em}, electromagnetic torque. P plot shows that active power status during fault active. Three-phase faults effects can be seen obviously more harmful than one-phase fault. Active power dropped to “0” values during fault. During fault electromagnetic toque touches extreme. When the fault is cleared, peak values are very high with respect to one-phase fault results. Voltage forms drop to zero in all phases as expected as seen in Figure 4.12. points.

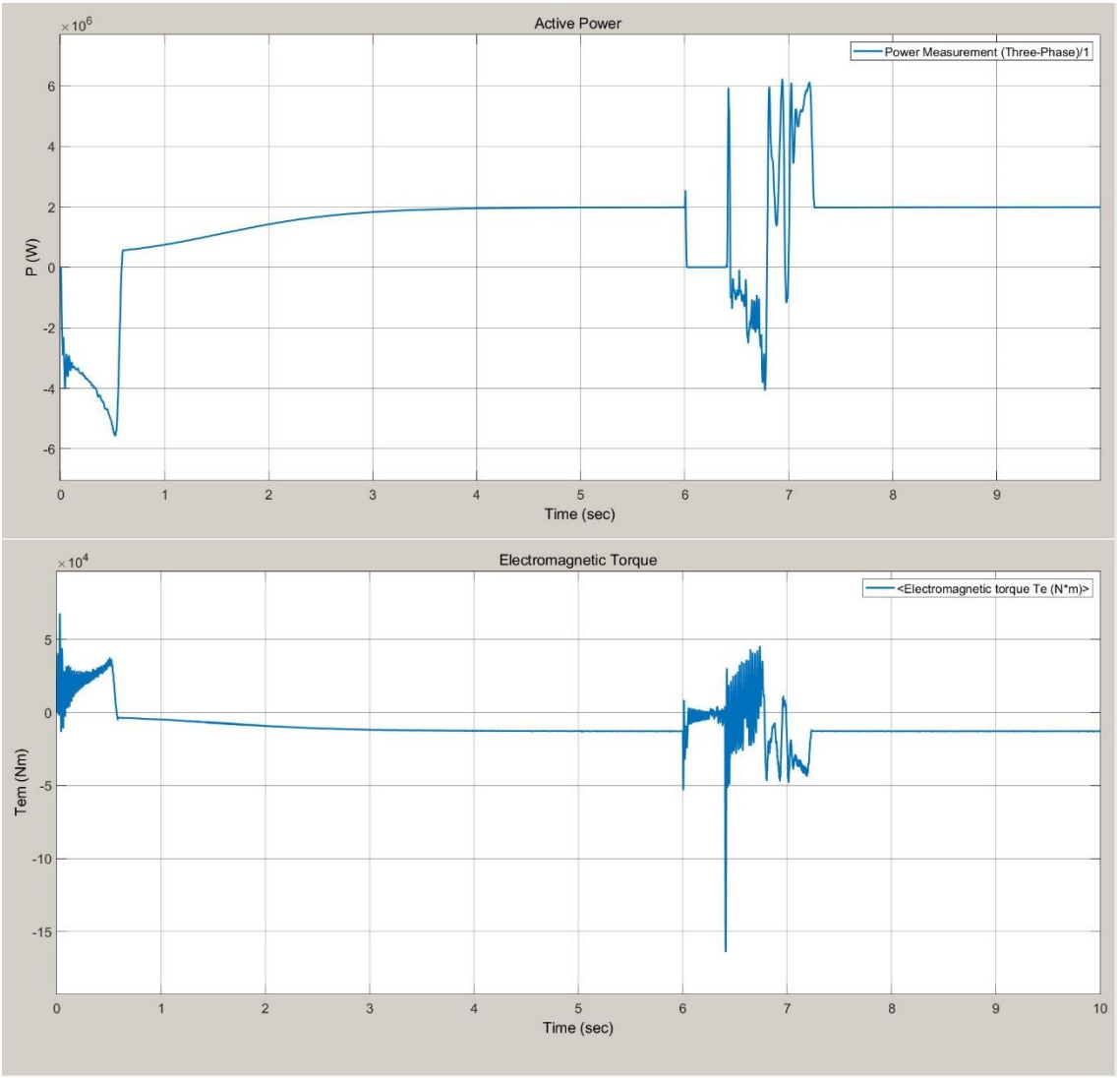

Figure 4.11. Scenario 5 power, electromagnetic torque

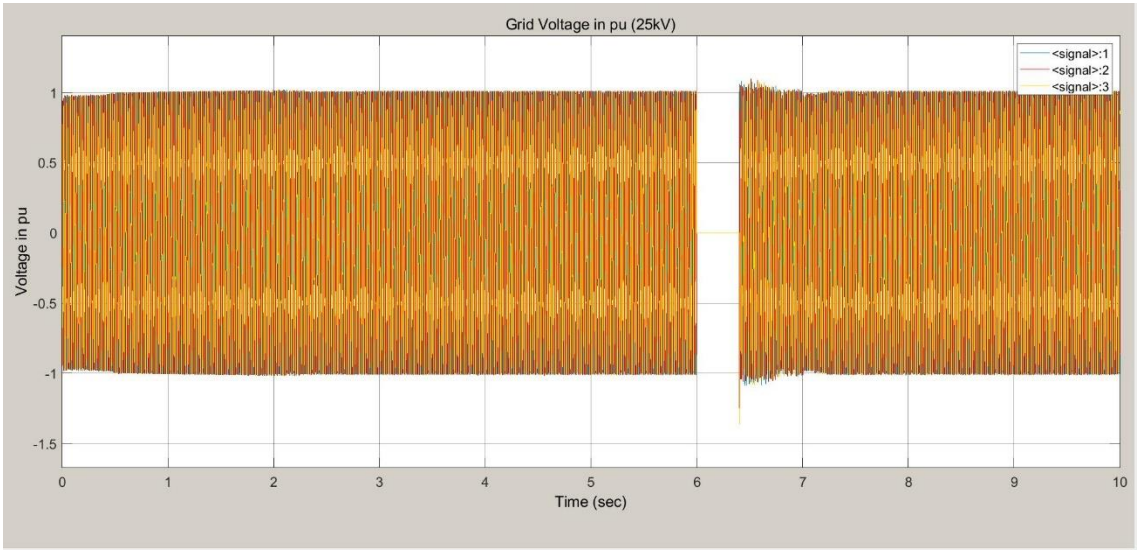

Figure 4.12. Scenario 5 power, electromagnetic torque and voltage analysis during fault

4.1.1.6. Scenario 6

Three-Phase to ground fault would be represented while Vgrid at 0.5p.u. At t=6 sec, for 400ms, three-phase to ground fault is applied.

Power and Electromagnetic Torque measurements would be examined. In Figure 4.13, Scenario 6 measured values can be seen, P for Active power, and T_{em}, electromagnetic torque. P plot shows that active power status during fault active. Three-phase faults effects can be seen obviously more harmful than one-phase fault. Active power could not reach its nominal rate and starting oscillation before faut applied and then active power is dropped to "0" values during fault.

When the fault is cleared, peak values are very high with respect to one-phase fault results. Voltage forms drop to zero in all phases as expected, which can be seen in Figure 4.14. During fault electromagnetic toque touches extreme points. Active power and electromagnetic torque could not settle down after fault and continue oscillation until the end of simulation.

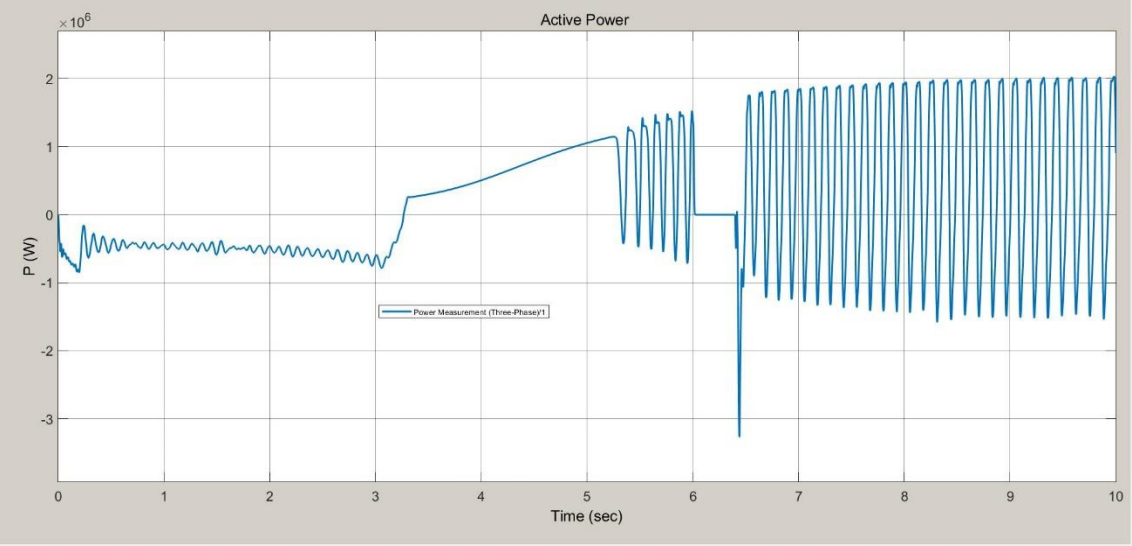

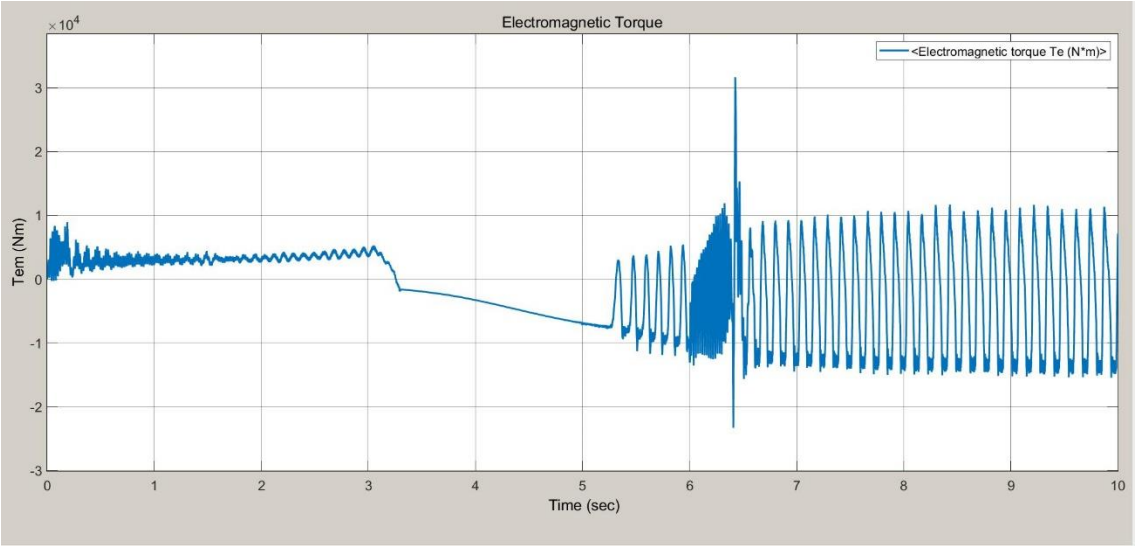

Figure 4.13. Scenario 6 power, power, electromagnetic torque analysis

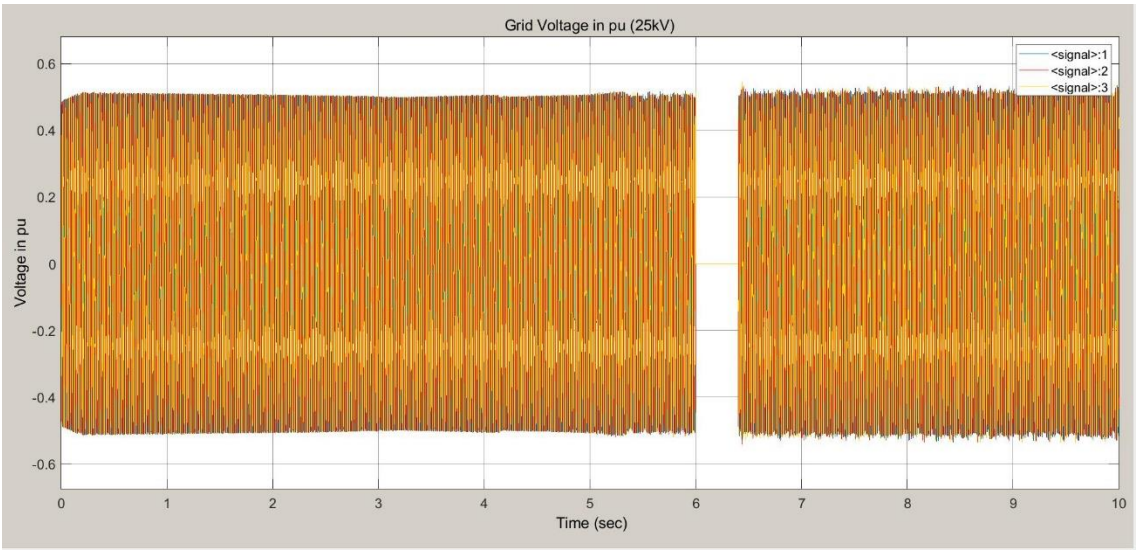

Figure 4.14. Scenario 6 power, electromagnetic torque and voltage analysis during fault

4.1.1.7. Scenario 7

Three-Phase to ground fault would be represented while Vgrid at 0.1p.u. At t=6 sec, for 400ms, three-phase to ground fault is applied.

Power and Electromagnetic Torque measurements would be examined. In Figure 4.15, Scenario 7 measured values can be seen, P for Active power and T_{em}, electromagnetic torque. P plot shows that active power status during fault active. Active power could not reach its nominal rate, obviously generation is dropped to very low values and starting oscillation before faut applied and then active power is dropped to nearly “0” values during fault.

When the fault is cleared, peak values are very high with respect to one-phase fault results. Voltage forms, which can be seen Figure 4.16, drop to zero in all phases as expected. During fault electromagnetic toque touches extreme points. Active power and electromagnetic torque could not settle down after fault and continue oscillation until the end of simulation.

4.1.1.8. Scenario 8

In this Scenario 8, there are two fault applied consecutively to the system, Both one-phase to ground and three-phase to ground fault would be applied to the system while Vgrid at 1p.u. At t=5 sec, for 400ms, one-phase to ground fault is applied and after that at t=6 sec, for 400ms, three-phase to ground fault is applied to the system.

Power and Electromagnetic Torque measurements would be examined. In Figure 4.17, Scenario 8 measured values can be seen, P for Active power, and T_{em}, electromagnetic torque. P plot shows that active power status during fault active. Active power reached its nominal rate, two consecutive one-phase and three-phase to ground faults effects can be seen. After both faults are cleared, it takes time to go back to its steady state rates for active power. On the other hand, peak active power values are very high for a period.

Starting from first fault until the time that both faults are cleared, electromagnetic toque touches extreme points, and oscillating for a long time. Grid voltage forms, which can be seen Figure 4.18, show one phase to ground fault and three-phase to ground fault in the same graphic.

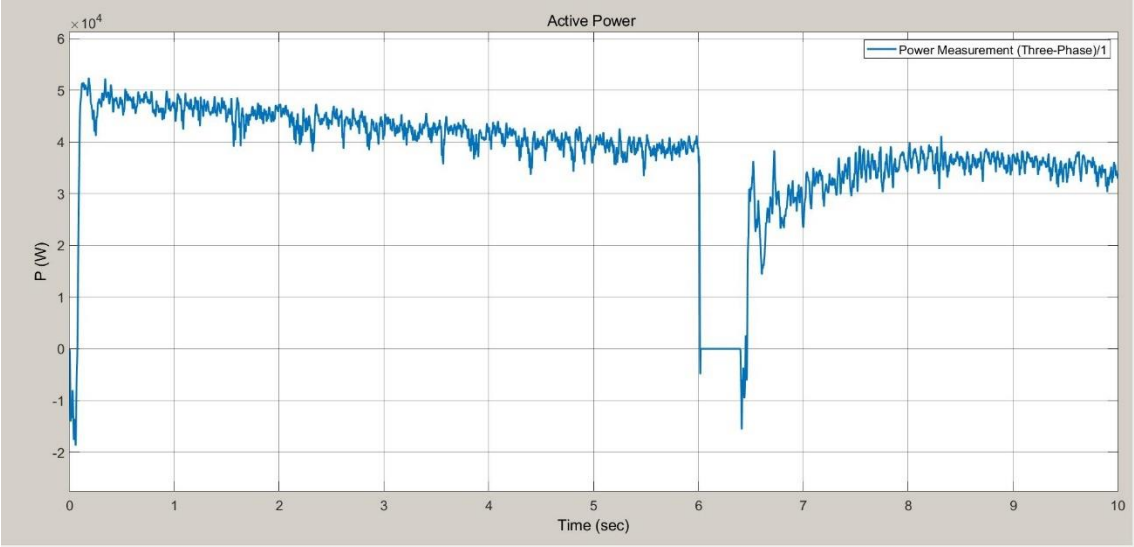

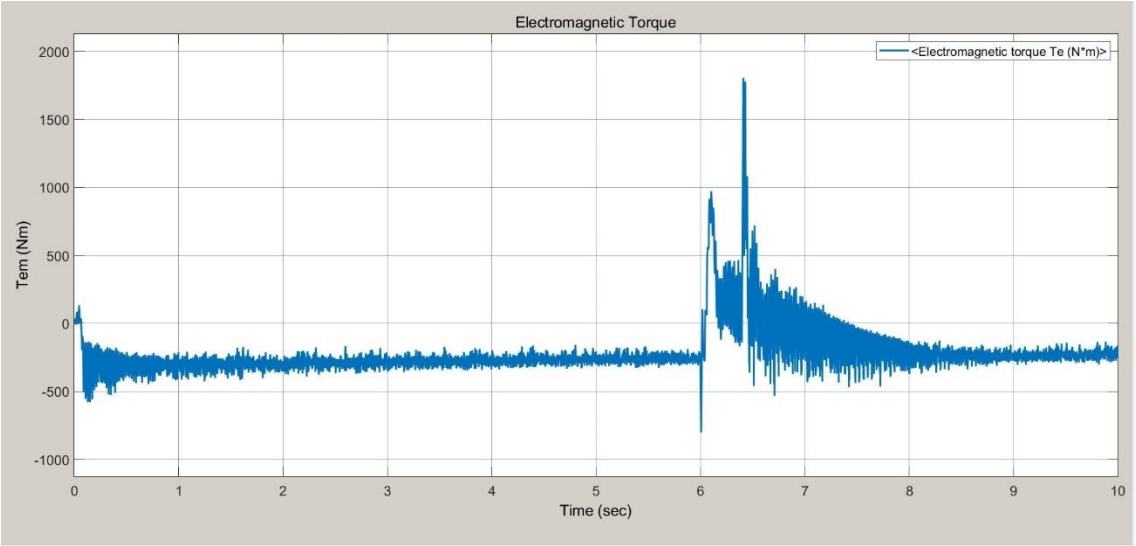

Figure 4.15. Scenario 7 power, electromagnetic torque

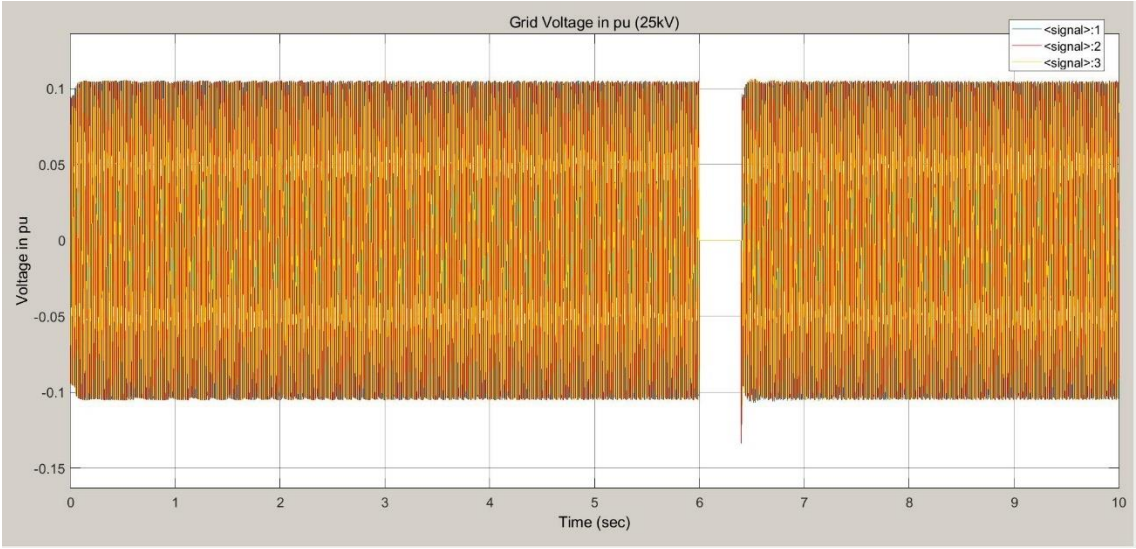

Figure 4.16. Scenario 7 power, electromagnetic torque and voltage analysis during fault

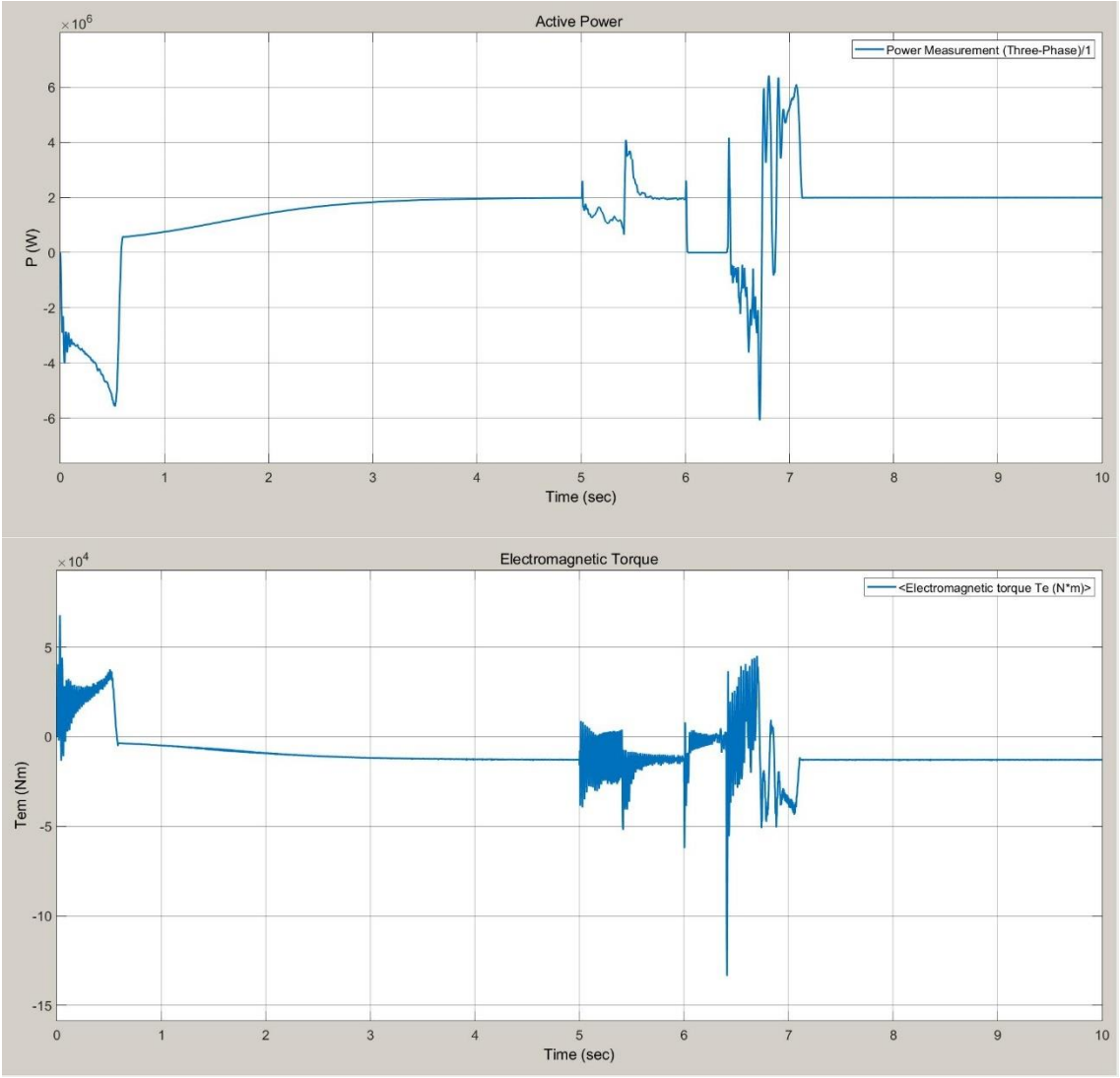

Figure 4.17. Scenario 8 power, electromagnetic torque

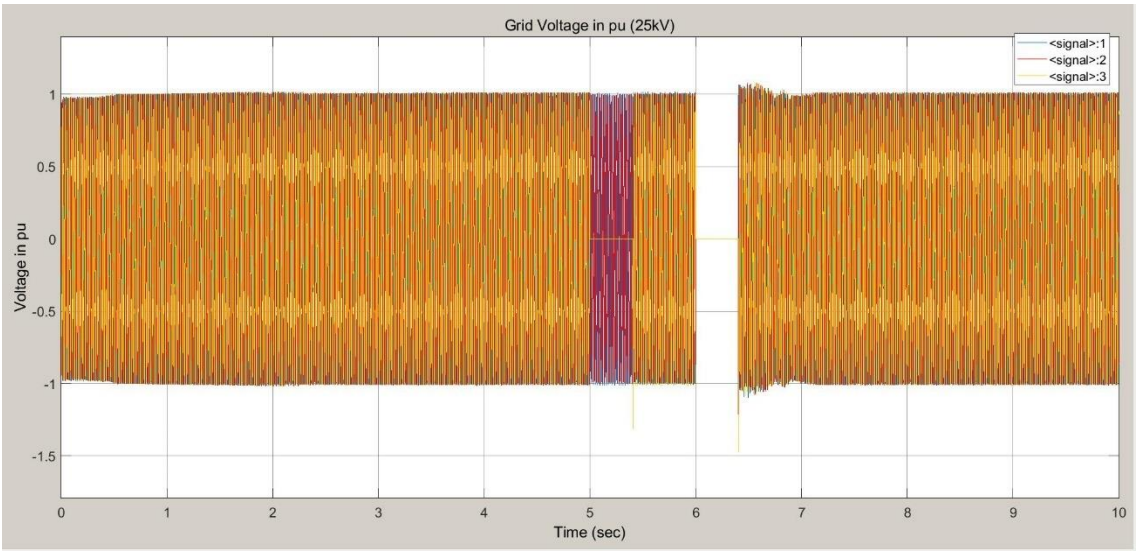

Figure 4.18. Scenario 8 power, electromagnetic torque and voltage analysis during fault

4.2. HAWC2 Model Run

Simulation Model run plan can be found in the following table. In Table 4.2, each simulation session the output of the simulations is defined.

Table 4.2. HAWC2 Simulation Plan

	Fault Effect	**Fault Type**	**Plots for Shaft, Tower, and Generator Torque**	**Description**
Simulation 1	No	NA	Yes	HAWC2 Model Verification
Simulation 2	Yes	Single Fault	Yes	Correlation with EE model
Simulation 3	Yes	Double Fault	Yes	Correlation with EE model

4.2.1. DTU 10MW Turbine Simulation Runs

HAWC2 tool runs with DTU 10MW turbine to get moment and force outputs for tower and shaft.

4.2.1.1. Simulation 1

DTU 10MW wind turbine model's "htc" files called from HAWC2 to run the simulation in order to get base plots related with model. Using Pdap (ver. 3.14.0) tools which is suggested from HAWC2 to visualize the output of the run is used to observation of model in terms of outputs of model run. Main body's moment and force as well as deflections of tower and blades can be seen with respect to simulation time. In Figure 4.19, general plotting of Pdap tools can be seen.

In simulation 1, tower base and tower top moments for x, y, and z axis as well as shaft moments and generator torque reference plots are obtained. Simulation time is set to 1000sec. Wind speed is set to 12 m/s for all simulations. In APPENDIX E all HAWC2 output's coordinate system for DTU 10MW wind turbine model can be found.

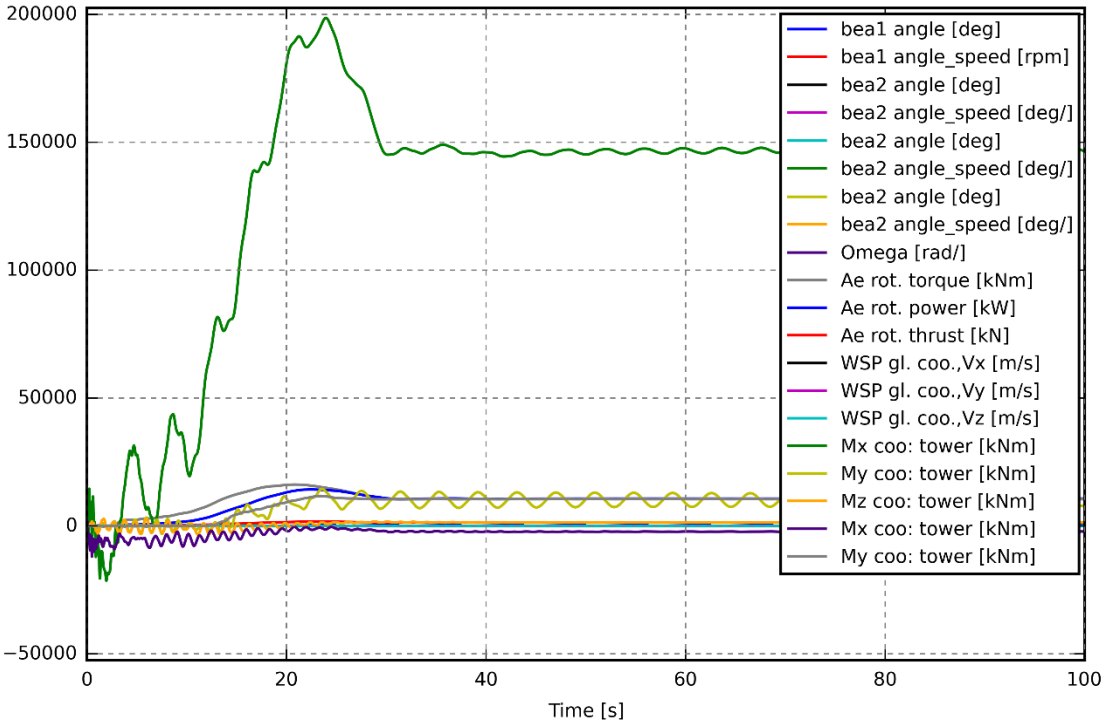

Figure 4.19. Pdap visualization tool example of plotting – general view

In Figure 4.20, tower top y-axis moment, in Figure 4.21 shaft z-axis moment and in Figure 4.22 generator torque reference can be seen.

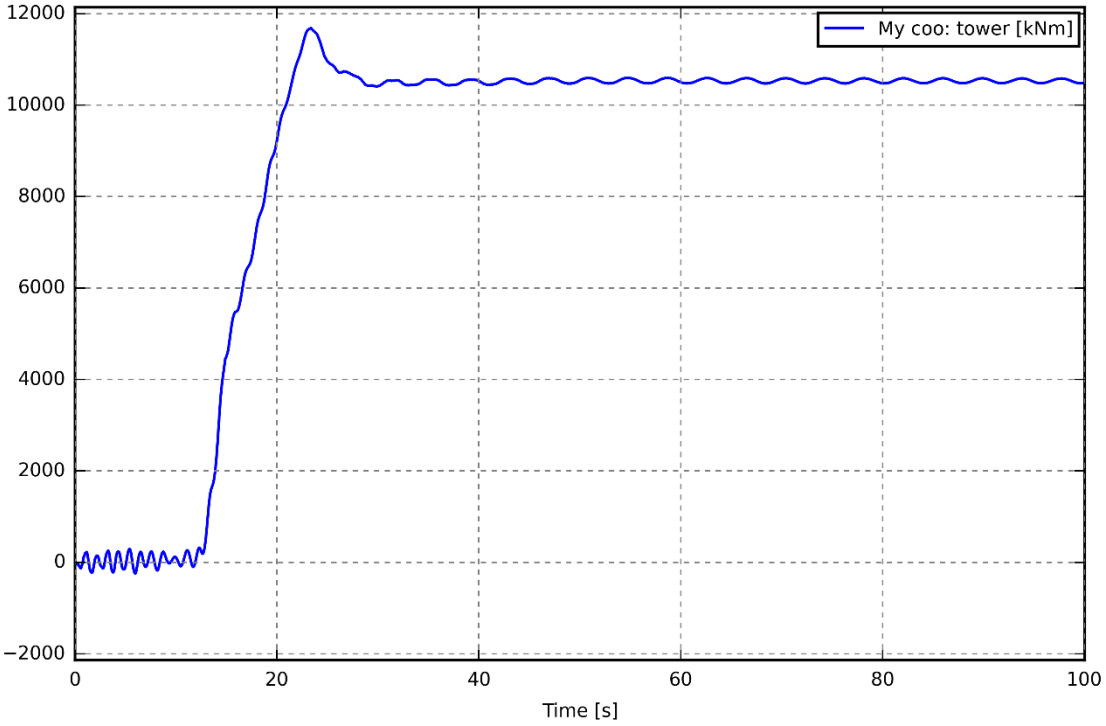

Figure 4.20. Tower top moment y-axis

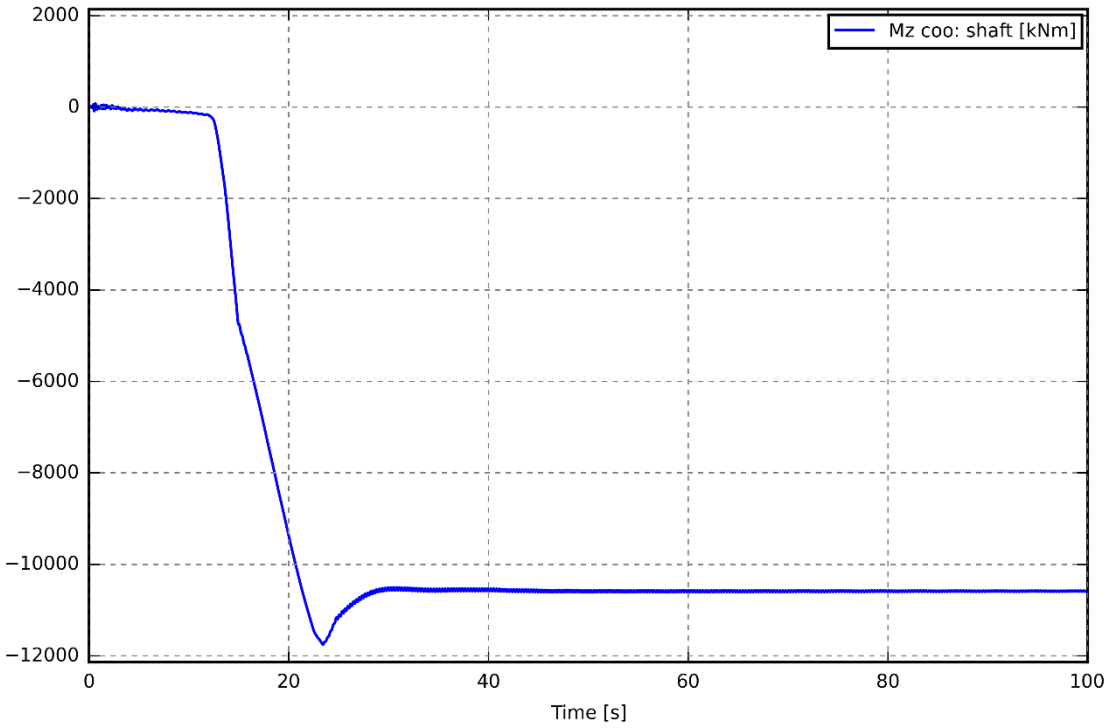

Figure 4.21. Shaft moment z-axis

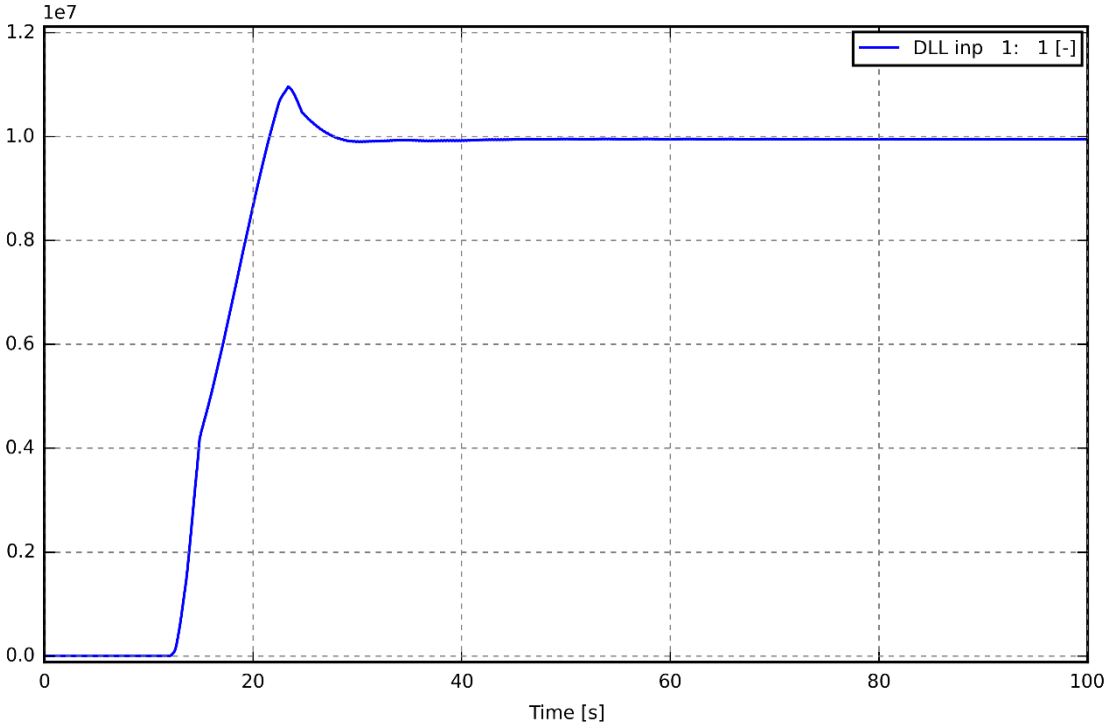

Figure 4.22. Generator torque reference

In Figure 4.23, tower top deflection in x-axis, in Figure 4.24, tower top deflection in y-axis and in Figure 4.25, transversal and axial deflection scattered plot can be found.

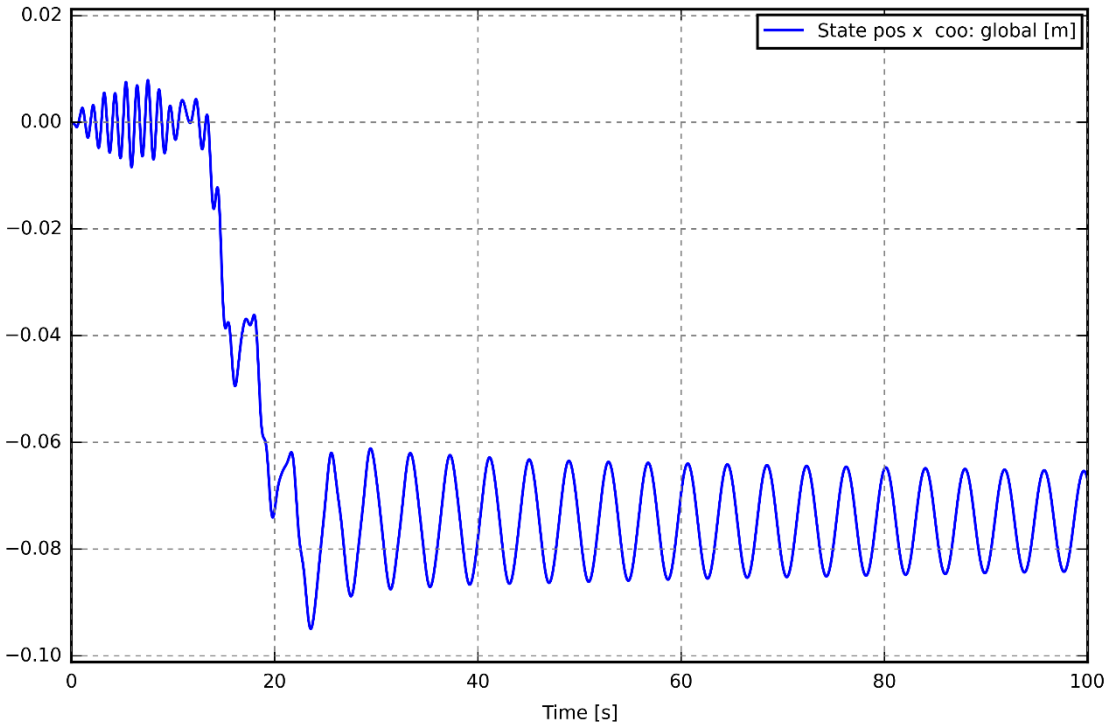

Figure 4.23. Tower top deflection in x-axis, m

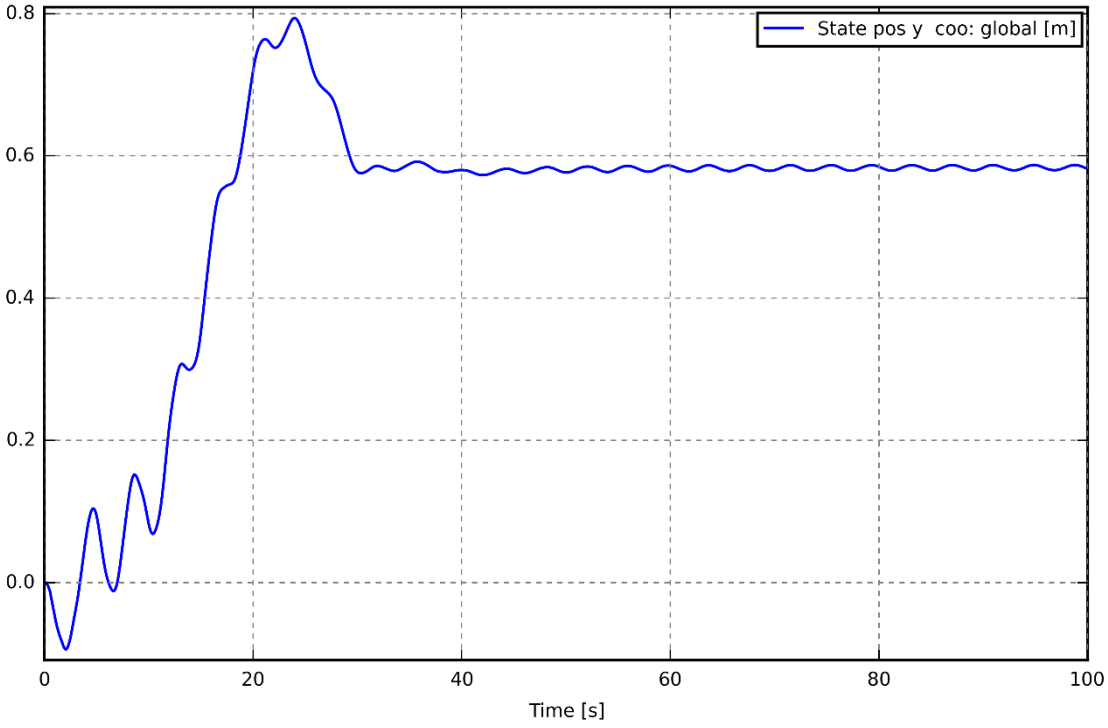

Figure 4.24. Tower top deflection in y-axis, m

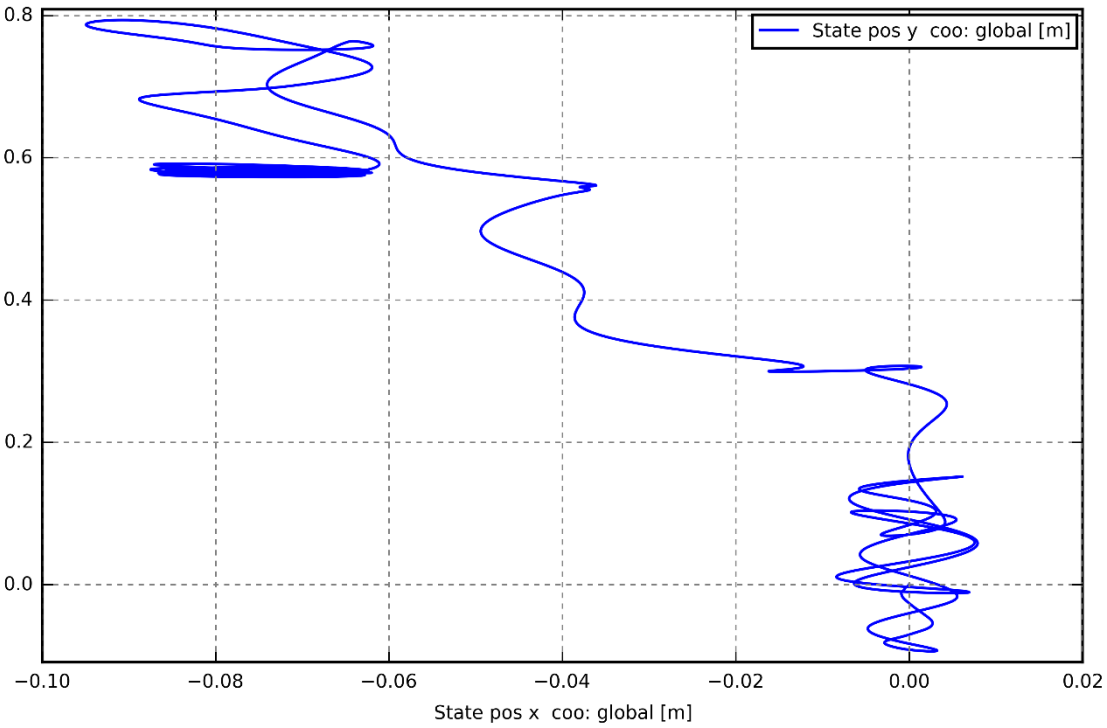

Figure 4.25. Tower top transversal and axial deflection

4.2.1.2. Simulation 2

DTU 10MW wind turbine model's advanced simulation "htc" files called from HAWC2 to run the simulation in order to get base plots related with model to show effects of fault.

In simulation 2, tower top moment in y-axis as well as shaft moments in z-axis and generator torque reference plots can be seen. Simulation time is set to 1000sec. Tower top deflection in x-axis and y-axis are studied and single fault applied simulation tower top deflection results are presented.

In Figure 4.26, tower top y-axis moment, in Figure 4.27, shaft z-axis moment and in Figure 4.28, generator torque reference can be seen.

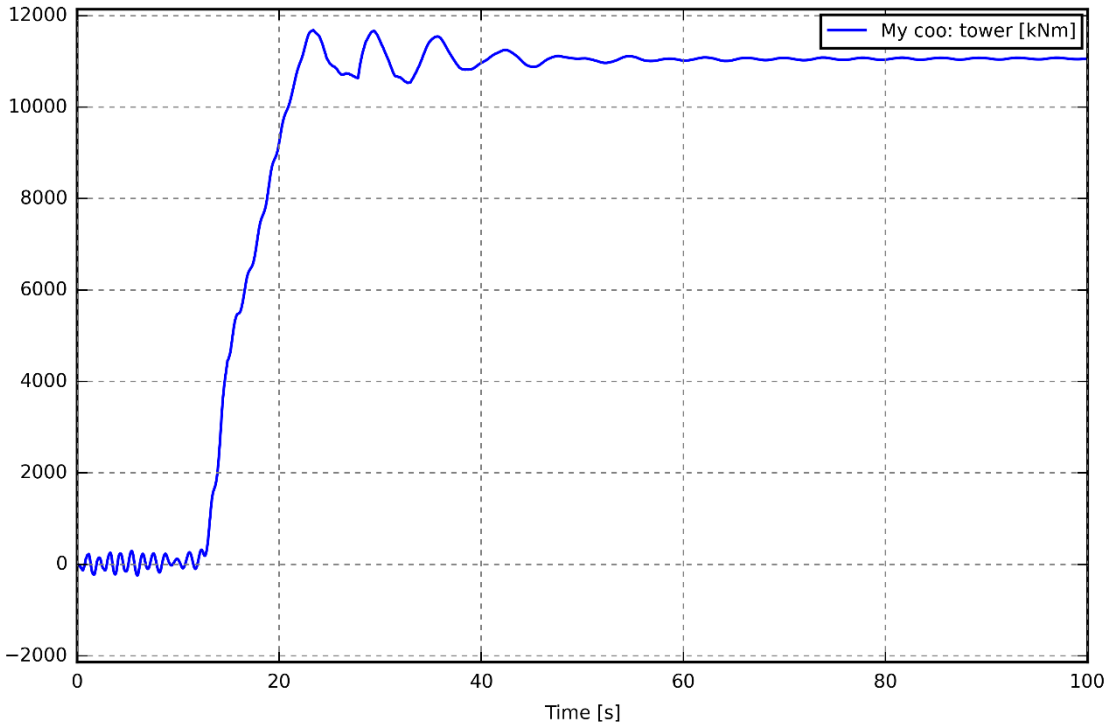

Figure 4.26. Tower top y-axis moment with single fault

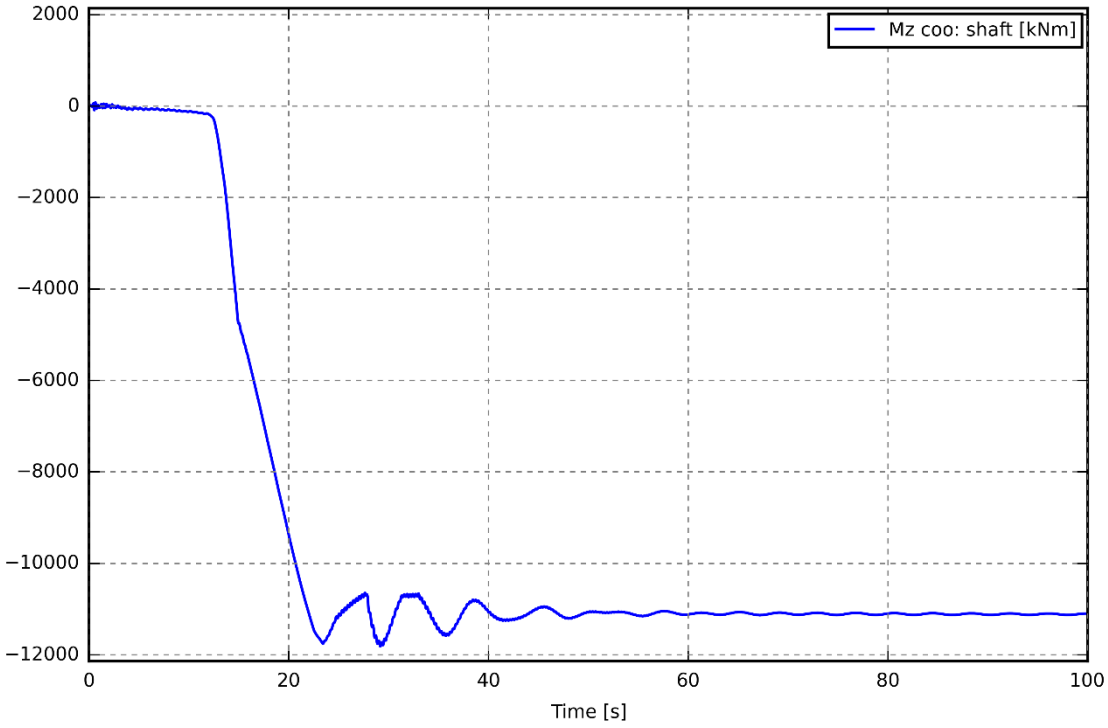

Figure 4.27. Shaft z-axis moment with single fault

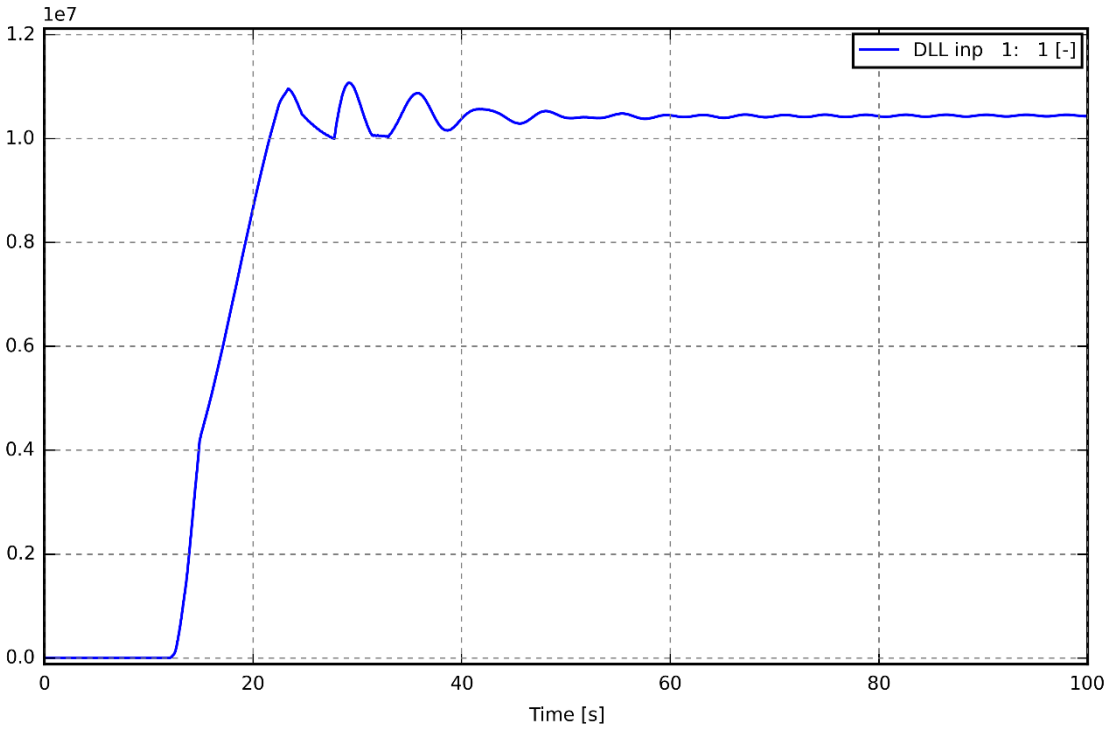

Figure 4.28. Generator torque reference, kN with single fault

In Figure 4.29, tower top deflection in x-axis, in Figure 4.30, tower top deflection in y-axis and in Figure 4.31 tower top transversal and axial deflection analysis can be found.

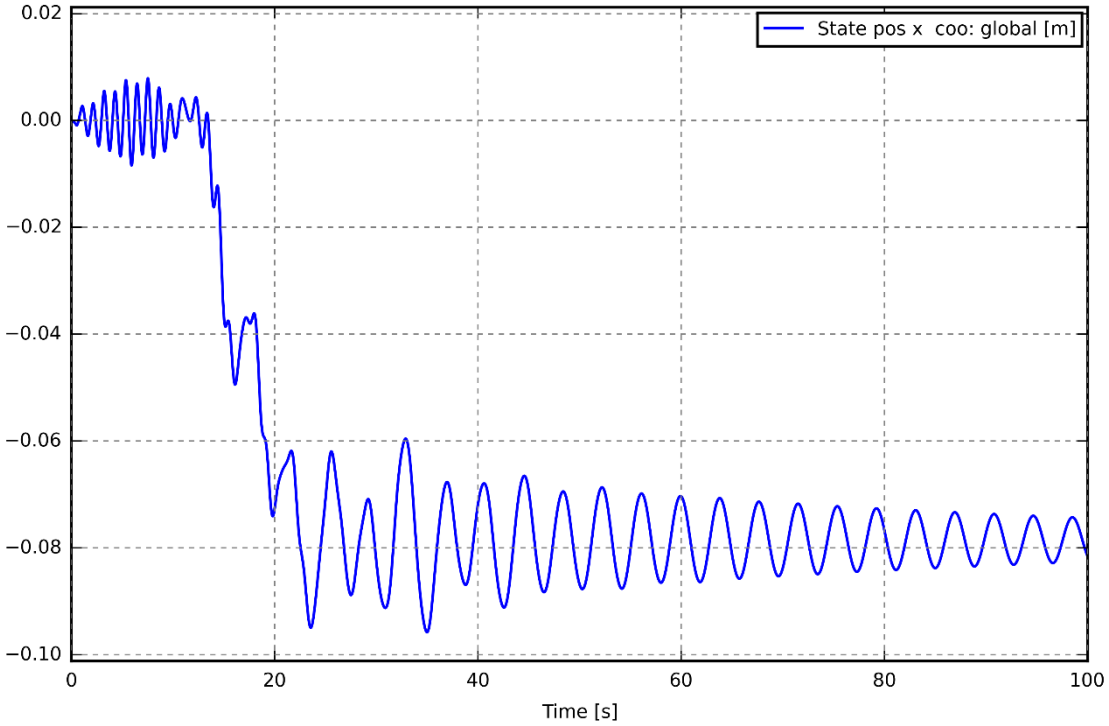

Figure 4.29. Tower top deflection in x-axis with single fault

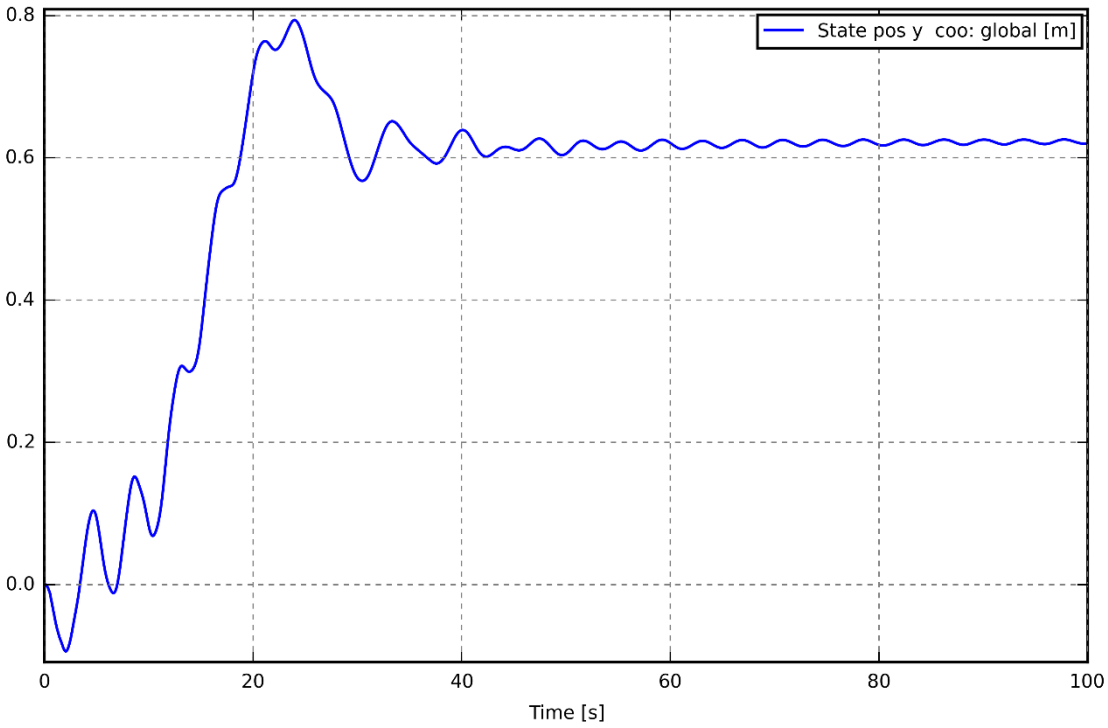

Figure 4.30. Tower top deflection in y-axis moment with single fault

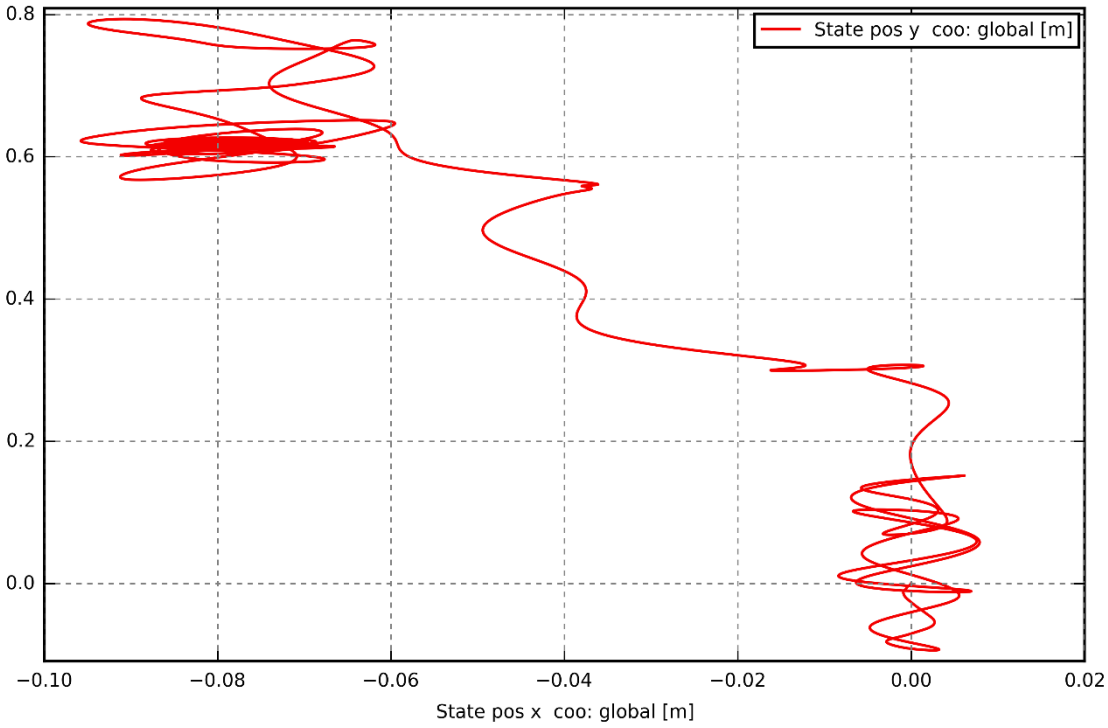

Figure 4.31. Tower top transversal and axial deflection with single fault

4.2.1.3. Simulation 3

DTU 10MW wind turbine model's advanced simulation "htc" files called from HAWC2 to run the simulation in order to get base plots related with model to show effects of fault.

In simulation 3, tower top moment in y-axis as well as shaft moment in z-axis and generator torque reference plots can be seen. Simulation time is set to 1000sec. Tower top deflection in both x-axis and y-axis and transversal and axial deflection analysis can be seen.

In Figure 4.32, tower top moment in y-axis moment, in Figure 4.33, shaft z-axis moment and in Figure 4.34, generator torque reference can be seen.

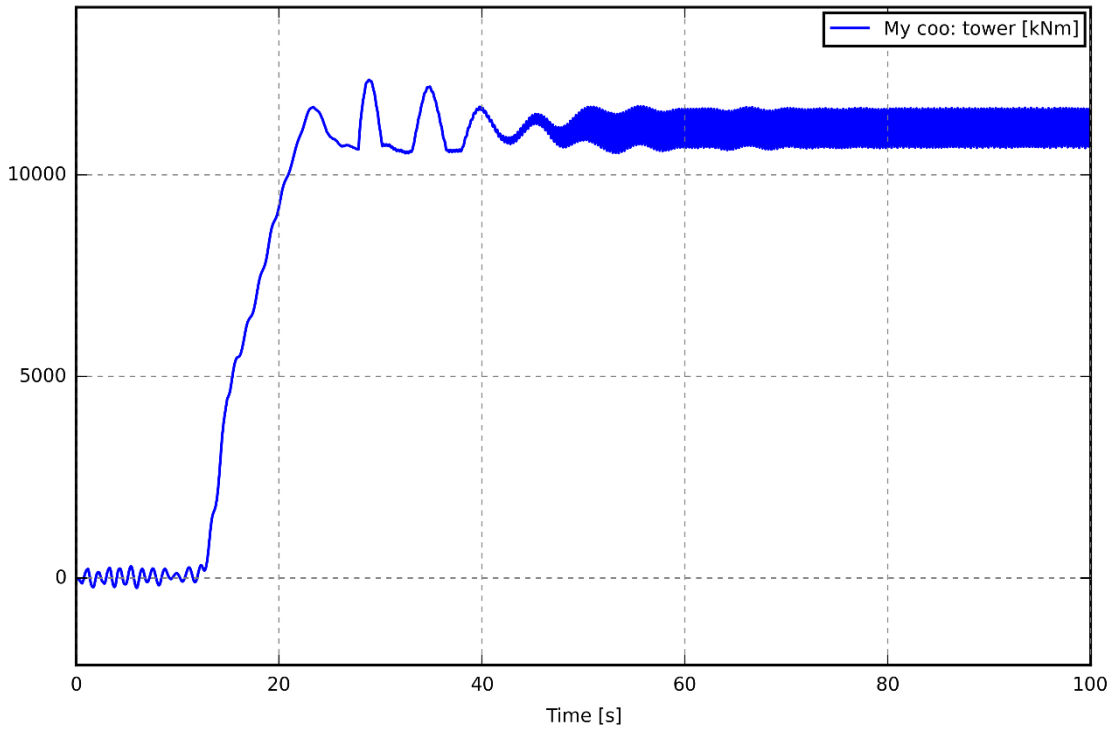

Figure 4.32. Tower top y-axis moment with double fault

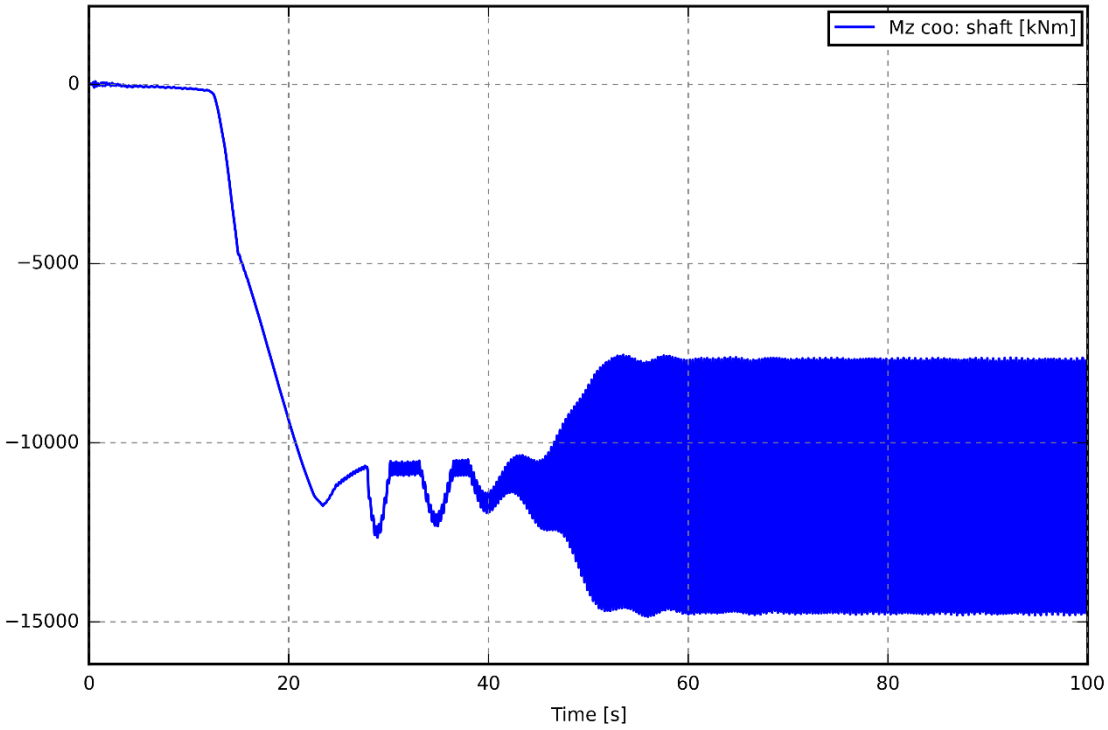

Figure 4.33. Shaft z-axis moment with double fault

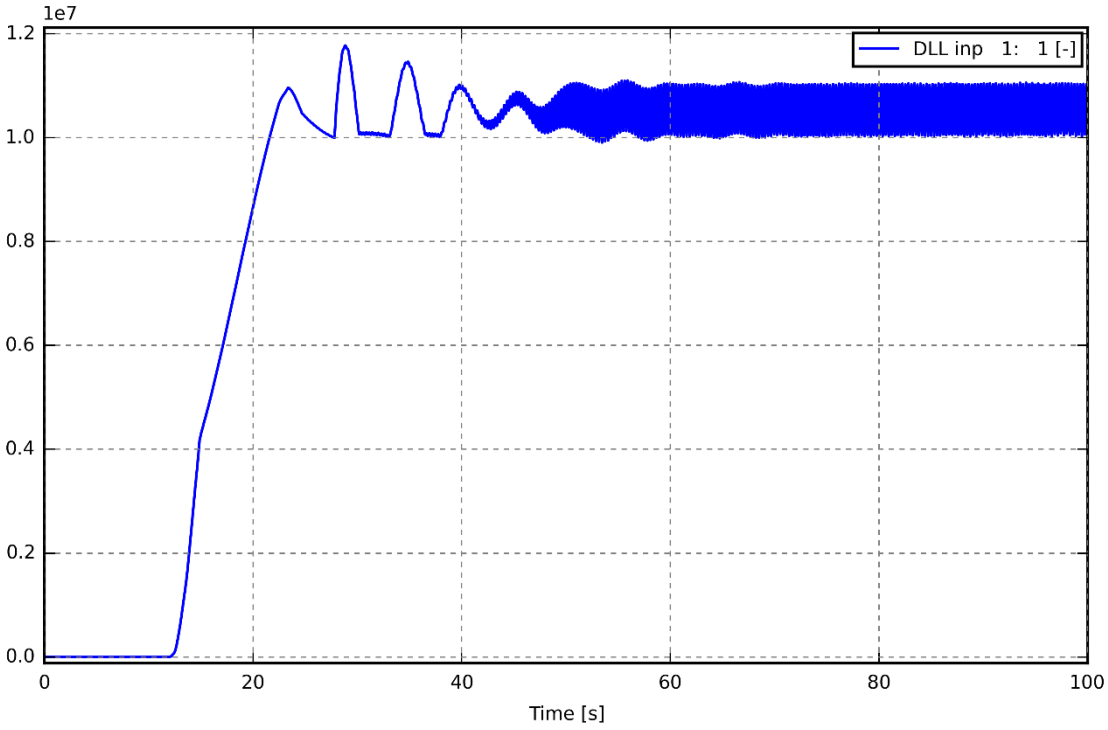

Figure 4.34. Generator torque reference with double fault

In Figure 4.35, tower top deflection in x-axis, in Figure 4.36, tower top deflection in y-axis and in Figure 4.37 tower top transversal and axial deflection analysis with double fault can be found.

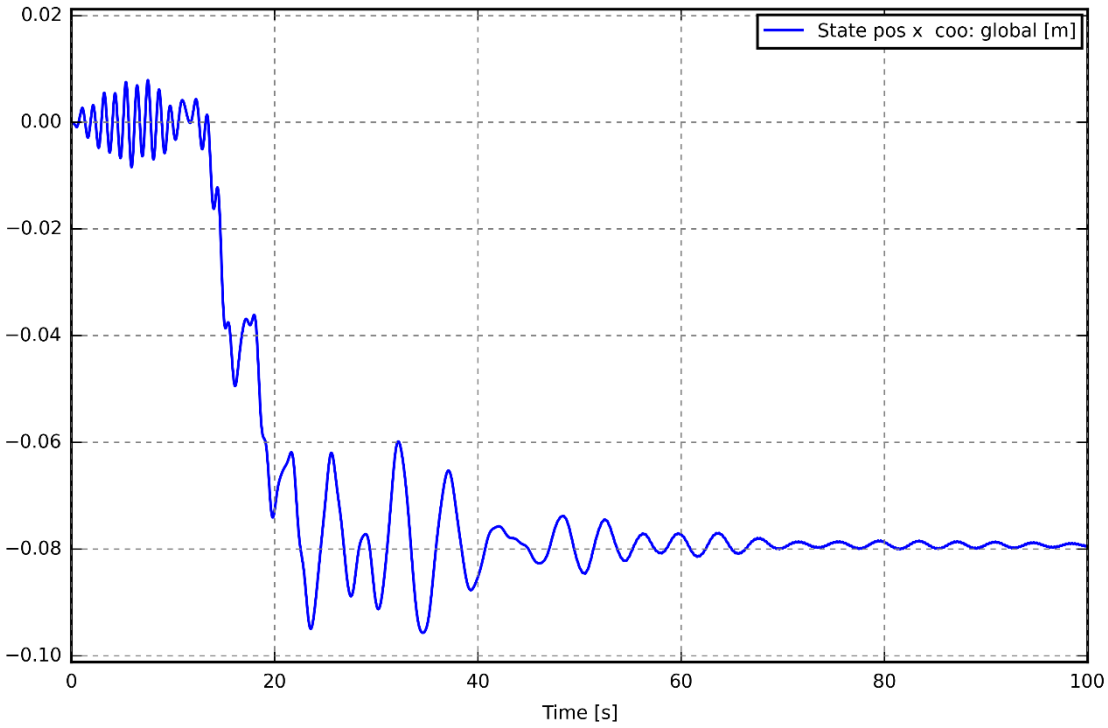

Figure 4.35. Tower top deflection in x-axis with double fault

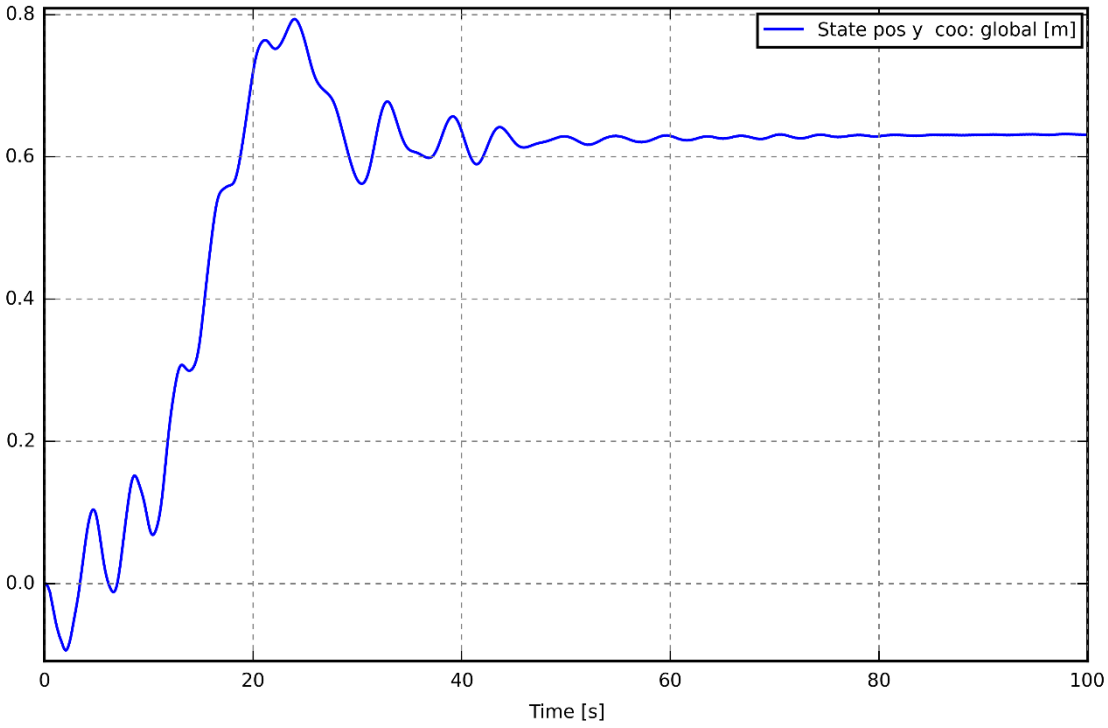

Figure 4.36. Tower top deflection in y-axis with double fault

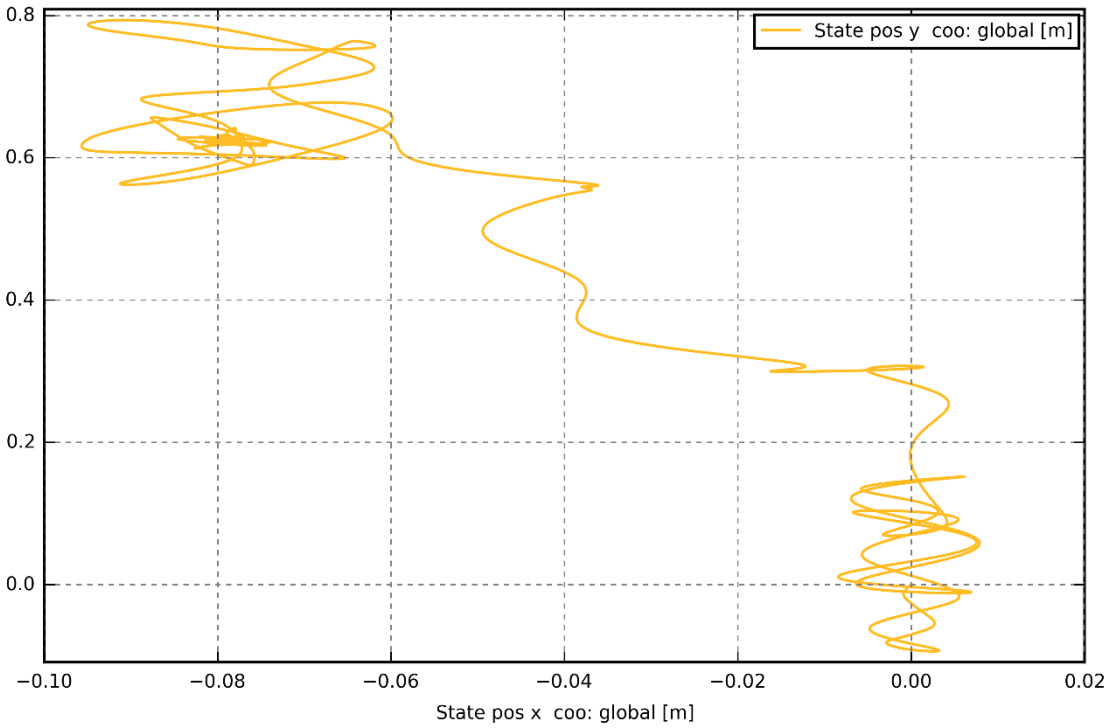

Figure 4.37. Tower top transversal and axial deflection analysis with double fault

4.2.1.4. Comparison of Tower Top Deflection in Base, Single and Double Fault Situations for 12 m/s Wind Speed

In Figure 4.38, tower top deflection in three situation is comparatively studied.

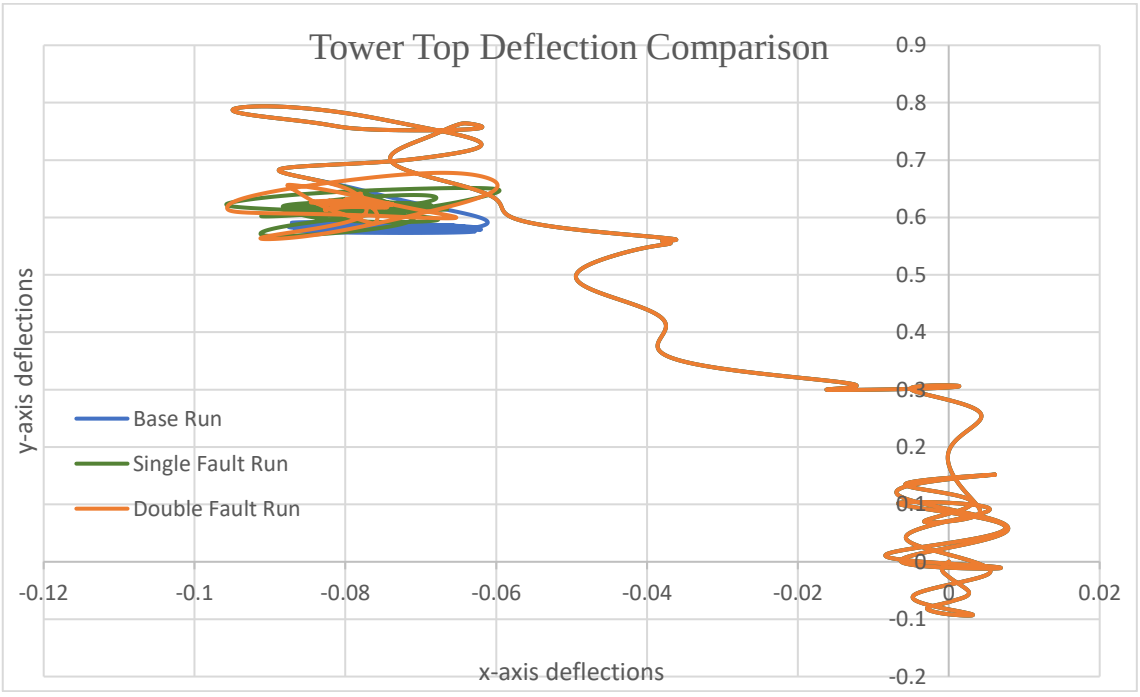

Figure 4.38. Tower top transversal and axial deflection analysis comparison

4.2.1.5. Comparison of Tower Top Deflection in Double Fault Situations for 6 m/s, 12 m/s and 18 m/s Wind Speed

In order to see deflections for different wind speeds, simulations are run in different wind speed with the worst case of fault situation such as double fault situation. Wind speed values as 6m/s which is less than nominal wind speed and 18 m/s higher than nominal wind speed are set in HAWC2 “htc” file and simulations are done with same fault situations.

In Figure 4.39, all three different wind speed simulation results for double fault situation examined. Tower top deflections are presented in one graphic for comparative study.

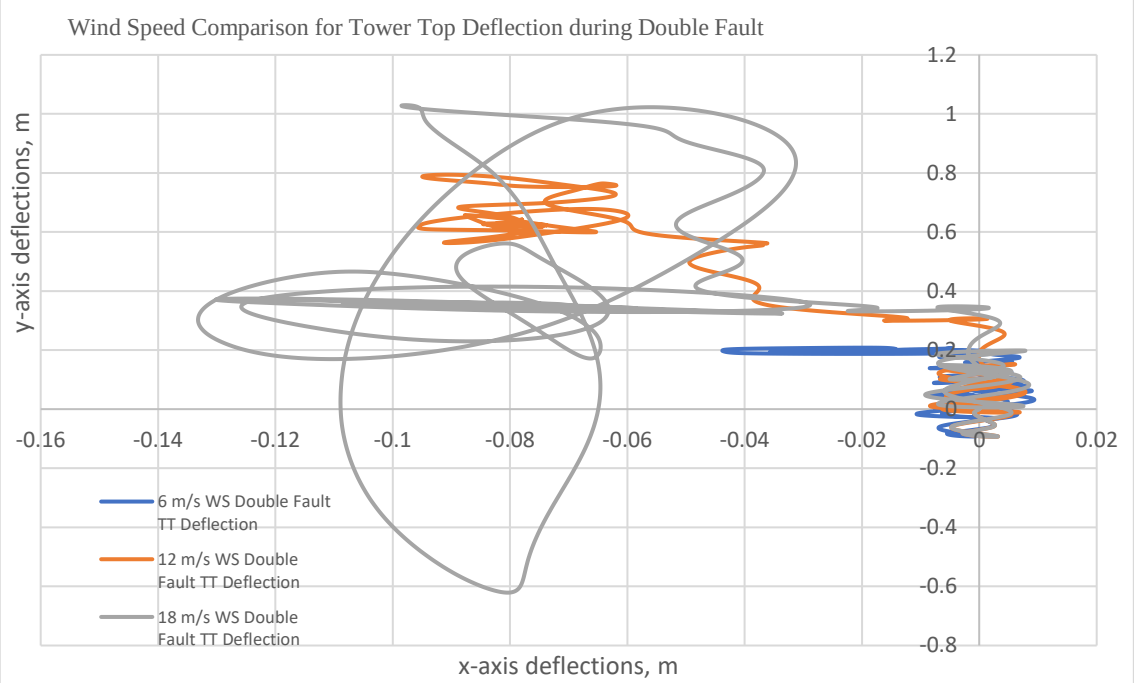

Figure 4.39. Tower top transversal and axial deflection analysis comparison for different wind speed

CHAPTER 5
DISCUSSION ON RESULTS

In this chapter, it is aimed to review the results which are obtained in Chapter 4, in which Power System Simulations and HAWC2 Simulations are performed. This study's purpose is to find the effects on mechanical systems during faults; therefore, comparison of both results is considered in this limitations. In their study Barahona et al. mention that the results show that Variable-speed wind turbines have shown that power supply conditions, specifically under voltage problems, can greatly affect structural stresses (Barahona et al. 2013). The findings demonstrated that a substantial decrease in the loads caused by an imbalanced voltage failure can be achieved. Moreover, Tarnowski and Claudio aimed to characterize the capabilities of variable speed wind turbines to provide inertial response (Tarnowski and Claudio 2012). Concerns include the effects on the drive train and tower, the maximum amount of energy that can be delivered, the decrease in power during the recovery period, and the protective measures against torque overload. Wind turbines do not experience excessive stress during this operation as long as appropriate overloading restrictions are enforced.

In this study, overview of the results can be declared as mechanical systems are impacted when power systems are faced with a fault from grid side according to fault ride through applications. This can be seen clearly from HAWC2 simulations results, especially for tower top deflection analysis. In their study, (Barahona et al. 2013) shows that the simulation findings indicate a link between the generator and the tower, as well as the blades. This thesis study shows comparable results with their paper with respect to HAWC2 exports.

In Table 5.1, power system test results can be seen for each scenario. Status of electromagnetic torque output of the generator are evaluated for comparison.

Table 5.1. Results of Power Systems for each scenario

	Low Voltage Fault 1 Phase to Ground	Low Voltage Fault 3 Phase to Ground	Description	Results
Scenario 1	No	No	MATLAB/Simulink Model Verification	Active Power Rated = 2.0 MW Tem Rated = 1.0 p.u
Scenario 2	Yes	No	1-phase to ground fault at Vgrid 1.0 p.u	Active Power Max = 3.2 MW Tem Max = 3.5 p.u
Scenario 3	Yes	No	1-phase to ground fault at Vgrid 0.5 p.u	Active Power Max = 1.8 MW Tem Max = 1.1 p.u
Scenario 4	Yes	No	1-phase to ground fault at Vgrid 0.1 p.u	Active Power Max = 0.05 MW Tem Max = 0.04 p.u
Scenario 5	No	Yes	3-phase to ground fault at Vgrid 1.0 p.u	Active Power Max = 6.0 MW Tem Max = 6.5 p.u
Scenario 6	No	Yes	3-phase to ground fault at Vgrid 0.5 p.u	Active Power Max = 1.8 MW Tem Max = 2.5 p.u
Scenario 7	No	Yes	3-phase to ground fault at Vgrid 0.1 p.u	Active Power Max = 0.05 MW Tem Max = 0.2 p.u
Scenario 8	Yes	Yes	1-phase to ground and 3-phase to ground fault at Vgrid 1.0 p.u	Active Power Max = 4.0 MW Tem Max = 6.0 p.u

In Table 5, according to summary of the results, for single faults 3-phase to ground fault has the worst case situation which is represented in Scenario 5. Electromagnetic torque has been reaching at the peak values for 0.5 seconds at that time fault is cleared and wind turbine is connected to grid. Then, electromagnetic torque graphics has fluctuations which is settled down after around 0.5 seconds. In their study, Zhang et al. emphasized that a three-phase to ground fault in a wind turbine is a crucial occurrence that can have a substantial influence on the performance and dependability of the wind

turbine power system (Zhang et al. 2015). The utilization of torque measurements, shaft displacement, and vibration analysis of the gearbox or electric machine is emphasized for the purpose of detecting faults in wind turbines.

From result summary table, Scenario 8 has the worst case of increasing electromagnetic torque from generator rotor. After faults, electromagnetic torque graphics has fluctuated and reach some peak values, however when fault cleared it takes around 1 or 1.5 seconds to reach rated value. These because we introduced successive double faults from grid side to power system. Lebranchu et al. highlighted the frequent occurrence of successive grid faults in wind turbine systems, which creates substantial difficulties (Lebranchu et al. 2019). To ensure the dependability and efficiency of wind turbine power systems, it is crucial to implement comprehensive approaches for detecting, withstanding, minimizing the impact of, and diagnosing faults. However, in literature it is rare to find that successive grid faults ride through capability and effectiveness analysis.

In HAWC2, comparison for simulation which without fault, with single and double fault situations are done in terms of tower top deflections. Transversal and axial deflections are examined to see the difference between situations. In the first attempt, effect analysis is done with respected rated wind speed. From the results, it was observed that, at 12 m/s wind speeds, transversal deflection of tower top body has the worst results in double fault applied simulation runs. Axial deflections are not so much changed against fault situations. According to results, it seems that even in the worst case scenario, deflections are reaming in the design limitations at the rated wind speed. According to Tarnowski and Claudio 2012, the study found that transverse tower deflections are mostly influenced by the rise in generator torque, specifically the amount of the power boost in inertial response (Tarnowski and Claudio 2012). Their simulation results indicate that the tower deflections during inertial response are likely to stay within the design constraints. However, it can be said that, during the inertial response rotor torque is lowering because of which in turn produced a reduction in the thrust against low voltage ride through application in which rotor torque increasing like this thesis study. Voltage drop faults would be more harmful than frequency changes in the system due to increasing in the swings of shaft main body.

On the other hand, while analyzing the wind speed effect with worst case fault scenario, it can be stated that axial deflection has increased significantly for 18 m/s wind speed. Transversal deflection is slightly increased also but it is closed to values that no

fault steady state situation. In their study, Tarnowski and Claudio 2012 stated that the variation in tower deflection can be observed across various wind speeds (Tarnowski and Claudio 2012). Furthermore, there is a direct correlation between the amount of energy given and the magnitude of the axial tower deflection. In their study, rated wind speed has the more deflection unlike this thesis study, that is because inertial response depends on aerodynamic efficiency which is the highest in rated speed.

In the study conducted for the thesis, it was observed that the occurrence of severe grid faults, which are necessary to maintain connection to the grid with fault ride through capability, has an impact on the response of electrical systems. This impact, in turn, leads to deflection on the main bodies of the system, specifically in terms of tower top transversal and axial deflections.

CHAPTER 6
CONCLUSION

This thesis has examined the power system of current wind turbines, focusing on their fault ride-through capabilities and the interconnections between subsystems. The objective is to demonstrate the impact of electrical systems on mechanical systems. Novel techniques and remedies were devised to address the unique issue of grid faults resulting in voltage drops. The wind turbine model, equipped with a double-fed induction generator, is employed to observe the impact of the electrical system's response on the mechanical system during a single-phase short circuit or consecutive one-phase and three-phase short circuit failures. The HAWC2 tool is used to thoroughly analyze the effects on mechanical systems for all fault cases with different wind speed situations.

The initial stage involves the construction of a Power System for a Double Fed Induction Generator (DFIG) Type Wind Turbine, which is then connected to a Grid. The initial simulation of the study involves analyzing the performance of the power system and validating its accuracy. The next step involves intentionally introducing grid faults, namely one-phase to ground and three-phase to ground faults, into the system. All scenarios include adjusting the grid voltage to observe the impact of grid faults on the electrical system of a DFIG Wind Turbine. The per unit values of electromagnetic torque are recorded to observe any variations.

The subsequent phase involves the preparation of HAWC2 simulations. Initially, the HAWC2 model is executed using a base model for a reference wind turbine. Subsequently, alterations are made to the HAWC2 model to incorporate variations in electromagnetic torque, thereby demonstrating the impact of faults on the mechanical system. This can be accomplished by inducing tower and shaft deflections in both axial and transverse directions. Conducting a comparative analysis of findings across various fault scenarios and wind velocities in order to determine the outcomes.

Electrical power systems are planned using MATLAB/Simulink, and all necessary simulations for each scenario are executed on Simulink. A 2MW Doubly Fed Induction Generator (DFIG) wind turbine is utilized to construct power systems and grid connections, while simulating fault scenarios. Conversely, the HAWC2 tool is utilized in conjunction with the DTU 10MW reference turbine for conducting simulations. The

correlation between these tools is managed offline. Electromagnetic torque values in per unit (p.u.) are sent from Simulink to HAWC2.

The most severe scenario, based on the Simulink results, is when there is a sequential fault involving three-phase to ground and single-phase to ground. In this scenario, the tower deflection reaches its highest value. As the wind speed rises, there is a corresponding increase in deflections along both axes. These results are significant since it is uncommon to examine consecutive faults on a Doubly Fed Induction Generator (DFIG) wind turbine using offline coupled instruments for fault ride through of power systems.

This thesis imagined that in wind turbine design, it is crucial to address the interactions between systems, as there will be repercussions for both sides. Hence, this thesis presents and validates a methodology for doing effect analysis, resulting in beneficial outcomes as intended. In future research, this study might be expanded to demonstrate the constraints of mechanical components by examining the stresses imposed on them during fault scenarios. Several types of defects can be analyzed, including fluctuations in grid frequency and voltage reductions. This would result in the integration of both inertial response and low voltage ride through capabilities. Advanced simulation tools will be chosen for the purpose of designing and combining them for iterative simulations, which will allow for the fine-tuning of control parameters for both subsystems.

REFERENCES

Abad, Gonzalo, Jesus Lopez, Miguel Rodriguez, Luis Marroyo, and Grzegorz Iwanski. 2011. Doubly Fed Induction Machine. John Wiley & Sons.

Abdelmalek, Samir, Sarah Rezazi, Azzeddine Bakdi, and Maamar Bettayeb. 2019. "VOLTAGE DIPS EFFECTS DETECTION and COMPENSATION for DOUBLY-FED INDUCTION GENERATOR BASED WIND ENERGY CONVERSION SYSTEM." Rev. Roum. Sci. Techn.-Électrotechn. Et Énerg 64: 199–204. http://www.revue.elth.pub.ro/upload/27804503_SAbdelmalek_RRST_3_2019_pp_199-204.pdf.

Ali, Saif. 2018. Simulation of Dynamic Systems with MATLAB® and Simulink®, Third Edition. CRC Press EBooks. https://doi.org/10.1201/9781315154176.

Altın, Müfit, Ömer Göksu, Remus Teodorescu, Pedro Rodriguez, Birgitte-Bak Jensen, and Lars Helle. 2010. "Overview of Recent Grid Codes for Wind Power Integration." IEEE Xplore. May 1, 2010. https://doi.org/10.1109/OPTIM.2010.5510521.

Asmuth, Henrik, Gonzalo P. Navarro Diaz, Helge Aagaard Madsen, Emmanuel Branlard, Alexander R. Meyer Forsting, Karl Nilsson, Jason Jonkman, and Stefan Ivanell. 2022. "Wind Turbine Response in Waked Inflow: A Modelling Benchmark against Full-Scale Measurements." Renewable Energy 191 (May): 868–87. https://doi.org/10.1016/j.renene.2022.04.047.

Barahona, Braulio, Nicolaos A. Cutululis, Anca D. Hansen, and Poul Sørensen. 2013. "Unbalanced Voltage Faults: The Impact on Structural Loads of Doubly Fed Asynchronous Generator Wind Turbines." Wind Energy 17 (8): 1123–35. https://doi.org/10.1002/we.1621.

Barlas, Thanasis, Néstor Ramos-García, Georg Raimund Pirrung, and Sergio González Horcas. 2021. "Surrogate-Based Aeroelastic Design Optimization of Tip Extensions on a Modern 10 MW Wind Turbine." Wind Energy Science 6 (2): 491–504. https://doi.org/10.5194/wes-6-491-2021.

Betti, Giulio, Marcello Farina, Giuseppe A Guagliardi, Andrea Marzorati, and Riccardo Scattolini. 2014. "Development of a Control-Oriented Model of Floating Wind Turbines." IEEE Transactions on Control Systems and Technology 22 (1): 69–82. https://doi.org/10.1109/tcst.2013.2242073.

Chandrasekaran, Subramanian, Claudio Rossi, Domenico Casadei, and Angelo Tani. 2013. "Improved Control Strategy for Low Voltage Ride through Capability of DFIG with Grid Code Requirements." SSRN Electronic Journal. https://doi.org/10.2139/ssrn.3425824.

Chen, Chao, Philippe Duffour, Paul Fromme, and Xugang Hua. 2021. "Numerically Efficient Fatigue Life Prediction of Offshore Wind Turbines Using

Aerodynamic Decoupling." Renewable Energy 178 (November): 1421–34. https://doi.org/10.1016/j.renene.2021.06.115.

Dimitrov, Nikolay, Mark C. Kelly, Andrea Vignaroli, and Jacob Berg. 2018. "From Wind to Loads: Wind Turbine Site-Specific Load Estimation with Surrogate Models Trained on High-Fidelity Load Databases." Wind Energy Science 3 (2): 767–90. https://doi.org/10.5194/wes-3-767-2018.

Ekanayake, J.B., L. Holdsworth, XueGuang Wu, and N. Jenkins. 2003. "Dynamic Modeling of Doubly Fed Induction Generator Wind Turbines." IEEE Transactions on Power Systems 18 (2): 803–9. https://doi.org/10.1109/tpwrs.2003.811178.

Engineering, WARSE The World Academy of Research in Science and. 2019. "DFIG Power Reserve Control Based on ADRC during Grid Frequency Fault." World Academy of Research in Science and Engineering, January. https://www.academia.edu/39789557/DFIG_power_reserve_control_based_on_ADRC_during_grid_frequency_fault.

Florin Iov, Frede Blaabjerg, and Anca Daniela Hansen. 2002. "A Simulation Platform to Model, Optimize and Design Wind Turbines. The Matlab/Simulink Toolbox." The Annals of "Dunarea de Jos" University of Galati. Fascicle III, Electrotechnics, Electronics, Automatic Control, Informatics 25: 83–89. https://www.gup.ugal.ro/ugaljournals/index.php/eeaci/article/view/762.

Florin Iov, Remus Teodorescu, Frede Blaabjerg, Björn Andresen, Jens Birk, and Javier Miranda. 2006. "Grid Code Compliance of Grid-Side Converter in Wind Turbine Systems," June. https://doi.org/10.1109/pesc.2006.1711744.

Fontanella, A., A. Zasso, and M. Belloli. 2022. "Wind Tunnel Investigation of the Wake-Flow Response for a Floating Turbine Subjected to Surge Motion." Journal of Physics: Conference Series 2265 (4): 042023. https://doi.org/10.1088/1742-6596/2265/4/042023.

Gaertner, Evan, Jennifer M Rinker, Latha Sethuraman, Frederik Zahle, Benjamin O Anderson, Garrett Barter, Nikhar Abbas, et al. 2020. "IEA Wind TCP Task 37: Definition of the IEA 15-Megawatt Offshore Reference Wind Turbine," March. https://doi.org/10.2172/1603478.

Gallego-Calderon, Juan, Anand Natarajan, and Nicolaos A. Cutululis. 2016. "Ultimate Design Load Analysis of Planetary Gearbox Bearings under Extreme Events." Wind Energy 20 (2): 325–43. https://doi.org/10.1002/we.2008.

Gashi, Ali, Gazmend Kabashi, Skender Kabashi, Skender Ahmetaj, and Valon Veliu. 2012. "Simulation the Wind Grid Code Requirements for Wind Farms Connection in Kosovo Transmission Grid." Energy and Power Engineering 04 (06): 482–95. https://doi.org/10.4236/epe.2012.46062.

Hansen, Anca D., Poul Sørensen, Florin Iov, and Frede Blaabjerg. 2006. "Centralised Power Control of Wind Farm with Doubly Fed Induction

Generators.” Renewable Energy 31 (7): 935–51. https://doi.org/10.1016/j.renene.2005.05.011.

Hansen, Anca D., and Gabriele Michalke. 2007. “Fault Ride-through Capability of DFIG Wind Turbines.” Renewable Energy 32 (9): 1594–1610. https://doi.org/10.1016/j.renene.2006.10.008.

Hansen, Anca D., Nicolaos A. Cutululis, Helen Markou, and Poul E. Sørensen. 2011. “Impact of Fault Ride-through Requirements on Fixed-Speed Wind Turbine Structural Loads.” Wind Energy 14 (1): 1–11. https://doi.org/10.1002/we.398.

Horcas, S G, N N Sørensen, F. Zahle, G R Pirrung, and T Barlas. 2022. “Vibrations of Wind Turbine Blades in Standstill: Mapping the Influence of the Inflow Angles.” Physics of Fluids 34 (5). https://doi.org/10.1063/5.0088036.

Hu, Jiabing, Heng Nian, Bin Hu, Yikang He, and Z. Q. Zhu. 2010. “Direct Active and Reactive Power Regulation of DFIG Using Sliding-Mode Control Approach.” IEEE Transactions on Energy Conversion 25 (4): 1028–39. https://doi.org/10.1109/tec.2010.2048754.

Huang, Hui, Chengxiong Mao, Jiming Lu, and Dan Wang. 2014. “Electronic Power Transformer Control Strategy in Wind Energy Conversion Systems for Low Voltage Ride-through Capability Enhancement of Directly Driven Wind Turbines with Permanent Magnet Synchronous Generators (D-PMSGs).” Energies 7 (11): 7330–47. https://doi.org/10.3390/en7117330.

Iov, F, Hansen, A D, Soerensen, P, and Blaabjerg, F. 2004. "Wind Turbine Blockset in Matlab/Simulink - General overview and description of the models." Denmark.

Jerin, Ann, Palanisamy Kaliannan, and Umashankar Subramaniam. 2017. “Testing of Low-Voltage Ride through Capability Compliance of Wind Turbines – a Review.” International Journal of Ambient Energy 39 (8): 891–97. https://doi.org/10.1080/01430750.2017.1340337.

Jiang, Zhiyu, Weifei Hu, Wenbin Dong, Zhen Gao, and Zhengru Ren. 2017. “Structural Reliability Analysis of Wind Turbines: A Review.” Energies 10 (12): 2099. https://doi.org/10.3390/en10122099.

Kalyani, V. Mohana, J. Preetha Roselyn, C. Nithya, and D. Devaraj. 2016. "Enhanced crowbar protection for fault ride through capability of wind generation systems." International Journal of Power Electronics and Drive Systems 7, no. 4.

Kumar, Anuj. 2015. “Transient Behavior of Doubly Fed Induction Generator Using Simulink Model in Wind Energy Conversion System.” International Journal of Innovative Research in Science, Engineering and Technology 04 (02): 450–54. https://doi.org/10.15680/ijirset.2015.0402032.

Kumar, Sushil, and Shilpa Manoj Rawte. 2013. "Grid voltage control by using DFIG during grid faults.‘." IOSR Journal of Engineering (IOSRJEN)’, e-ISSN: 2250-3021.

Larsen, Torben, Anders Hansen, and Melchior. 2007. “How 2 HAWC2, the User’s Manual.” https://orbit.dtu.dk/files/7703110/ris_r_1597.pdf.

Lebranchu, Alexis, Sylvie Charbonnier, Christophe Bérenguer, and Frédéric Prévost. 2019. “A Combined Mono- and Multi-Turbine Approach for Fault Indicator Synthesis and Wind Turbine Monitoring Using SCADA Data.” ISA Transactions 87 (April): 272–81. https://doi.org/10.1016/j.isatra.2018.11.041.

Lio, Wai Hou, Gunner Chr. Larsen, and Gunhild R. Thorsen. 2021. “Dynamic Wake Tracking Using a Cost-Effective LiDAR and Kalman Filtering: Design, Simulation and Full-Scale Validation.” Renewable Energy, March. https://doi.org/10.1016/j.renene.2021.03.081.

Morren, J., and S.W.H. deHaan. 2005. “Ridethrough of Wind Turbines with Doubly-Fed Induction Generator during a Voltage Dip.” IEEE Transactions on Energy Conversion 20 (2): 435–41. https://doi.org/10.1109/tec.2005.845526.

Mullane, A., G. Lightbody, and R. Yacamini. 2005. “Wind-Turbine Fault Ride-through Enhancement.” IEEE Transactions on Power Systems 20 (4): 1929–37. https://doi.org/10.1109/tpwrs.2005.857390.

Nunes, M.V.A., J.A. PecasLopes, H.H. Zurn, U.H. Bezerra, and R.G. Almeida. 2004. “Influence of the Variable-Speed Wind Generators in Transient Stability Margin of the Conventional Generators Integrated in Electrical Grids.” IEEE Transactions on Energy Conversion 19 (4): 692–701. https://doi.org/10.1109/tec.2004.832078.

Pao, Lucy Y. 2021. “Active Power Control of Wind Power Plants for Grid Integration.” Springer EBooks, January, 1–6. https://doi.org/10.1007/978-3-030-44184-5_272.

Papi, Francesco, Pier Francesco Melani, Jörg Alber, Francesco Balduzzi, Giovanni Ferrara, Christian Navid Nayeri, and Alessandro Bianchini. 2022. “Potential of Mini Gurney Flaps as a Retrofit to Mitigate the Performance Degradation of Wind Turbine Blades Induced by Erosion.” Journal of Physics: Conference Series 2265 (3): 032046–46. https://doi.org/10.1088/1742-6596/2265/3/032046.

Pratap, R. 2016. “Getting Started with MATLAB.” Oxford University Press, SA.

Ren, Zhengru, Zhiyu Jiang, Roger Skjetne, and Zhen Gao. 2018. “Development and Application of a Simulator for Offshore Wind Turbine Blades Installation.” Ocean Engineering 166 (October): 380–95. https://doi.org/10.1016/j.oceaneng.2018.05.011.

Shi, Wei, Xiang Tan, Zhen Gao, and Torgeir Moan. 2016. “Numerical Study of Ice-Induced Loads and Responses of a Monopile-Type Offshore Wind Turbine in Parked and Operating Conditions.” Cold Regions Science and Technology 123 (March): 121–39. https://doi.org/10.1016/j.coldregions.2015.12.007.

Siavash Beheshtaein. 2014. “Optimal Hysteresis Based DPC Strategy for STATCOM to Augment LVRT Capability of a DFIG Using a New Dynamic References Method.” International Symposium on Industrial Electronics, June. https://doi.org/10.1109/isie.2014.6864682.

Sim, Jun-Bo, Ki-Cheol Kim, Rak-Won Son, and Joong-Ki Oh. 2012. "Ride-through of PMSG wind power system under the distorted and unbalanced grid voltage dips." Journal of Electrical Engineering & Technology 7, no. 6: 898-904.

Sitharthan, R, and M Geethanjali. 2015. “Application of the Superconducting Fault Current Limiter Strategy to Improve the Fault Ride-through Capability of a Doubly-Fed Induction Generator–Based Wind Energy Conversion System.” SIMULATION 91 (12): 1081–87. https://doi.org/10.1177/0037549715615428.

Slootweg, J.G., H. Polinder, and W.L. Kling. 2003. “Representing Wind Turbine Electrical Generating Systems in Fundamental Frequency Simulations.” IEEE Transactions on Energy Conversion 18 (4): 516–24. https://doi.org/10.1109/tec.2003.816593.

Tang, Rundong, and Renjing Cao. 2023. “Numerical Investigation on Wake Characteristics of Floating Offshore Wind Turbine under Pitch Motion.” Iet Renewable Power Generation 17 (11): 2765–78. https://doi.org/10.1049/rpg2.12741.

Tarnowski, Germán, and Claudio. 2012. “Coordinated Frequency Control of Wind Turbines in Power Systems with High Wind Power Penetration.” Accessed February 9, 2024. https://orbit.dtu.dk/files/75259610/gctarnowski_thesis1.pdf.

Thapa, Khagendra, Jinho Kim, and Yong Cheol Kang. 2016. “Coordinated Control for Low Voltage Ride-through of a PMSG-Based Wind Power Plant.” Journal of International Council on Electrical Engineering 6 (1): 242–51. https://doi.org/10.1080/22348972.2016.1251533.

Thapa, Khagendra, Jinho Kim, and Yong Cheol Kang. 2016. “Coordinated Control for Low Voltage Ride-through of a PMSG-Based Wind Power Plant.” Journal of International Council on Electrical Engineering 6 (1): 242–51. https://doi.org/10.1080/22348972.2016.1251533.

Tuhfe Göçmen, Filippo Campagnolo, Thomas Duc, Irene Eguinoa, Søren Juhl Andersen, Vlaho Petrović, Lejla Imširović, et al. 2022. “FarmConners Wind Farm Flow Control Benchmark – Part 1: Blind Test Results.” Wind Energy Science 7 (5): 1791–1825. https://doi.org/10.5194/wes-7-1791-2022.

Wang, Jianing, Yuan Fu, and Xiangyu Zhang. 2023. “Adaptive Control of DFIG-Based Wind Turbines for Fault Ride-through and Reactive Power Support Based on Stator Current Transient Component.” Journal of Physics: Conference Series 2564 (1): 012060–60. https://doi.org/10.1088/1742-6596/2564/1/012060.

Wang, Shaofeng, and Torben Juul Larsen. 2019. “Permanent Accumulated Rotation of an Offshore Monopile Wind Turbine in Sand during a Storm.” Ocean

Engineering 188 (September): 106340. https://doi.org/10.1016/j.oceaneng.2019.106340.

Wu, Zaijun, Chanxia Zhu, and Minqiang Hu. 2013. “Improved Control Strategy for DFIG Wind Turbines for Low Voltage Ride Through.” Energies 6 (3): 1181–97. https://doi.org/10.3390/en6031181.

Xu, Guanqun, Wei Yu, and Taeseong Kim. 2022. “Wind Turbine Load Estimation Using Machine Learning and Transfer Learning.” Journal of Physics: Conference Series 2265 (3): 032108. https://doi.org/10.1088/1742-6596/2265/3/032108.

Yan, Xiangwu, Giri Venkataramanan, Yang Wang, Qing Dong, and Bo Zhang. 2011. “Grid-Fault Tolerant Operation of a DFIG Wind Turbine Generator Using a Passive Resistance Network.” IEEE Transactions on Power Electronics 26 (10): 2896–2905. https://doi.org/10.1109/tpel.2010.2087037.

You, Rui, Braulio Barahona, Jianyun Chai, and Nicolaos Cutululis. 2013. “A Novel Wind Turbine Concept Based on an Electromagnetic Coupler and the Study of Its Fault Ride-through Capability.” Energies 6 (11): 6120–36. https://doi.org/10.3390/en6116120.

Zhang, Kun, Chengxiong Mao, Jiming Lu, Dan Wang, Junfeng Zhang, and Xun Chen. 2015. “Power Control of Directly Driven Wind Generation System Based on Superconducting Magnetic Energy Storage.” Electric Power Components and Systems 43 (7): 747–58. https://doi.org/10.1080/15325008.2014.1002586.

CHAPTER 7
APPENDICIES
APPENDIX A

1. HAWC2 License Information

HAWC2 provides a variety of software license agreements that are tailored to accommodate diverse users and objectives. The term "standard" refers to a widely accepted or established level of quality, performance,

The One-Year Commercial License is the standard license granted for commercial use. The 3-month commercial license refers to a commercial license with a shorter duration than standard licenses. HAWC2 offers a complimentary trial license for a duration of three months. The trial edition of this software does not provide assistance or access to online training resources. However, users have the option to purchase a separate restricted support package if desired.

The Cooperative Research License is designed for individuals involved in publicly sponsored cooperative research initiatives with DTU Wind. This license is specifically suited to facilitate collaborative research endeavors.

Academic License is designed for individual students or researchers involved in academic research endeavors. This includes endeavors such as the completion of theses or research projects that yield reports or publications that are accessible to the public. The academic license is provided at no cost and grants users access to online e-learning resources. However, it should be noted that support is not included as a default feature. Nevertheless, supplementary support packages are available for acquisition. Academic licenses are exclusively accessible to individuals who are either students or staff affiliated with universities or national laboratories. The process of obtaining such licenses necessitates submitting a formal request using an email address associated with an academic institution.

2. Running HAWC2

HAWC2 is run by calling the HAWC2 executable from a Windows Command Prompt on the input file, which has a .htc file extension:

<path to HAWC2 executable> <path to htc file>

For example, if the current working directory of the Command Prompt contains both HAWC2 executable and an input file called “turbine_model.htc” the command to run HAWC2 would be:

> HAWC2MB.exe turbine_model.htc

Example of running HAWC2 with an HTC file can be:

…\HAWC2\NREL5MWReferenceWindTurbinev50>C:\Users\90505\Desktop\HAWC2\HAWC2_12.9_win32\HAWC2MB.exe .\htc\NREL_5MW_reference_wind_turbine.htc

After execution of above command HAWC2 start running; License file would be loaded and checked then related DLL files are included for simulation in which HTC to be run step by step. CMD screen information about all these can be seen from Figure 1.

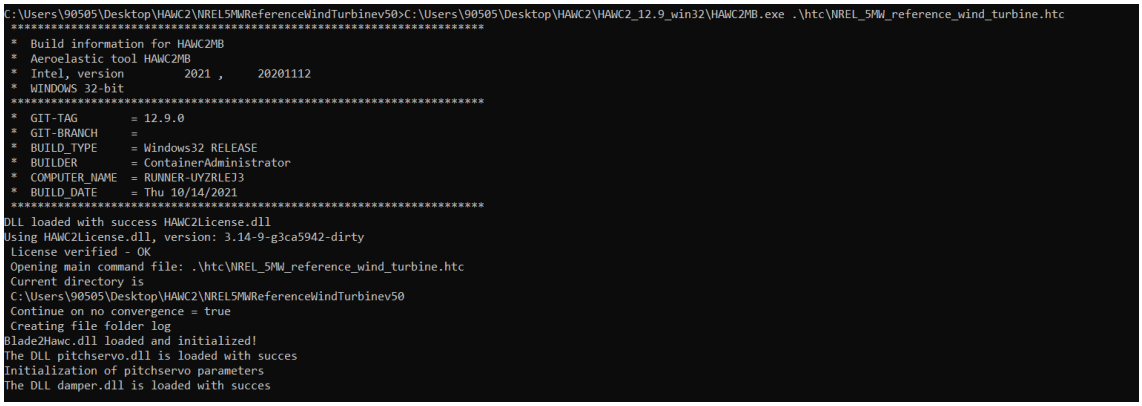

Figure 7.1. CMD command and status for HAWC2 run

APPENDIX B

Fortran Example:

```
//
!
! External Torque Input
!
SUBROUTINE TorqueDLL(time,M)
!DEC$ ATTRIBUTES DLLEXPORT::TorqueDLL
!DEC$ ATTRIBUTES ALIAS:'torqueDLL' :: TorqueDLL
! input
DOUBLE PRECISION :: time ! time
DOUBLE PRECISION ,DIMENSION(3) :: M ! External torque in reference
! node (global base)
! locals
LOGICAL, SAVE :: bInit = .FALSE. ! Initialization flag
!
! Initialise on first call
! Time check - Similar time interval should be same!!!!,
! 3 dimension M check
IF (.NOT.bInit) THEN
bInit = .TRUE.
! Open file and read mass
OPEN(10,FILE="Tem1.dat")
READ(10,*) Tem
CLOSE(10)
ENDIF
!
!
M[0]=Tem
END SUBROUTINE TorqueDLL
```

APPENDIX C

Table 7.1. DLL command, external force, and moment

Command 1	Command 2	Attributes Explanation
mbdy	force_ext	An external force is placed on the structure. Unit is [N]. 1. main body name 2. node number on main body 3. component (1 = F_x, 2 = F_y, 3 = F_z), if negative number the force is inserted with opposite sign. 4. coordinate system (possible options are: mbdy name," global", "local").
mbdy	moment_ext	An external moment is placed on the structure. Unit is [Nm]. 1. main body name 2. node number on main body 3. component (1 = M_x, 2 = M_y, 3 = M_z), if negative number the moment is inserted with opposite sign. 4. coordinate system (possible options are: mbdy name," global"," local").
mbdy	force_int	An internal force with a reaction component is placed on the structure. Unit is [N]. 1. main body name for action force 2. node number on main body 3. component (1 = F_x, 2 = F_y, 3 = F_z), if negative number the force is inserted with opposite sign. 4. coordinate system (possible options are: mbdy name," global"," local"). "local" means local element coo on the inner element. 5. main body name for reaction force 6. Node number on this main body
mbdy	moment_in	An internal force with a reaction component is placed on the structure. Unit is [Nm]. 1. main body name for action moment 2. node number on main body 3. component (1 = "G, 2 = "H, 3 = "I), if negative number the moment is inserted with opposite sign. 4. coordinate system (possible options are: mbdy name,"global","local"). "local" means local element coo on the inner element. 5. main body name for reaction moment 6. Node number on this main body

APPENDIX D

```
;
begin type2_dll;
   name gear;
   filename  ./control/hss_convert.dll ;
   arraysizes_init  1000 10 ;
   arraysizes_update  1000 10 ;
   begin init;
    constant 1 2.0 ;     number of used sensors - in this case only 1
    constant 2 1000;     unit conversion factor
   end init;
   begin output;
         mbdy moment_int shaft 1 1 shaft;
         mbdy moment_int shaft 2 1 shaft;
         mbdy moment_int shaft 3 1 shaft;
   end output;
;
   begin actions;
    mbdy moment_int shaft 1 1 global shaft 1;
         mbdy moment_int shaft 1 2 global shaft 2;
         mbdy moment_int shaft 1 3 global shaft 3;
         mbdy moment_int shaft 2 1 global shaft 1;
         mbdy moment_int shaft 2 2 global shaft 2;
         mbdy moment_int shaft 2 3 global shaft 3;
    mbdy moment_int shaft 3 1 global towertop;
         mbdy moment_int shaft 3 2 global towertop;
         mbdy moment_int shaft 3 3 global towertop;
   end actions;
end type2_dll;
;
```

APPENDIX E

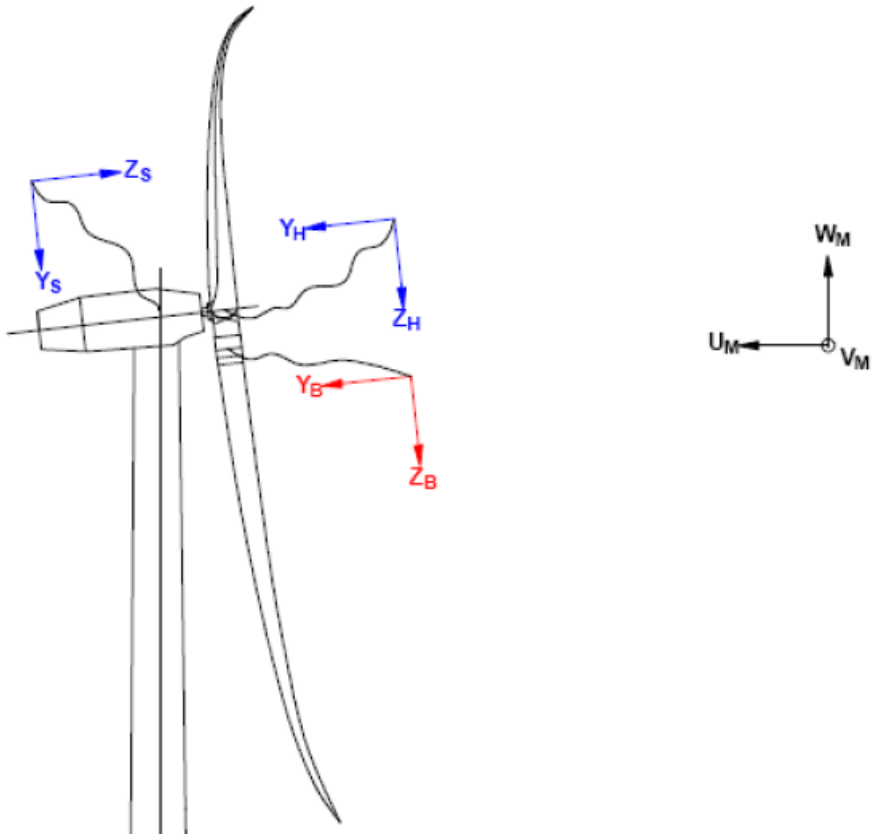

Figure 7.2. Coordinate system representation

APPENDIX F

Rotor Side Converter measurements:

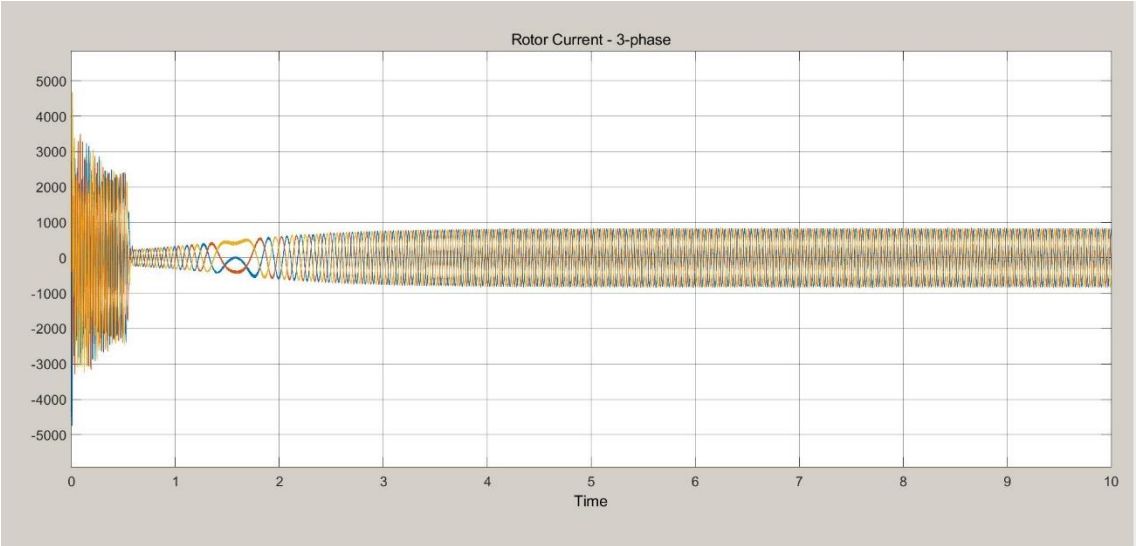

Figure 7.3. Rotor side converter current Ir, in 3-phase

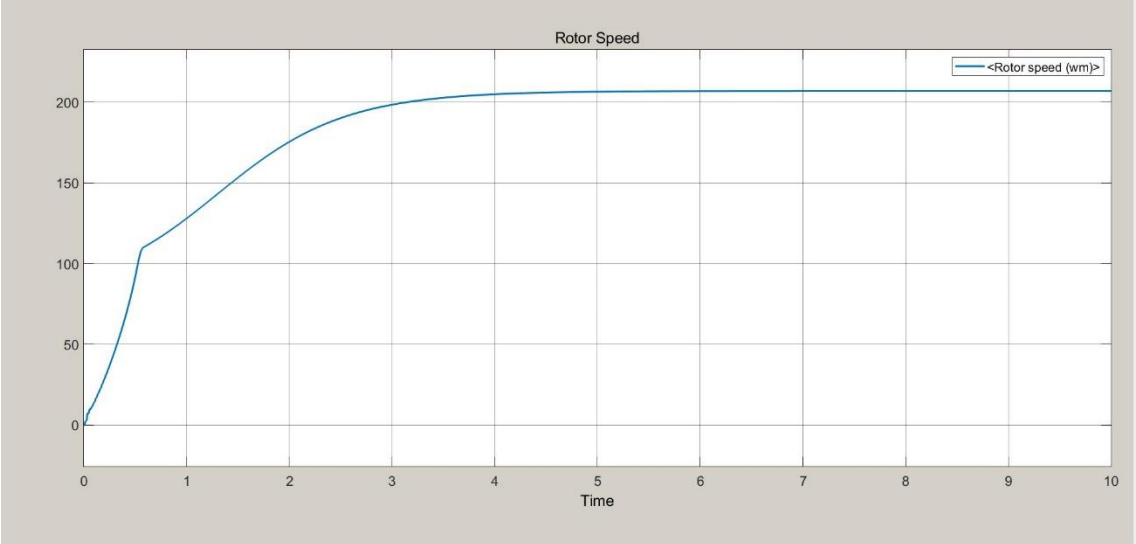

Figure 7.4. Rotor speed

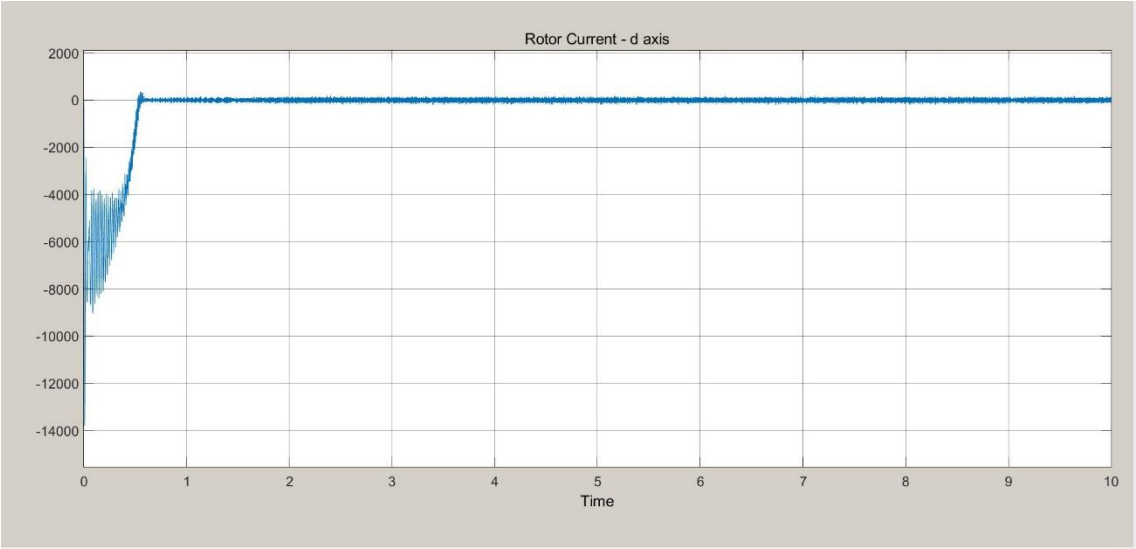

Figure 7.5. Rotor side converter current in d axis form

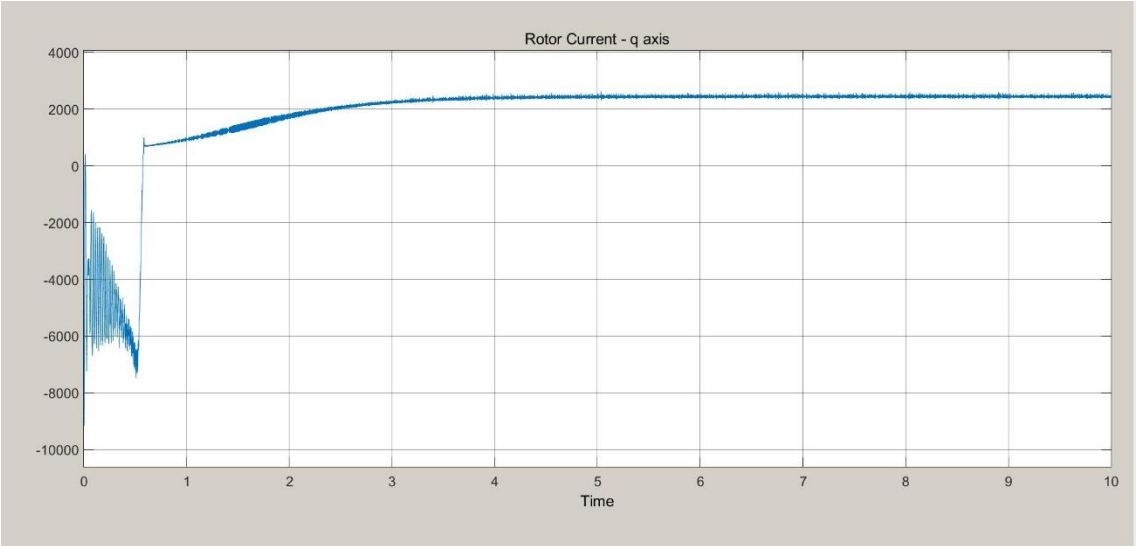

Figure 7.6. Rotor side converter current in q axis form

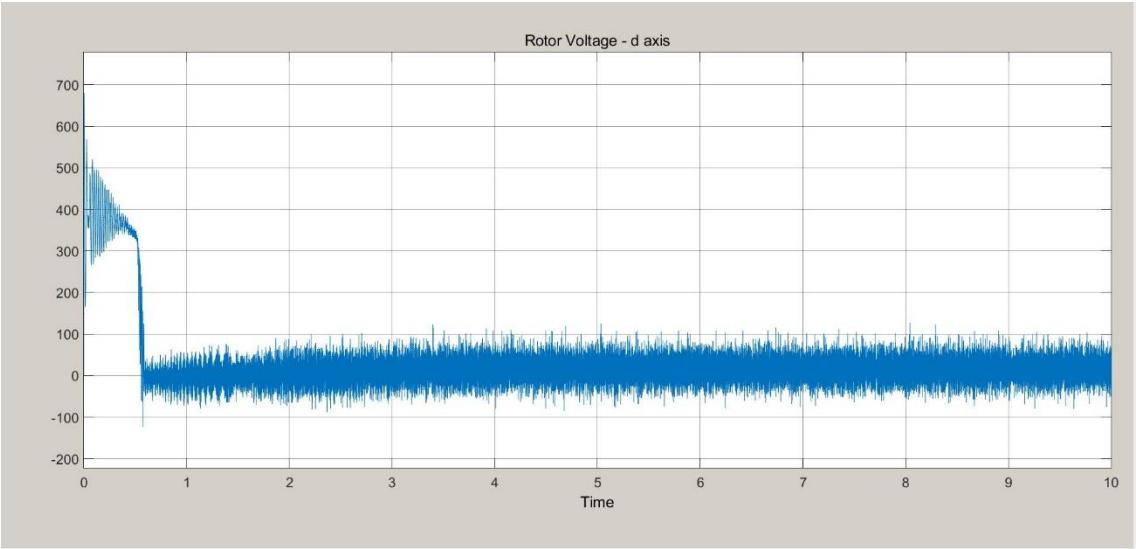

Figure 7.7. Rotor side converter voltage in d axis form

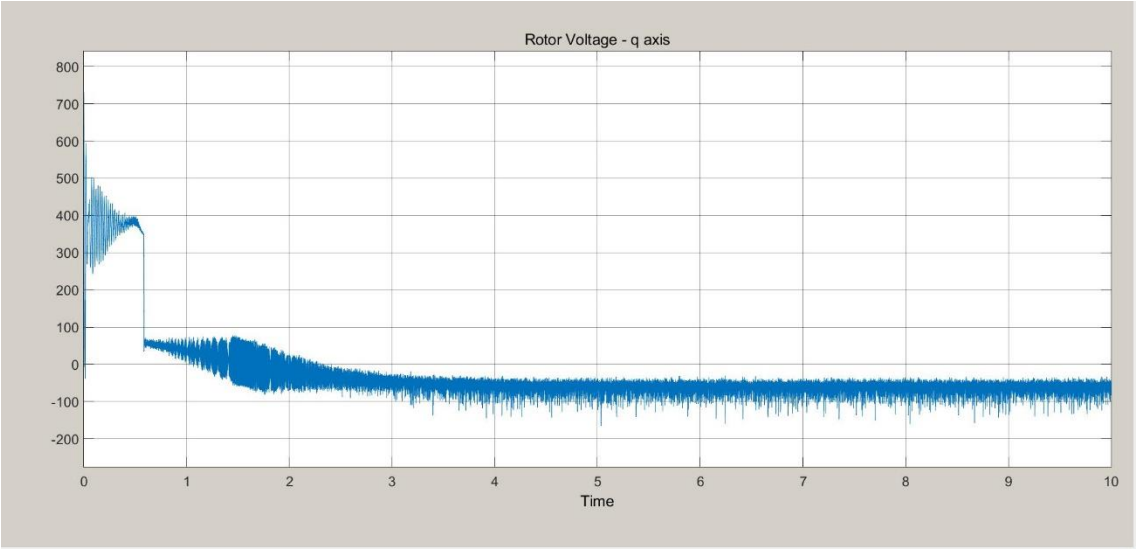

Figure 7.8. Rotor side converter voltage in q axis form

Stator side converter measurements:

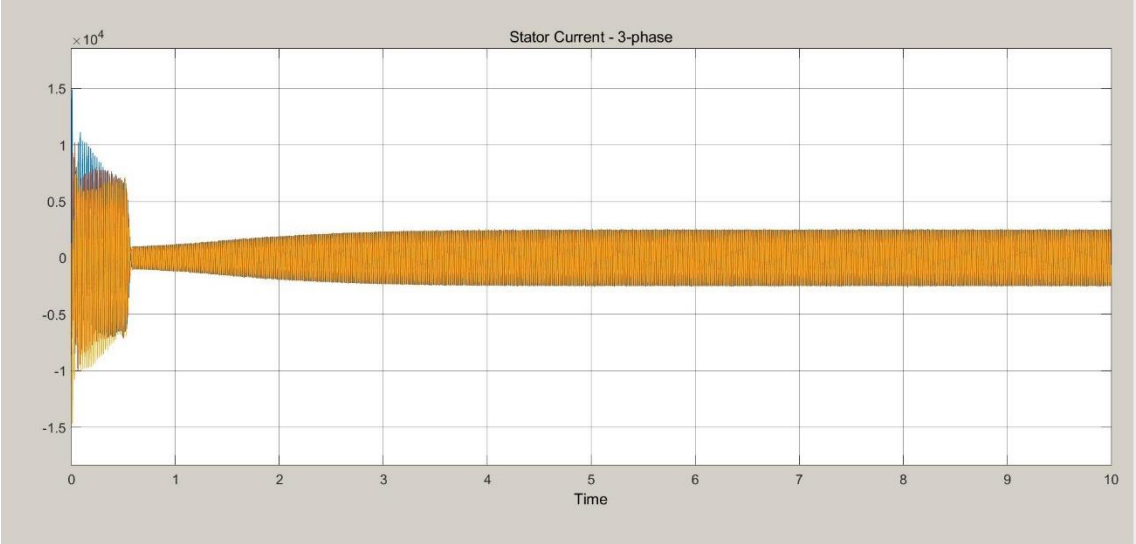

Figure 7.9. Stator side converter current – 3-phase

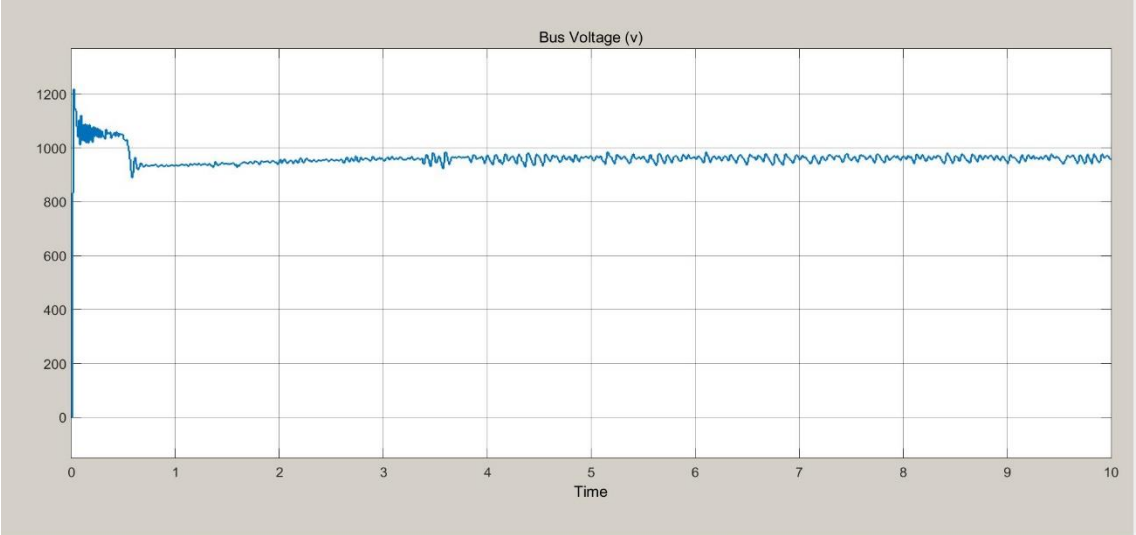

Figure 7.10. Bus voltage

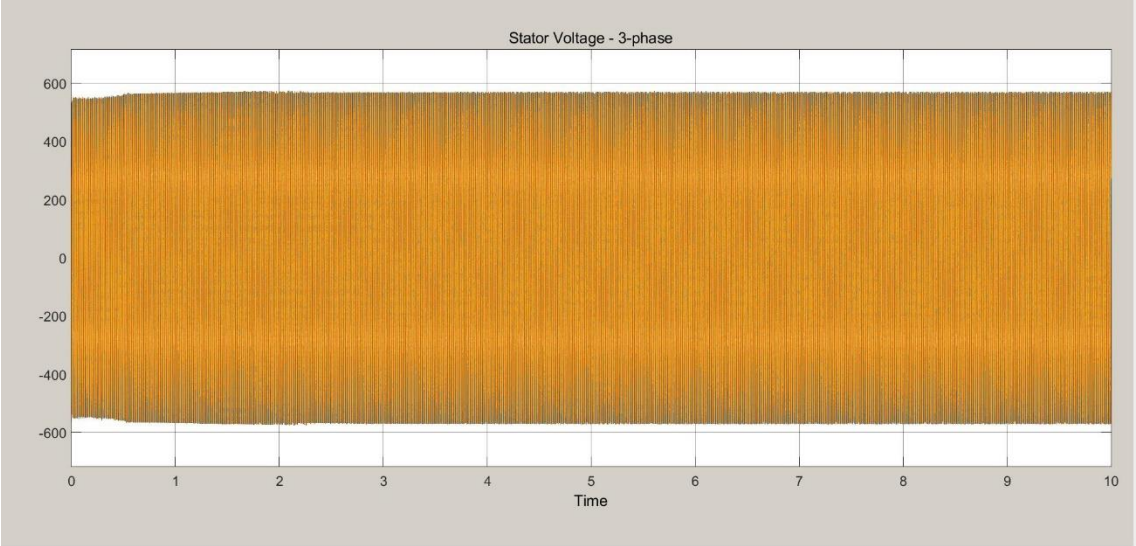

Figure 7.11. Stator side converter voltage in 3-phase

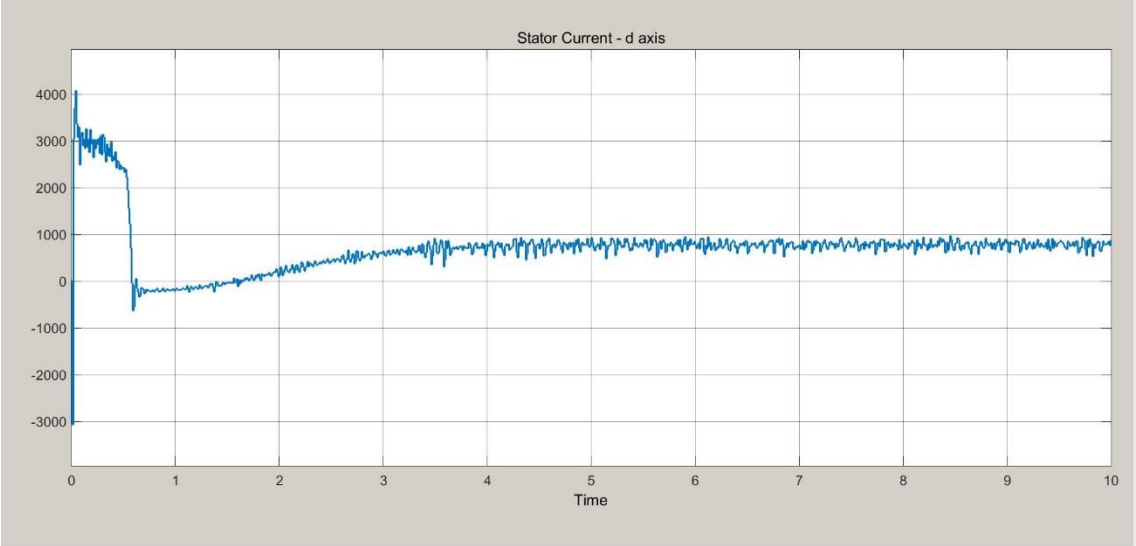

Figure 7.12. Stator side converter current in d axis

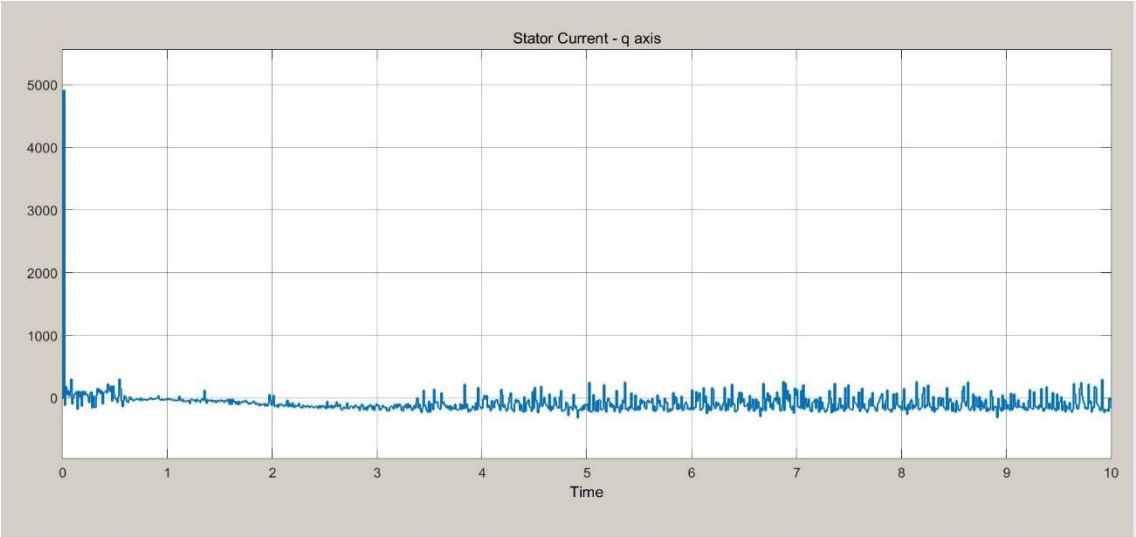

Figure 7.13. Rotor side converter current in q axis

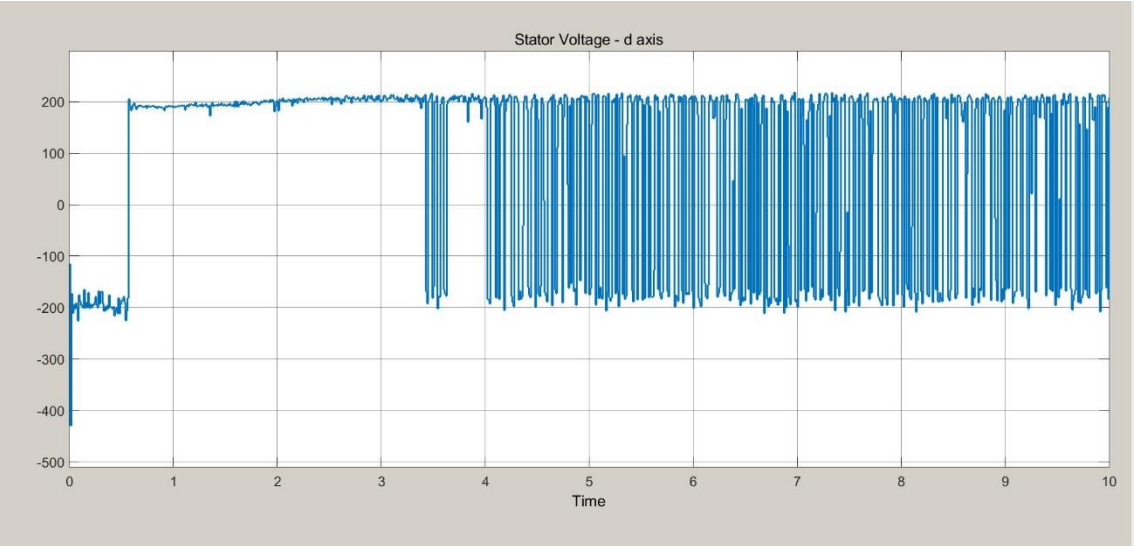

Figure 7.14. Rotor side converter voltage in d axis

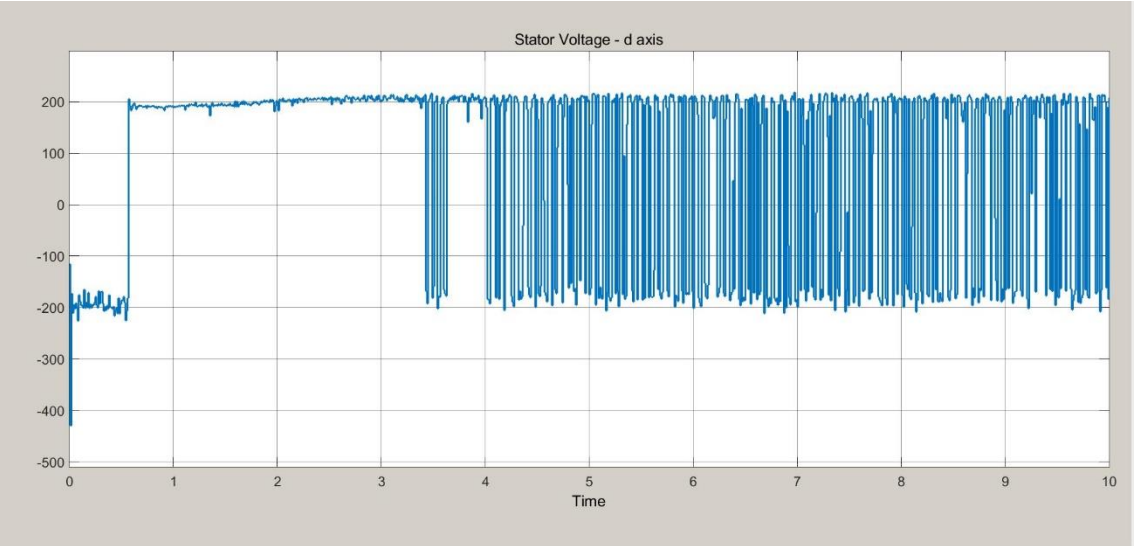

Figure 7.15. Rotor side converter voltage in q axis